NASA CR-66488

A STOP-START STUDY OF SOLID PROPELLANTS (U)

By G. E. Jensen

Distribution of this report is provided in the interest of information exchange. Responsibility for the contents resides in the author or organization that prepared it.

Prepared under
Contract No. NAS 1-6601
by
United Technology Center
DIVISION OF UNITED AIRCRAFT CORPORATION
SUNNYVALE, CALIFORNIA

for

NATIONAL AERONAUTICS AND SPACE ADMINISTRATION

CONTENTS

Page

SUMMARY 1

INTRODUCTION 3

EXPERIMENTAL STUDIES 5

Equipment and Experimental Procedures 5

Slab Motor 5
Window Motor 8

Experimental Results 11

Depressurization Studies 13
High-Speed Film Tests. 46
L* Studies 54

DISCUSSION AND ANALYSIS 73

THEORETICAL STUDIES 85

CONCLUSIONS 91

REFERENCES 93

ILLUSTRATIONS

Figure		Page
1	Schematic Diagram of Combustion Termination Apparatus	6
2	Slab-Motor Systems	7
3	Schematic of L* Window Motor	9
4	L* Window Motor	10
5	Schematic Top View of Window Motor and Camera System	12
6	Strand Burning Rates of Nonaluminized Propellants	15
7	$\dot{P}$ Characteristics of UTX-9394: CTPB - 84% AP	17
8	$\dot{P}$ Characteristics of UTX-9377: PBAN - 84% AP	18
9	$\dot{P}$ Characteristics of UTC-9377-4: PBAN - 84% AP	19
10	$\dot{P}$ Characteristics of UTX-9389: PU - 84% AP	20
11	$\dot{P}$ Characteristics of UTX-9395: PEP - 84% AP	21
12	$\dot{P}$ Characteristics of UTX-9379: UTREZ - 84% AP	22
13	Comparison of Critical Depressurization Limit Lines as a Function of Binder System - 84% AP	23
14	$\dot{P}$ Characteristics of UTX-9710: UTREZ/1.5 MAPO - 84% AP	25
15	$\dot{P}$ Characteristics of UTX-9712: UTREZ/MAPO/EPOXY - 84% AP	26
16	Stress vs Strain Behavior of UTREZ Propellants	27
17	$\dot{P}$ Characteristics of UTX-9711: PBAN/MAPO - 84% AP	28
18	$\dot{P}$ Characteristics of UTX-9775: CTPB/EPOXY - 84% AP	29
19	Strand Burning Rate of UTREZ Propellants	31
20	Strand Burning Rate of UTREZ Propellants	32
21	$\dot{P}$ Characteristics of UTX-9713: UTREZ - 80% AP	34
22	$\dot{P}$ Characteristics of UTX-9714: UTREZ - 76% AP	35
23	Effect of Oxidizer Loading Level Upon $\dot{P}$ Termination of UTREZ Propellants	36
24	Effect of Oxidizer Particle Size Upon $\dot{P}$ Termination of UTX-9754: UTREZ - 84% AP (400μ Large Diameter Particle, 70:30 Coarse to Fine)	37
25	$\dot{P}$ Characteristics of UTX-9757: UTREZ - 80% Solids, Large Diameter Particles Coated with 1.5% Kel-F	39

ILLUSTRATIONS (Continued)

Figure		Page
26	$\dot{P}$ Characteristics of UTX-9715: UTREZ - 84% Solids - 0.25% Iron Oxide	40
27	$\dot{P}$ Characteristics of UTX-9717: UTREZ - 84% Solids - 0.5% Iron Oxide	41
28	$\dot{P}$ Characteristics of UTX-9720: UTREZ - 84% Solids - 0.13% Copper Chromite	42
29	$\dot{P}$ Characteristics of UTX-9718: UTREZ - 84% Solids - 0.25% Copper Chromite	43
30	$\dot{P}$ Characteristics of UTX-9719: UTREZ - 84% Solids - 0.5% Copper Chromite	44
31	Comparison of Critical Depressurization Limits as a Function of Catalyst - UTREZ Binder - 84% Solids	45
32	$\dot{P}$ Characteristics of UTX-9755: UTREZ - 80% AP - 4% Aluminum	47
33	$\dot{P}$ Characteristics of UTX-9756: UTREZ - 76% AP - 8% Aluminum	48
34	$\dot{P}$ Characteristics of UTX-9759: 68% AP - 16% Aluminum	49
35	$\dot{P}$ Characteristics of UTX-9772: UTREZ - 16% Al (4% Needles)	50
36	Effect of Grain Size and Environmental Conditions upon Combustion Termination	53
37	Photomicrographs of $\dot{P}$ Terminated Propellant Surfaces	55
38	Representative L* Data Trace	59
39	L* Termination Characteristics of UTREZ, CTPB, and PEP Propellants - 84% AP	61
40	L* Termination Characteristics of Polyurethane, PBAN, and UTREZ Propellants - 84% AP	62
41	Effect of Oxidizer Loading Level upon L* Behavior of UTREZ Propellants	63
42	Effect of Catalyst upon L* Behavior of UTREZ Propellants	64
43	Effect of Kel-F Coating of AP Particles	65
44	Effect of Aluminum Concentration upon L* Behavior of UTREZ Propellants	67
45	Photomicrographs of L* Terminated Propellants	68

ILLUSTRATIONS (Concluded)

Figure		Page
46	Predicted Termination Requirement vs Experimental Results (500 psi)	74
47	Predicted Termination Requirement vs Experimental Requirements (100 psi)	77
48	Effect of Polymer in Arc-Image Furnace Delays as a Function of Environmental Pressure (N_2) for a Constant Flux Level	79
49	Effect of Flux Upon Ignition Delay of UTREZ Propellants for Different Environmental Pressures (N_2)	81

TABLES

Table		Table
I	Binder Formulation Studies	13
II	Coarse AP Screen Analysis	14
III	Compositions of UTREZ Propellants	30
IV	High-Speed Film Test Results	51
V	L* Test Data	60
VI	Predicted and Experimental Depressurization Rates (500 psi)	75
VII	Predicted and Experimental Depressurization Rates (100 psi)	76

ABBREVIATIONS AND SYMBOLS

AP	ammonium perchlorate
atm	atmosphere
b	constant
CTPB	carboxy-terminated polybutadiene
$\frac{dP}{dt}$	rate of depressurization
exp	experimental
ID	inside diameter
L*	chamber volume/nozzle throat area
max	maximum
n	burning rate exponent
OD	outside diameter
P	pressure
$\dot{P}$	rapid depressurization; rate of depressurization
P*	minimum ignition pressure
P_c	chamber pressure
P_{dl}	deflagration pressure
P_{ex}	extinction pressure
P_f	pressure at initiation of instability
P_L	light sensor-indicated extinction pressure
PBAN	polybutadiene-acrylic acid-acrylonitrile
PEP	nitrate-plasticized imine-cured polyester binder
PIB	polyisobutylene
PU	polyurethane
pred	predicted
$\dot{r}$	burning rate
$\bar{r}$	steady-state burning rate
SCTPB	saturated carboxy-terminated polybutadiene
t	time
UTC	United Technology Center
UTREZ	polyisobutylene
α	propellant thermal diffusivity
τ	time from initiation of depressurization to extinction
λ	constant

A STOP-START STUDY OF SOLID PROPELLANTS

by G. E. Jensen

United Technology Center
A Division of United Aircraft Corporation
Sunnyvale, California

SUMMARY

Rapid-depressurization ($\dot{P}$) and critical chamber geometry (L*) extinction characteristics of a series of composite propellants were investigated using a windowed end-burning grain motor for $\dot{P}$ and L* extinguishment tests and a slab motor for $\dot{P}$ tests. Systematic variation in the binder, binder curing agent, catalyst type and concentration, oxidizer concentration, and aluminum loading level were studied to elucidate the mechanisms of composite propellant combustion extinguishment.

The binder-polymer structure was found to have major influence upon the rapid depressurization termination characteristics of the tested non-aluminized propellants. Propellants containing CTPB, PBAN, and PEP binders were the most difficult to terminate and had similar termination characteristics (-60 000 psi/sec at 500 psia). Propellants formulated with PU and PIB were found to be much easier to terminate (-26 000 psi/sec at 500 psia). The critical depressurization rate for termination was found to be less a function of burning rate than predicted by Von Elbe[1*] and Paul[2], but more directly related to the thermal and oxidative degradation characteristics of the binder polymer. Those propellants exhibiting greater susceptibility to oxidative degradation of the binder (CTPB and PBAN) were more difficult to terminate than the more easily thermally-degraded propellants (PIB and PU).

The effect of curative type and polymer-to-curative equivalence ratio was explored using the PIB polymer-based propellants. While this series of propellants exhibited a wide range of tensile properties, the termination characteristics of the propellants were negligibly affected by the curative type or equivalence ratio. In contrast, increasing the fuel content of another series of PIB propellants resulted in a significant lowering of the termination limits. However, substitution of aluminum for AP had little effect upon the termination limits, nor did inclusion of copper chromite and iron oxide burning rate catalysts significantly affect the termination behavior of the basic PIB propellant system.

---

*Superscript numbers denote references appearing on page 93.

The propellant binder system also was found to control the L* extinction behavior. Propellants formulated with PIB and PU demonstrated higher extinction pressures than the propellants formulated with CTPB, PEP, and PBAN binders. In addition, it was found that increasing the fuel content or substitution of aluminum for AP further increased the extinction pressure of PIB propellants. Inclusion of burning rate catalysts resulted in no change of the extinction pressure level.

High-speed motion pictures were used to supplement the characterization tests. Good picture quality was obtained and several significant points were discernible in the film sequences. In those instances where the rate of chamber pressure depressurization was significantly above the rate necessary for termination, extinguishment was achieved shortly after initiation of chamber venting and at a chamber pressure above the exhaust or ambient pressure level (14.7 psia). In cases where the depressurization rate was much less than that needed for extinction, there was no discernible pause in the combustion of the grain, although there was an adjustment of the burning rate to the imposed pressure change. In some instances, at rates slightly less than the critical depressurization rate, the grain was extinguished but reignition occurred several seconds later. Reignition at the propellant/inhibitor interface was noted in some tests. Such interfaces, which are likely to occur in working motors, must necessarily be considered in the design of any termination system.

INTRODUCTION

This final technical report is submitted in accordance with the requirements of Contract No. NAS 1-6601. The principal objective of these studies was to experimentally and theoretically investigate the basic parameters controlling solid propellant extinguishment and thrust modulation resulting from rapid depressurization or critical chamber-geometry extinguishment. Using two types of depressurization motors and an L* extinguishment apparatus, solid propellant combustion termination behavior was investigated as a function of formulation variables. Systematic variation in the binder, type of catalyst, oxidizer concentration, reactivity at the oxidizer fuel interface, and metal additives were used to study the extinguishment behavior and provide guidelines for solid propellant optimization. Additionally, a theoretical model of combustion termination behavior was developed and programmed for computer solution.

Numerous experimental and theoretical[3,4,5,6,7,8,and 9] studies have shown the rate of depressurization needed for successful termination to be a function of the propellant formulation and to be modifiable by the addition of formulation additives. L* correlated combustion termination has been postulated to occur by rapid depressurization generated by low-frequency instabilities, and the ease of termination by this mode has also been shown to be affected by formulation differences in much the same manner as that found for $\dot{P}$ termination.

Termination of propellant combustion requires that the rate of heat generation in the combusting surface be reduced to a point where the exothermic processes are no longer self-sustaining. Thus, the function of any termination system is to reduce the pressure and temperature in the combustion zone such that heat generation by gas-phase combustion feedback, exothermic oxidizer decomposition, and oxidative degradation of the binder is less than the heat loss by conduction and thermal degradation of the binder. While the overall aspects of these processes are qualitatively simple in nature, quantitative and usable understanding of the mechanisms of combustion termination is lacking.

Ignition and combustion studies [9,10,11] conducted at UTC suggested that the related processes of combustion termination and ignition of AP propellants are affected to a significant extent by the thermal and oxidative characteristics of the binder and the pressure level at which these processes occur.

To interrelate the effect of binder and other formulation differences with environmental conditions and to further define the mechanisms of propellant termination, the experimental and theoretical investigation as reported herein was conducted. Basically, the program consisted of three

aspects: (1) an experimental study of $\dot{P}$ behavior including high-speed film studies, (2) an experimental study of L* extinction behavior, and (3) the development of an analytical model of combustion extinction behavior. The experimental portions of the program constituted the primary effort during the period of performance and thus make up the major portion of this report. The theoretical model which has evolved from the experimental studies is discussed following the experimental results.

EXPERIMENTAL STUDIES

The depressurization studies were conducted using two similar rapid-depressurization motors. The bulk of the characterization studies were performed in a dual-nozzle motor using a 1-lb slab grain. A second window motor utilizing smaller free-standing grains was used for high-speed film studies and for the study of environmental effects. Details of both motors and the experimental techniques associated with their usage and the experimental results are presented in subsequent sections.

Equipment and Experimental Procedures

Slab motor. - The slab motor used for rapid depressurization characterization is shown schematically in figure 1 and pictorially in figure 2. The basic element is a small motor containing propellant slabs (1-lb) with dual-nozzle assemblies located at the motor centerline. The smaller assembly is the steady-state nozzle used during the entire test time, and the large assembly is the depressurization nozzle. This depressurization nozzle consists of a double-burst disc assembly with a pressurization port located between the discs. The motor has been designed such that a liner may be attached to all of the internal motor surfaces if desired. The propellant slabs were positioned in the forward end of the box, allowing better developed flow conditions for both nozzles. Though the test apparatus may be attached to a surge tank, as illustrated in figure 1, to simulate various exhaust conditions, the motor was exhausted to the atmosphere (14.7 psia) in all the studies reported herein. Instrumentation consisted of light sensors, pressure transducers, recorders, and time-sequencing circuits.

Depressurization was accomplished by bursting the downstream disc of the double-disc assembly with a momentary overpressure in the chamber between the burst discs. This rupture resulted in a large pressure difference being developed across the upstream disc which burst the disc and opened the termination nozzle. If correctly sized, the combination of the two nozzles results in a depressurization rate sufficient to terminate combustion.

The testing cycle was a programmed operation. At time zero, t_0, the fire switch activated the recorder. After a short time delay, t_1, which assured that the recorder attained the proper chart speed, the igniter was initiated. Following another delay, t_2, which allowed sufficient time for the motor to reach steady-state conditions, the termination solenoid was activated, causing the overpressure of the downstream disc. The remaining delay, t_3, allowed sufficient time for the actual termination period before recorder shutdown.

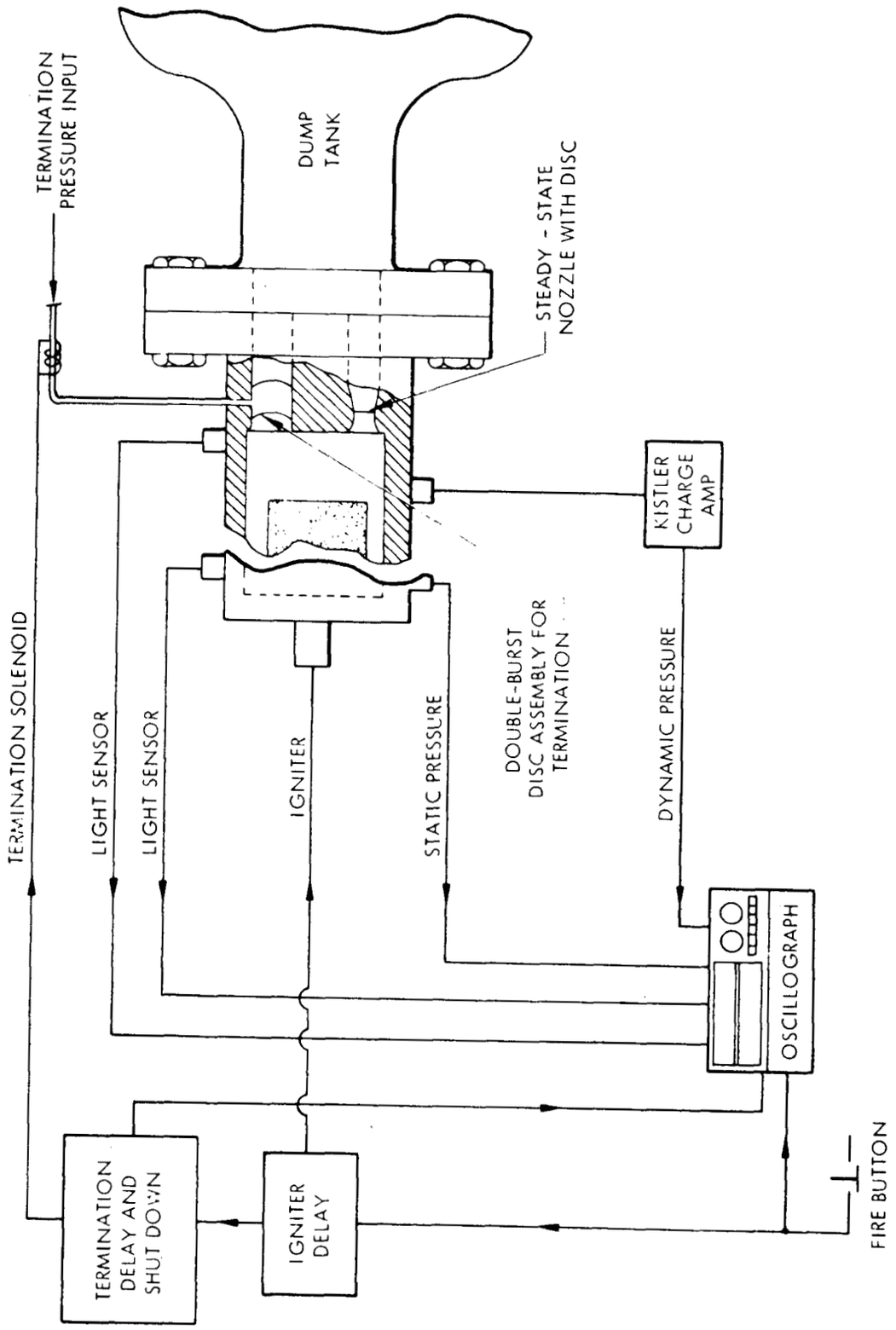

Figure 1. Schematic Diagram of Combustion Termination Apparatus

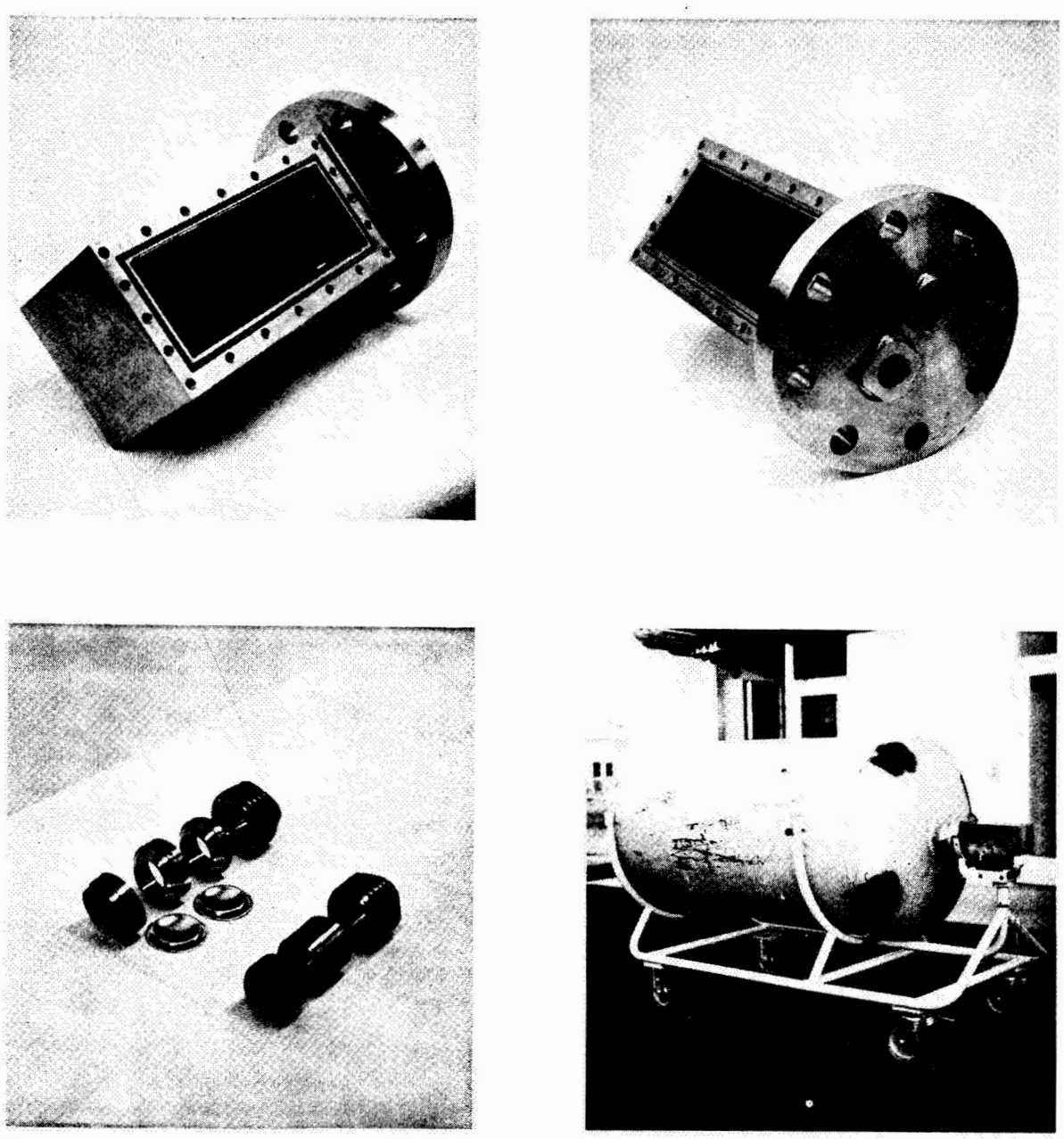

P-31770

Figure 2. Slab-Motor Systems

During the test cycle, two Texas Instrument LS-223 photovoltaic light sensors were used to monitor the propellant flame conditions and a 0 to 1000 psig strain gage transducer was used to follow the pressure transient. The motor has been used successfully at pressures up to 700 psia. Using the largest termination nozzle (0.99 in.) and reducing the motor volume by the addition of steel blocks, depressurization rates of -90 000 psi/sec can be obtained. This rate also represents the upper accuracy limits of the instrumentation system.

As a result of the programmed operation, a wide range of test conditions can be studied using one propellant grain in several tests. The time delays, t_1, t_2, and t_3, are all adjustable over reasonably wide ranges.

Window motor. - The window motor depicted in figures 3 and 4 has a dual-nozzle system with a steady-state nozzle on top of the motor and a depressurization nozzle at the end of the motor opposite the end-burning, solid propellant grain. High-pressure stainless steel tubing 3-in. OD by 2-in. ID was used for the body of the motor and the window tubes. Ladish high-pressure flanges were attached to the ends of the body with double welding. A safe operating pressure limit of 1200 psi with a 300 psi safety margin was provided by 1-in. thick by 3-in. diameter tempered Pyrex windows. Replacing the Pyrex windows with steel blanks provided a means of operating at pressures up to 2500 psi. The Pyrex windows have a clear diameter of 2.0 in. and were held in place with a 6-bolt flange and a Viton-A gasket assembly. Provision was made to provide nitrogen flushing of the windows should it become necessary during photographic studies.

As shown schematically in figure 3, the initial face of the end-burning grain was held to the left of the centerline of the window tubes. After the face was ignited, the grain regressed toward the centerline. Rapid depressurization and filming of the termination process can be programmed to begin when the grain face regresses to the centerline or to any any other convenient point. Programming was achieved by a timer system.

The propellant grains were ignited by mounting a patterned nichrome heating wire on the face of the grain, the leads being passed through the back end of the sample-holder. Combustion pressures were controlled by sizing the pyrolytic graphite steady-state nozzles mounted on top of the motor.

Depressurization of the motor was accomplished by puncturing a brass or Mylar burst disc mounted just aft of the termination nozzle. Both types of discs were burst by the firing console energizing the upper solenoid shown in figure 4, causing the spike to be driven into the diaphragm. Upon bursting of the diaphragm, the motor was exhausted through a stainless steel nozzle sized for the desired rate of depressurization. With throat diameters up to 2.0 in., depressurization rates as high as -1.2×10^6 psi/sec at 500 psi can be obtained.

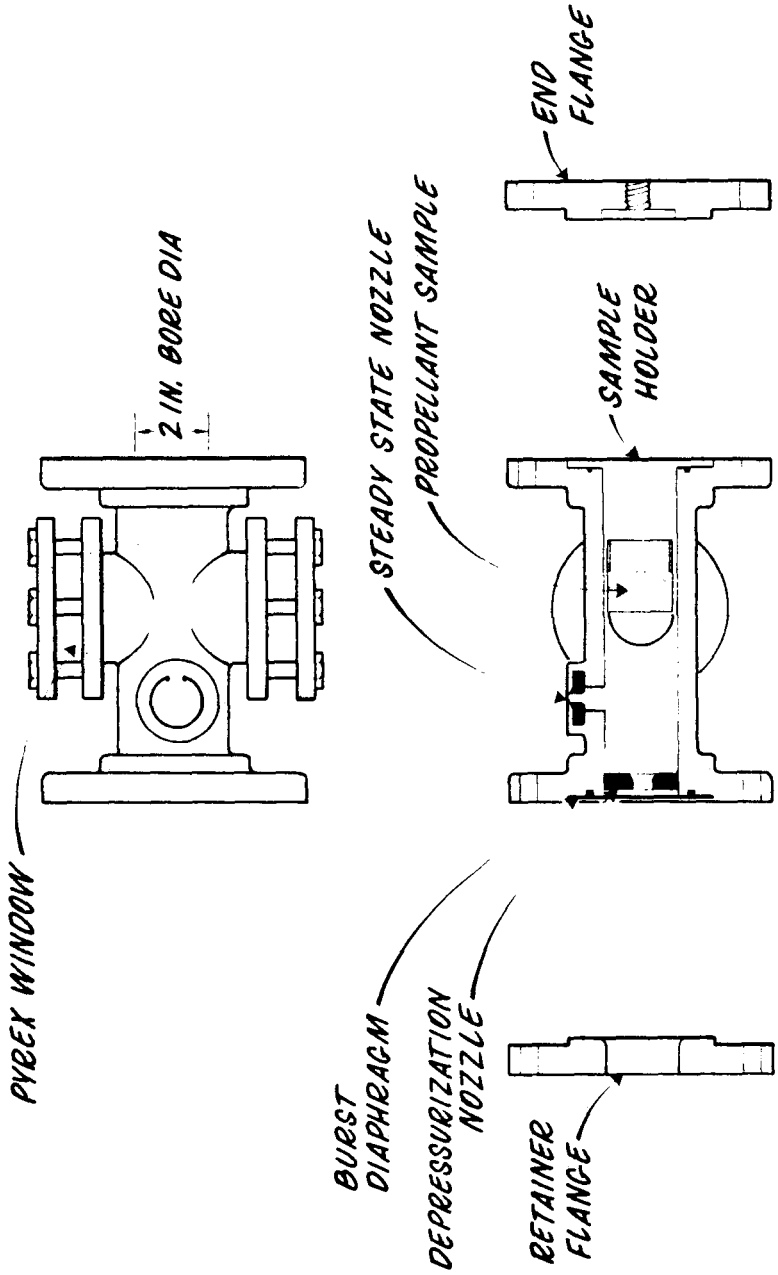

Figure 3. Schematic of L* Window Motor

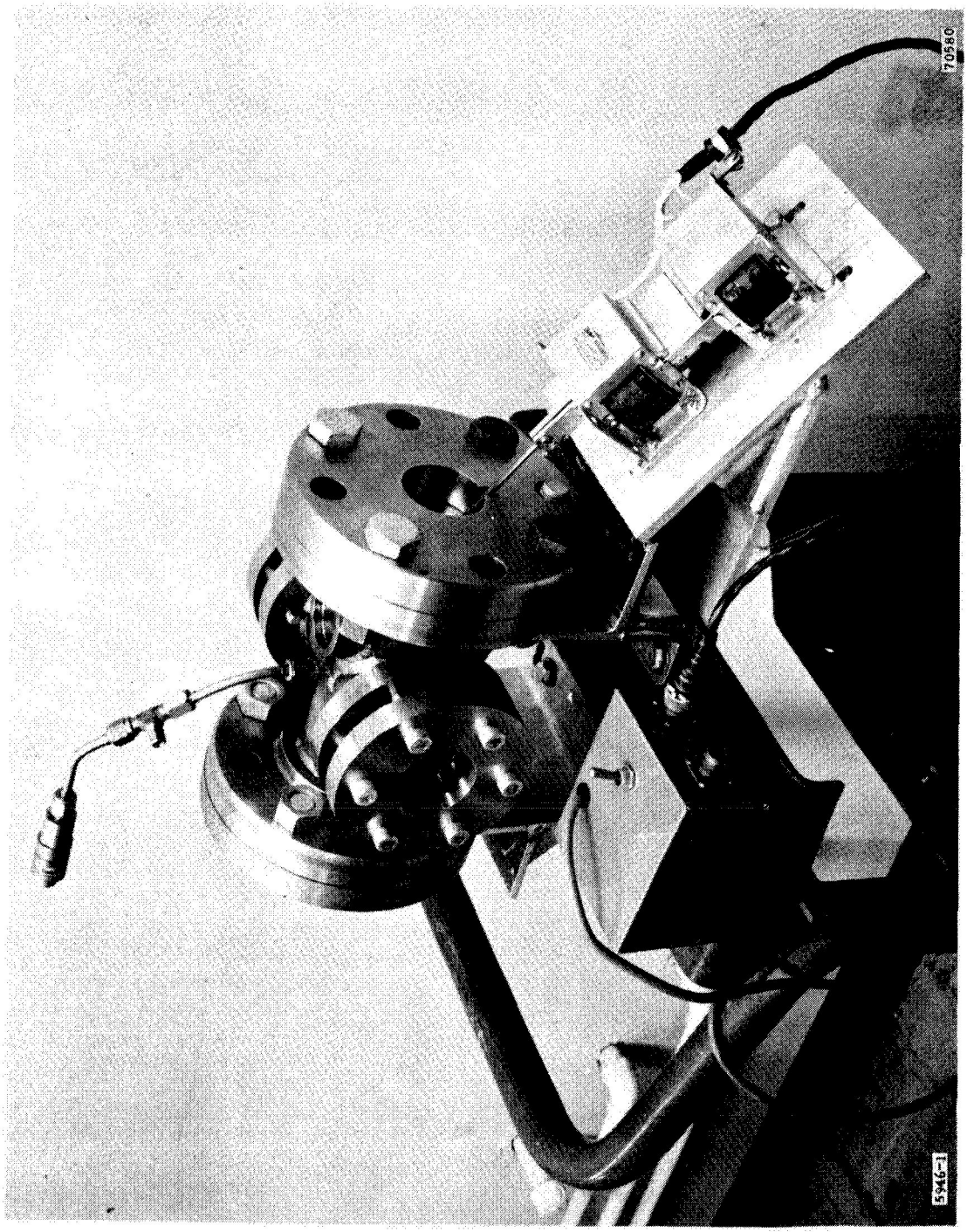

Figure 4. L* Window Motor

By plugging the upper steady-state nozzle and using the termination nozzle as a steady-state nozzle, L* tests were run in the same apparatus using cylindrical regressive-burning grains rather than neutral-burning end burners. For the L* tests, a 1000-liter vacuum chamber was attached to the test apparatus. Instrumentation for both L* and $\dot{P}$ tests consisted of two Texas Instrument LS-223 photovoltaic light sensors and strain-gage pressure transducers. Signals from these instruments were recorded on a Consolidated Electrodynamics Corporation 124 oscillograph at paper chart speeds of 64 in./sec.

Initially, the chamber pressure was measured using a 10 to 3000-psi Kistler quartz pressure transducer with a rise time of 3μsec. The electrical signal from the transducer charge amplifier was recorded on film using a Tetronix oscilloscope with a 5 msec/cm sweep speed. In order to catch the first portion of the depressurization transient, the scope signal was triggered by the signal used for energizing the depressurization solenoid. In order to achieve proper bursting, it was necessary to use discs which would self-burst at a pressure just above the desired operating pressure. Some discs would burst prematurely and the scope signal would not be triggered. Since comparison between the depressurization rates obtained using the strain-gage transducer system and the Kistler transducer system showed less than 5% difference for depressurization rates up to -35 000 psi/sec., the Kistler system was not used in later tests.

The bulk of the high-speed film tests were performed using a 500 frame/second 16 mm camera and the light system shown in figure 5. With the camera aligned approximately 30 degrees to the combusting face of the sample, filming was initiated immediately prior to ignition of the sample and stopped 500 to 1000 msec after chamber depressurization. An ASA 125 color film was used with a 1/2500 sec. shutter speed and an aperture stop of about 8.0, depending on the expected luminosity.

A limited number of tests were performed using a 2-sec. flashback lamp and a Red Lakes camera operating at 2000 frame/second. However, the intensity of the light was low and a shadowgraph-like picture resulted from the lack of a forelight. Since the results were not satisfactory, this system was not further developed.

Experimental Results

As discussed in the previous section, the 1-lb. slab motor was used for the $\dot{P}$ characterization while the window motor was used in the film studies as an aid to elucidating the mechanisms of combustion termination. As a consequence, the experimental findings of this study have been divided into two parts: "Experimental Studies," describing the results of the characterization studies, and "High-Speed Film Tests," describing the findings of the film studies. A discussion of the interrelation of these two portions of the program, the L* studies and interpretation of the results, is presented in the section entitled, "Discussion and Analysis."

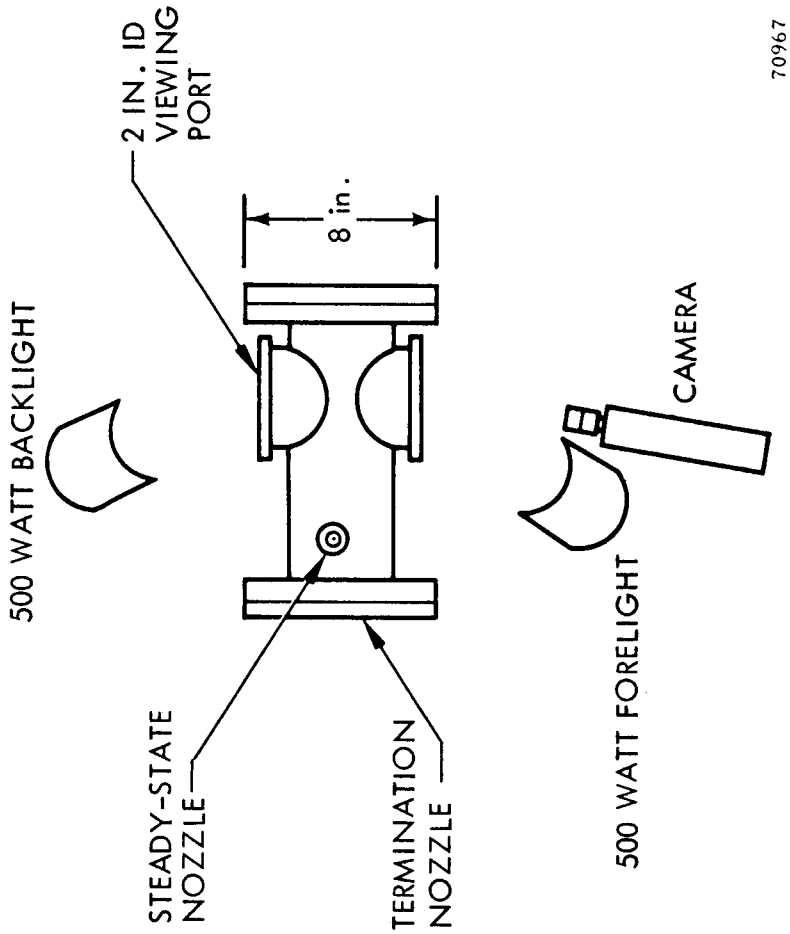

Figure 5. Schematic Top View of Window Motor and Camera System

Depressurization studies.- Six basic formulation variables were evaluated in the course of the program: (1) binder-polymer/curative system, (2) fuel or binder concentration, (3) AP particle size distribution, (4) AP particle coatings, (5) catalyst type and concentration, and (6) aluminum loading level. The formulation of these propellants and the experimental results are detailed in the following paragraphs.

Binder-curative studies: The basic propellants used for the study of polymer and curative system effects all contained 84% AP with a 70:30 coarse-to-fine ratio and were nonaluminized. As indicated in table I, the effect of binder-polymer structure upon combustion termination was studied using five basic polymer systems: PBAN, CTPB, UTREZ, PU, and PEP. Aziridinyl (MAPO), epoxy and aziridinyl/epoxide curative agents were used for formulation of the PBAN, CTPB, UTREZ, and PEP binder systems, while the PU propellant was formulated with an isocyanate cure system. With the exception of the PEP propellant, all propellants were plasticized with dioctyl adipate.

TABLE I. - BINDER FORMULATION STUDIES

Propellant UTX-	Binder	Curing agent(s)	Binder equivalents/ Curing agent equivalents
9394	CTPB	Epoxy/Aziridinyl(MAPO	1.0:4:0.9
9377	PBAN	Epoxy	0.5: (1.3:5)[a]
9711	PBAN	Aziridinyl	1.0:1.2
9389	PU	Isocyanate	0.4:1.0
9379	UTREZ	Aziridinyl	1.0:1.2
9710	UTREZ	Aziridinyl	1.0:1.5
9712	UTREZ	Aziridinyl/Epoxy	1.0:1.0/0.3
9395	PEP	Aziridinyl	1.0:1.5
9775	CTPB	Epoxy	0.8 (1.3:2)

[a] 1.3 equivalents of epoxy resin, 0.5 equivalents epoxy crosslinking agent.

In an effort to maintain propellant uniformity from batch to batch, large single lots of each of the binders were used during the course of the program to reduce variations in binder properties. Differences caused by AP variations are not as easily controlled. The use of one lot of oxidizer does not provide adequate control because of the natural agglomeration of the oxidizer crystals during a 1-year program. However, an attempt was made to minimize agglomeration in the large lot by repackaging the material in smaller 20-lb lots, using plastic bags with a dessicant in each bag. However, in spite of this precaution, during the second quarter of performance it was found that the finely ground AP was agglomerating severely. The stored fines were then discarded and the remainder of the

propellants formulated with freshly-ground fine AP and the stored large-particle AP which showed little agglomeration during the course of the program. Screen-analysis data of the coarse and fine AP are listed in table II. Screening of the ground (or fine) AP showed 10% of the material to be less than 3μ in diameter, 50% to be less than 6.3μ in diameter, and 90% to be less than 10.4μ in diameter.

TABLE II. - COARSE AP SCREEN ANALYSIS

Sieve no. (Tyler)		Percent cumulative retained	
		Minimum	Maximum
16	(1000μ)	0	0
48	(297μ)	4	12
65	(210μ)	30	50
100	(149μ)	62	80
200	(74μ)	95	99
325	(44μ)	98	100

Mean particle diameter - 190μ

The measured strand-burning rates of the propellants listed in table I are presented in figure 6. Within the pressure limits of the rapid-depressurization tests (0 to 1000 psi), the PEP propellant (UTX-9395) had the highest burning rate, burning at the rate of 0.355 in./sec at 1000 psig with a burning rate exponent, n, of 0.25. The two PBAN propellants had the highest burning rate exponents ($n \simeq 0.4$) and had nearly identical burning rate characteristics. The slowest burning propellants were those formulated with UTREZ. These propellants did not burn in strand form at 1000 psi; however, nearly identical UTREZ formulations have been successfully fired in micromotors at pressures up to 2500 psi. A measure of the effect of batch-to-batch formulation differences upon burning rate can be obtained from the CTPB strand data plotted in figure 6. The open and closed circles represent burning rates for two batches of propellant mixed several weeks apart. While slight differences in burning rate can be noted, these differences are less than the experimental differences for different strands from any one batch.

Qualitative physical differences between the tested propellants were noted. The PU propellant exhibited poor interfacial bonding between the fuel and AP crystals. Cutting or machining of the propellants, or even handling of cut surfaces, resulted in significant loss of AP from the surface. The other propellants did not exhibit these characteristics; however, the propellant formulated with CTPB (UTX-9394) had a more plastic consistency, while the UTREZ (UTX-9710) formulated with 1.5 equivalents of the aziridinyl curative was an extremely hard propellant. In the latter case, samples for the window-motor studies were machined to size, rather than cut in the normal manner.

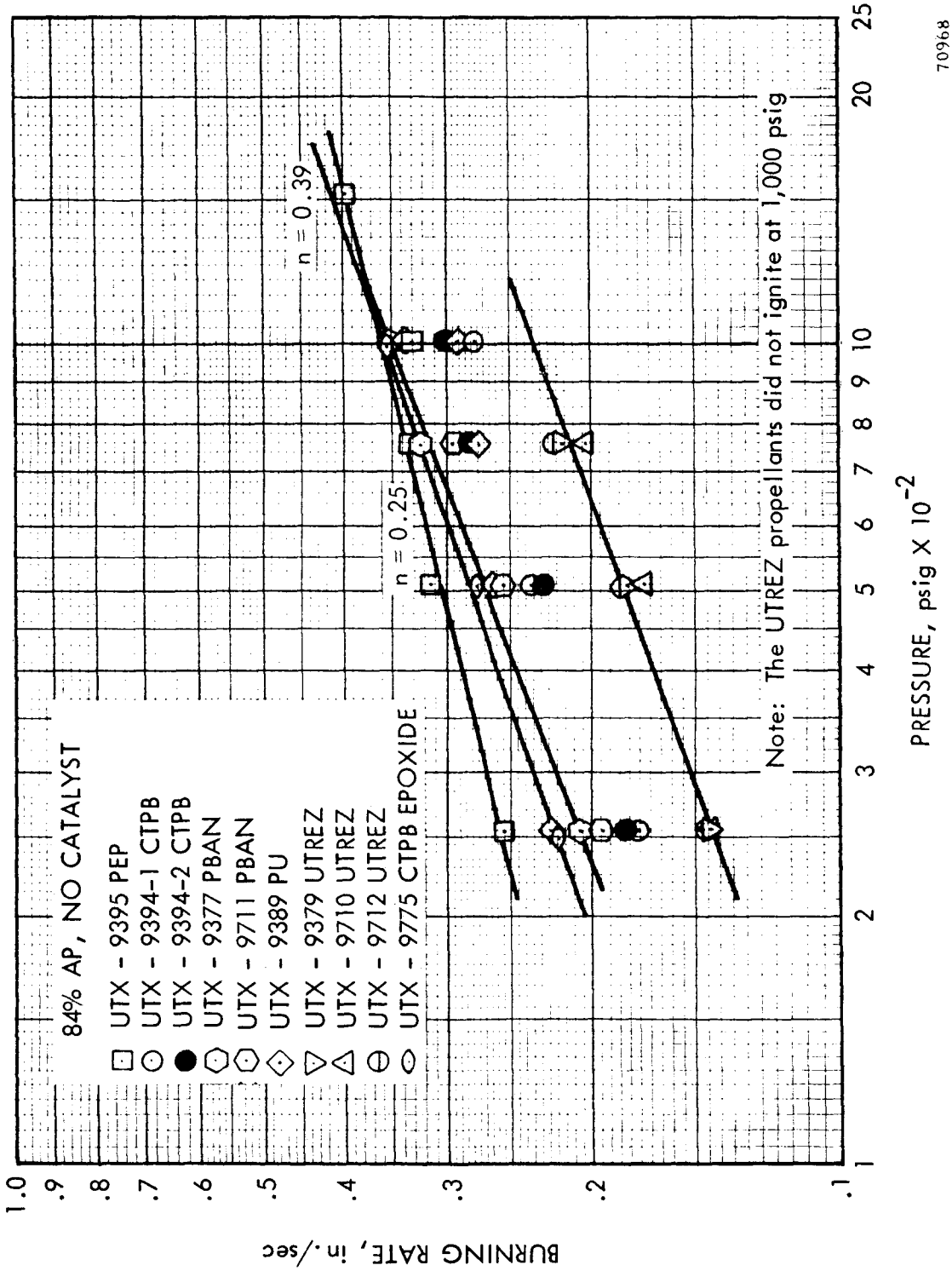

709648

Figure 6. Strand Burning Rates of Nonaluminized Propellants

Individual rapid depressurization data were obtained for all nine propellants. For reporting purposes, the maximum rate of chamber depressurization (initial rate of depressurization) has been plotted versus the chamber pressure at initiation of chamber venting. These data can be plotted on alternate bases and additional parameters (i.e., ambient pressure level, motor geometry, and depressurization path) rather than chamber pressure and rate of depressurization can be utilized to define the absolute combustion termination limits. However, for purposes of discrimination between formulation differences, the representation used here is considered sufficient.

The effect of normal batch-to-batch formulation differences upon the termination characteristics of the CTPB propellant (UTX-9394) is shown in figure 7. The lines shown in figure 7 and in subsequent figures are the best line separating the zone of combustion termination from the zone of reignition or nontermination of combustion. The flagged points represent data obtained using a propellant batch formulated several weeks after formulation of the original batch. In this instance, there is possibly some difference between the results obtained using the two batches, although these differences are of the same order as the uncertainties in determining the rate of depressurization. Similar batch differences effects are shown in figure 8 for the PBAN propellant UTX-9377. In this case, there is even less divergence at low pressures, but at higher pressures, the data are completely incongruous. The second batch of PBAN propellant required considerably higher depressurization rates for successful termination at chamber pressures of 200 psi and above. Further investigation revealed that the second batch of propellant had been formulated with AP fines which had agglomerated. It was also noted that the data obtained with the first propellant batch are completely in agreement with data obtained on an in-house project using a similar PBAN propellant. Though other factors may have caused this inconsistency, it was felt that the agglomeration of the AP apparently altered the combustion termination characteristics of the second batch. In order to explore this possibility further, a third batch of propellant, using unagglomerated crystals, was evaluated. These data were found to coincide with those for the second or agglomerated batch of propellant. Results obtained with a fourth batch of propellant, formulated several months later, are shown in figure 9. These data, although quantitatively different from the first results, do tend to support the original results. The causes for these differences are open to speculation. For comparison purposes, the data of figure 9 are used since they represent a mean of the various test results.

The binder-polymer structure was found to have major influence upon the termination characteristics of the tested propellants. As evidenced in figures 7 through 12, the PEP and CTPB propellants were the most difficult propellants to terminate and had nearly identical termination characteristics. The epoxy-cured PBAN propellant was only slightly less difficult than the PEP and CTPB propellants, but was more difficult to extinguish than the UTREZ and PU grains which had similar characteristics. These differences can best be seen in figure 13 where the different critical limit lines are compared. Interpretation of these results is presented in the section entitled, "Discussion and Analysis."

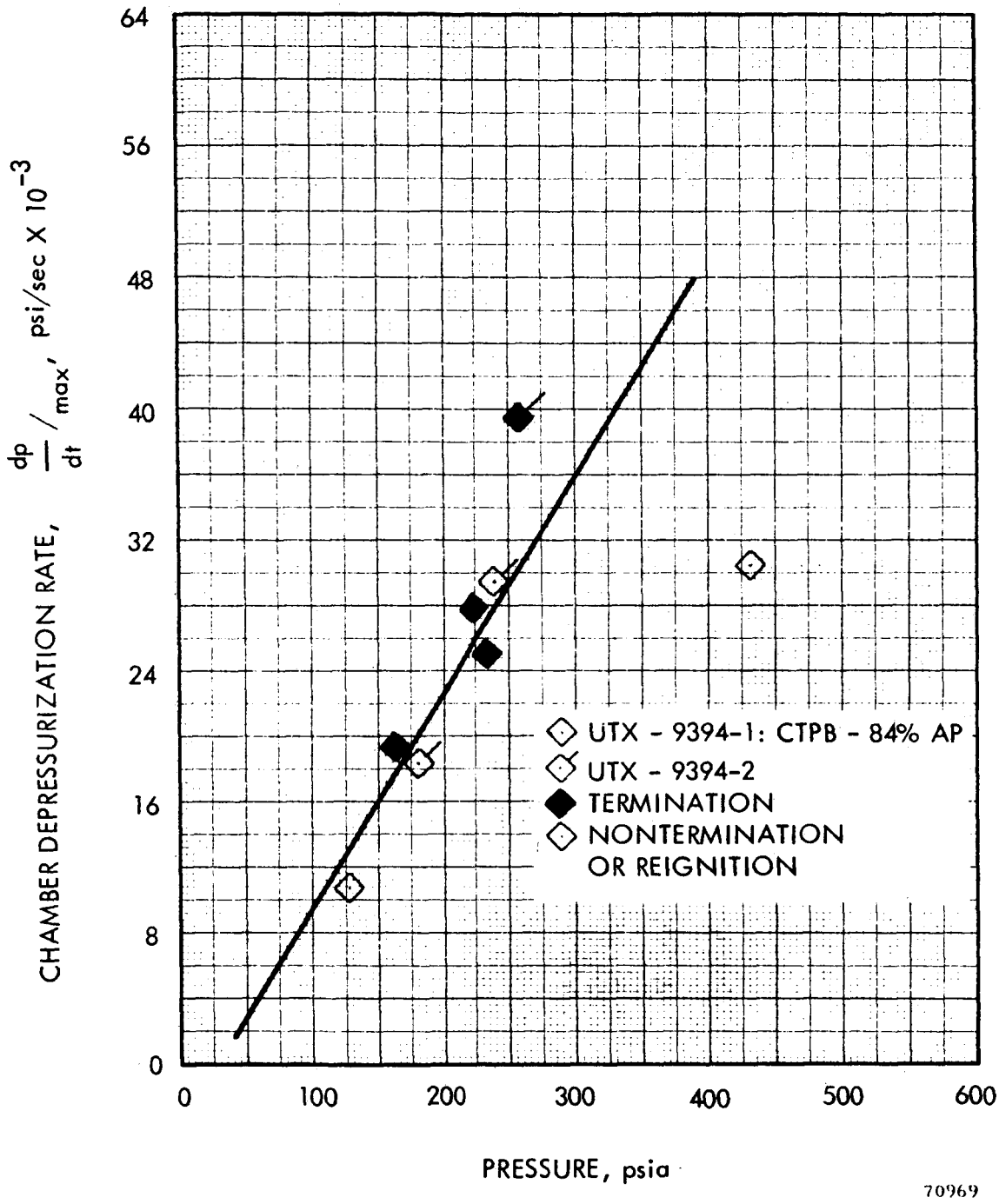

Figure 7. $\dot{P}$ Characteristics of UTX-9394: CTPB - 84% AP

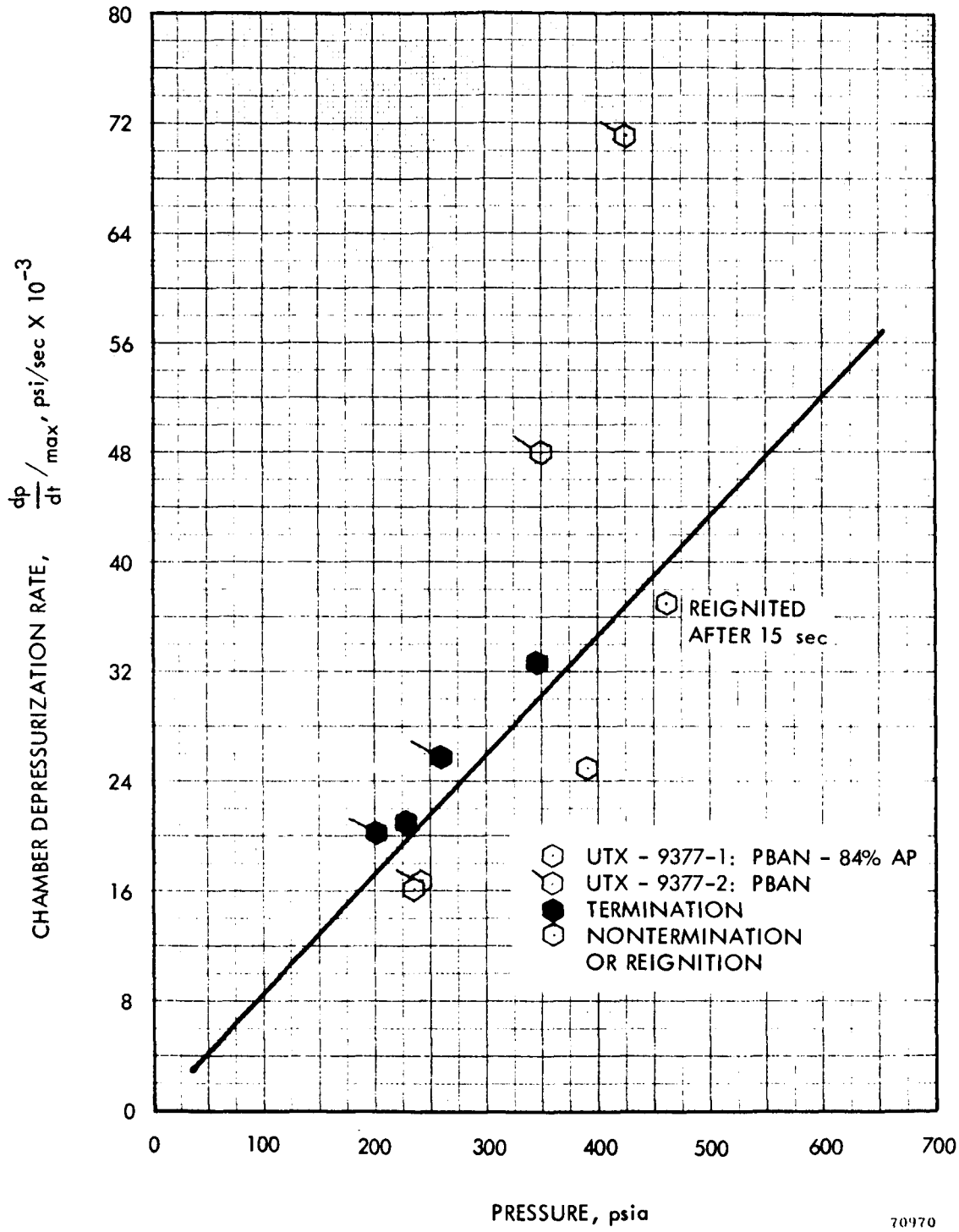

Figure 8. $\dot{P}$ Characteristics of UTX-9377: PBAN - 84% AP

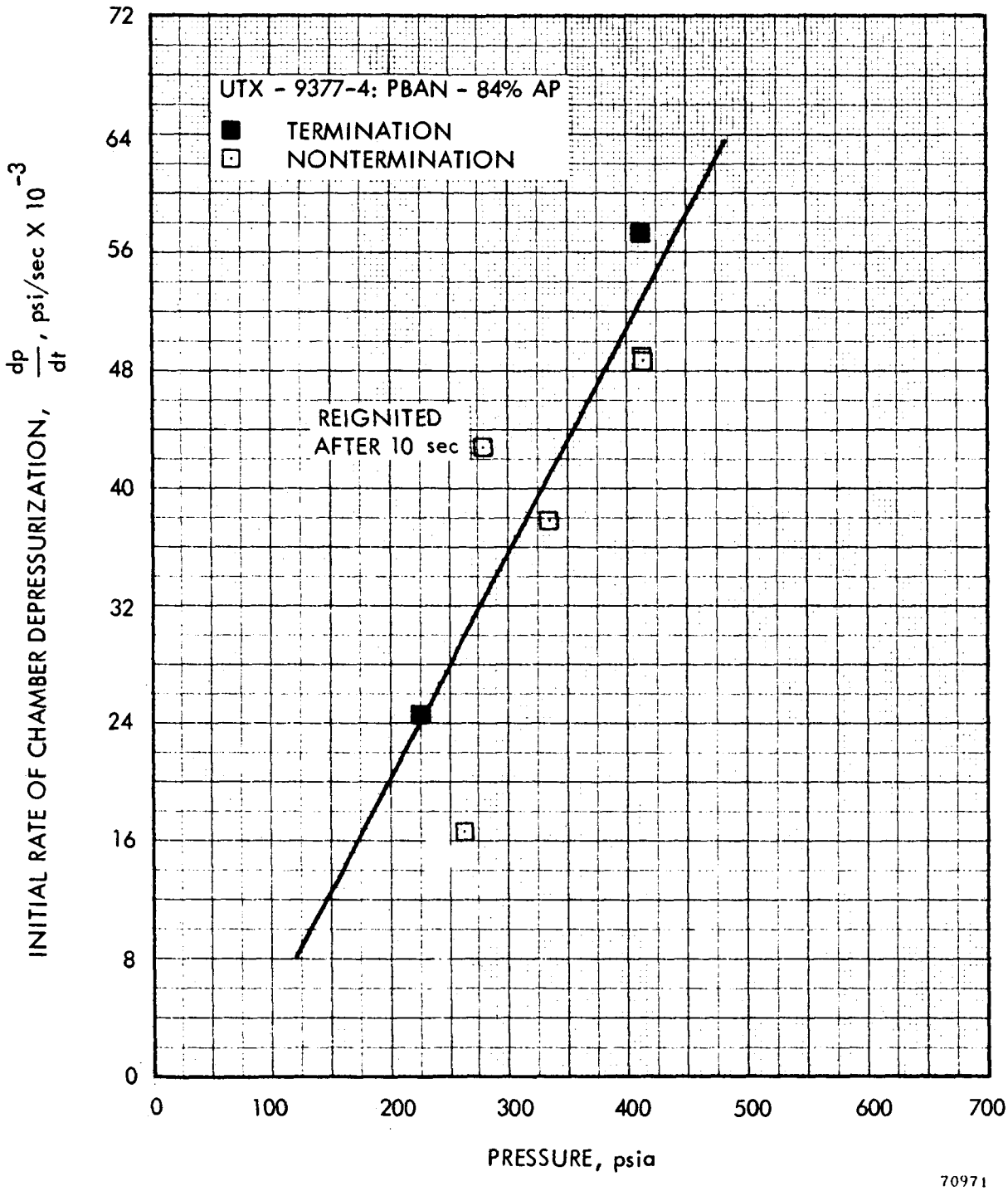

Figure 9. $\dot{P}$ Characteristics of UTX-9377-4: PBAN - 84% AP

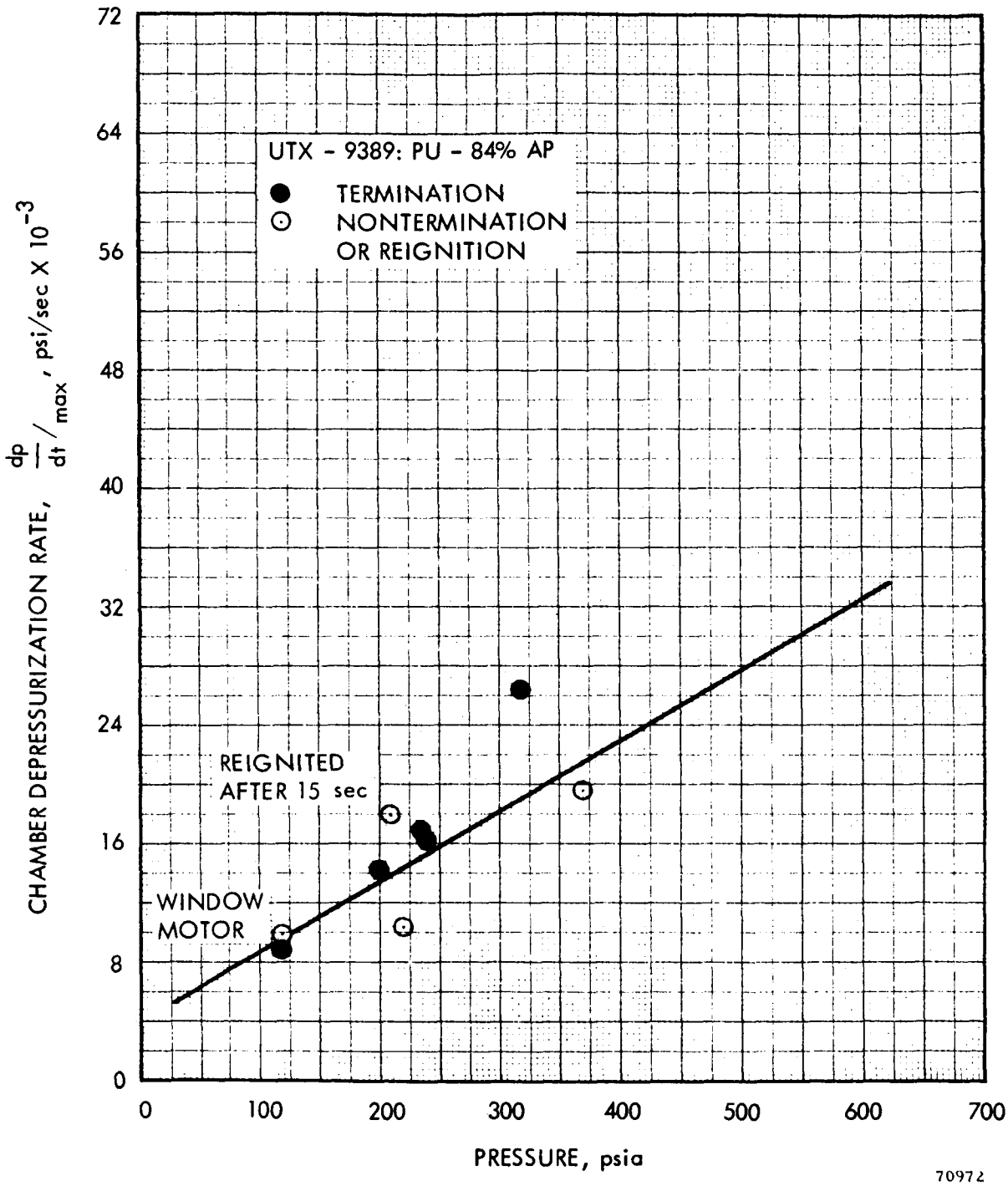

Figure 10. $\dot{P}$ Characteristics of UTX-9389: PU - 84% AP

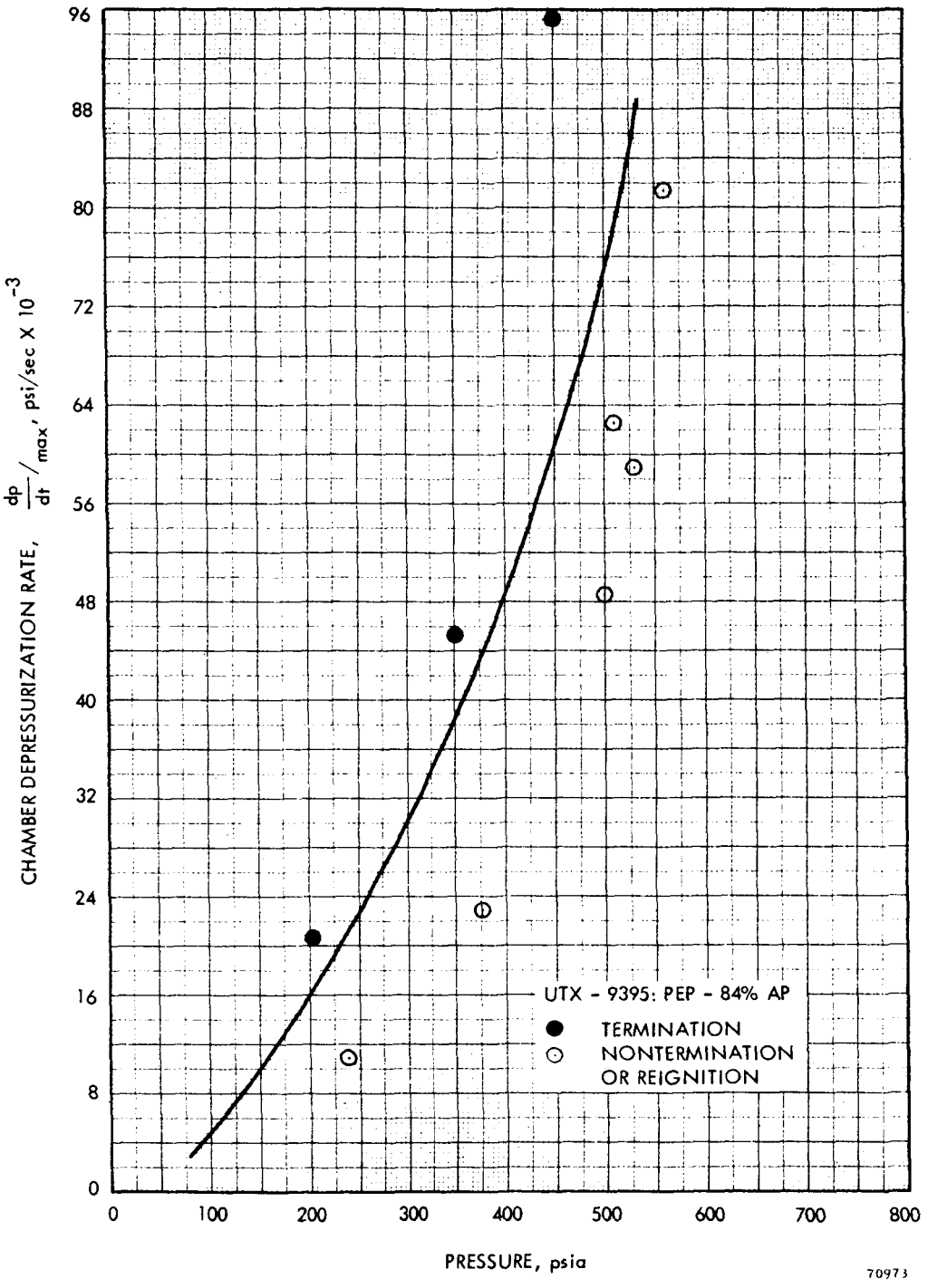

Figure 11. $\dot{P}$ Characteristics of UTX-9395: PEP - 84% AP

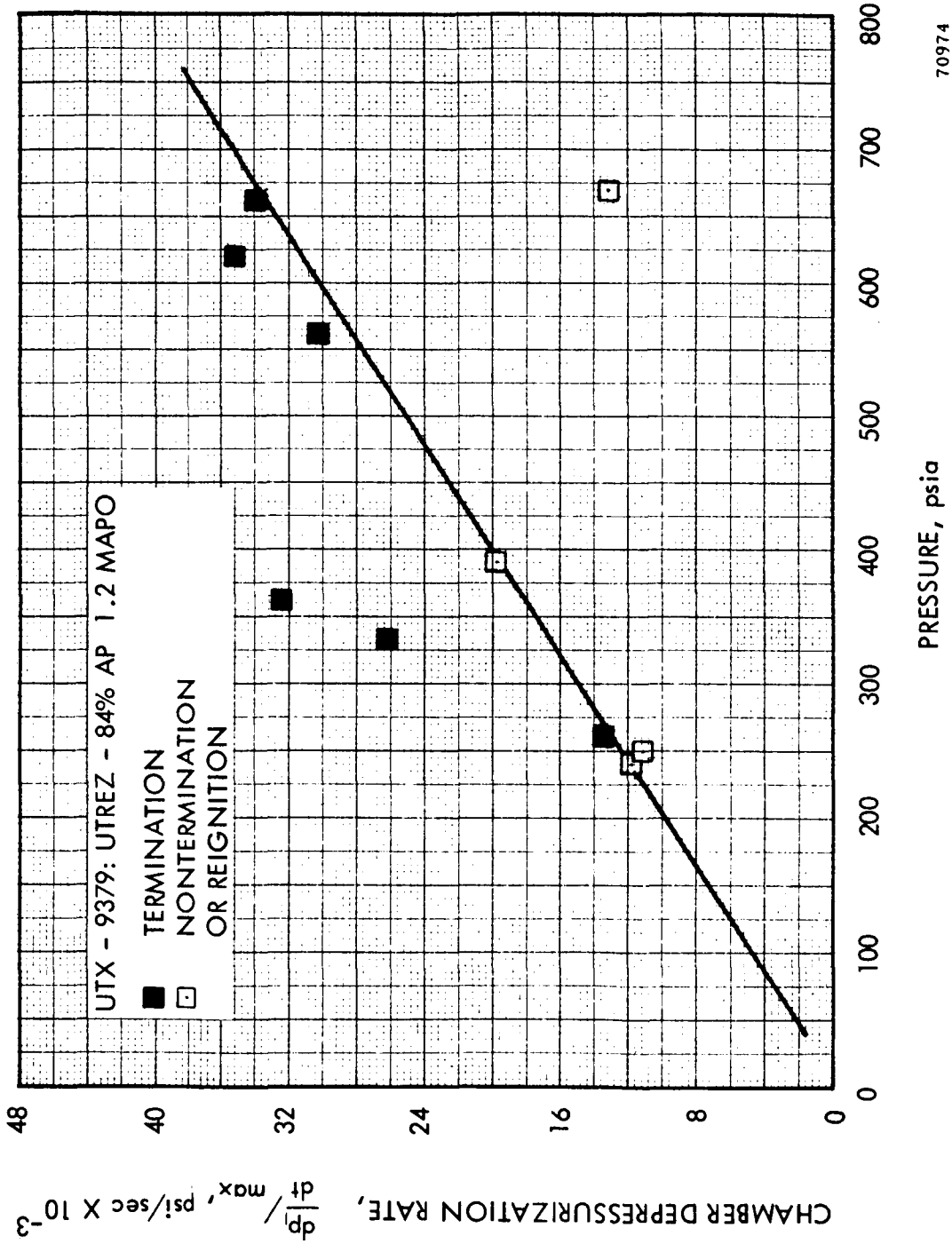

Figure 12. $\dot{P}$ Characteristics of UTX-9379
UTREZ - 84% AP

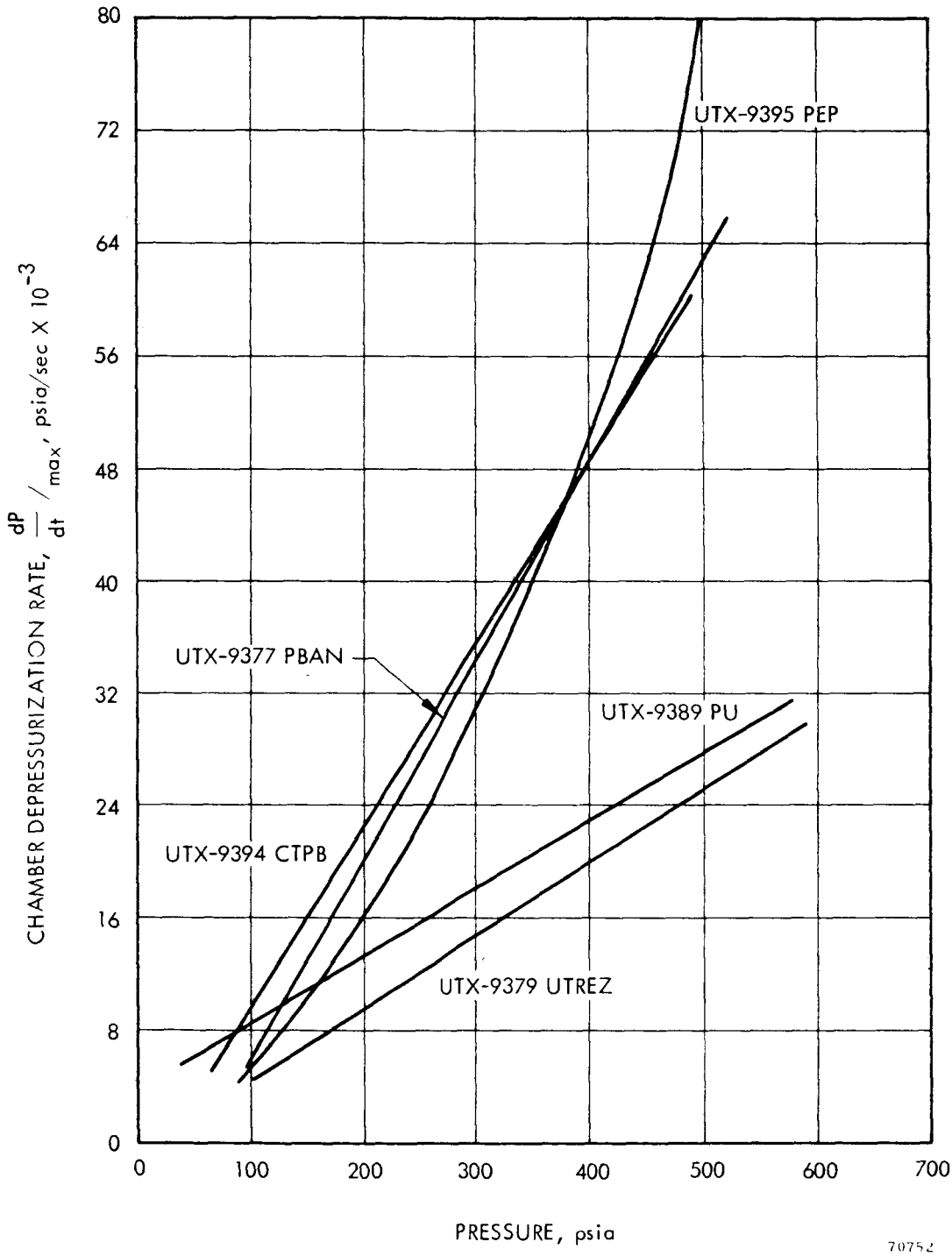

Figure 13. Comparison of Critical Depressurization Limit Lines as a Function of Binder System — 84% AP

The effect of curative type and polymer-to-curative equivalence ratio was explored using UTREZ, PBAN, and CTPB polymers. As evidenced in figure 14, an increase in the aziridinyl to UTREZ equivalence ratio from 1.2 to 1.5 resulted in a slight increase in termination requirements. However, the increase of aziridinyl produced an extremely hard propellant which had to be machined rather than cut. Figure 15 presents data obtained using a third UTREZ propellant, UTX-9712, formulated with 1.0 equivalents of aziridinyl and 0.3 equivalents of epoxide. This propellant has the same characteristics as UTX-9379 containing 1.2 aziridinyl equivalents. The mechanical properties of UTX-9712 are compared with those of the hard UTX-9710 in figure 16. Increasing the crosslinking density increased the modulus by a factor of two for the strain rates used in the evaluations (0.7 sec^{-1}). On the basis of this information, it was concluded that for saturated polymers, bulk mechanical property differences resulting from increased crosslinking have little effect on termination behavior.

As shown in figure 17, UTX-9711 containing PBAN formulated with the aziridinyl curative has significantly higher termination requirements than the previously tested epoxide-cured PBAN propellant. At the higher pressure levels, the termination characteristics of the UTX-9711 exceed the capabilities of the slab motor. However, as in the case of the anomalous results obtained with the two batches of UTX-9377, this increase may result from uncontrolled minor formulation differences rather than differences in curative systems. A reverse effect was found for the CTPB propellants. As shown in figure 18, the completely epoxy-cured CTPB propellant, UTC-9775, could not be terminated in the slab motor although the reference MAPO/epoxy-cured propellant could be. It was not determined if the increase in termination limits was significant since the reference CTPB MAPO/epoxy propellant requires rates near the upper limit of the apparatus. Thus, on the basis of the contradictory evidence obtained with the two basically similar polybutadiene binder systems, no conclusions can be made concerning the effect of curative system.

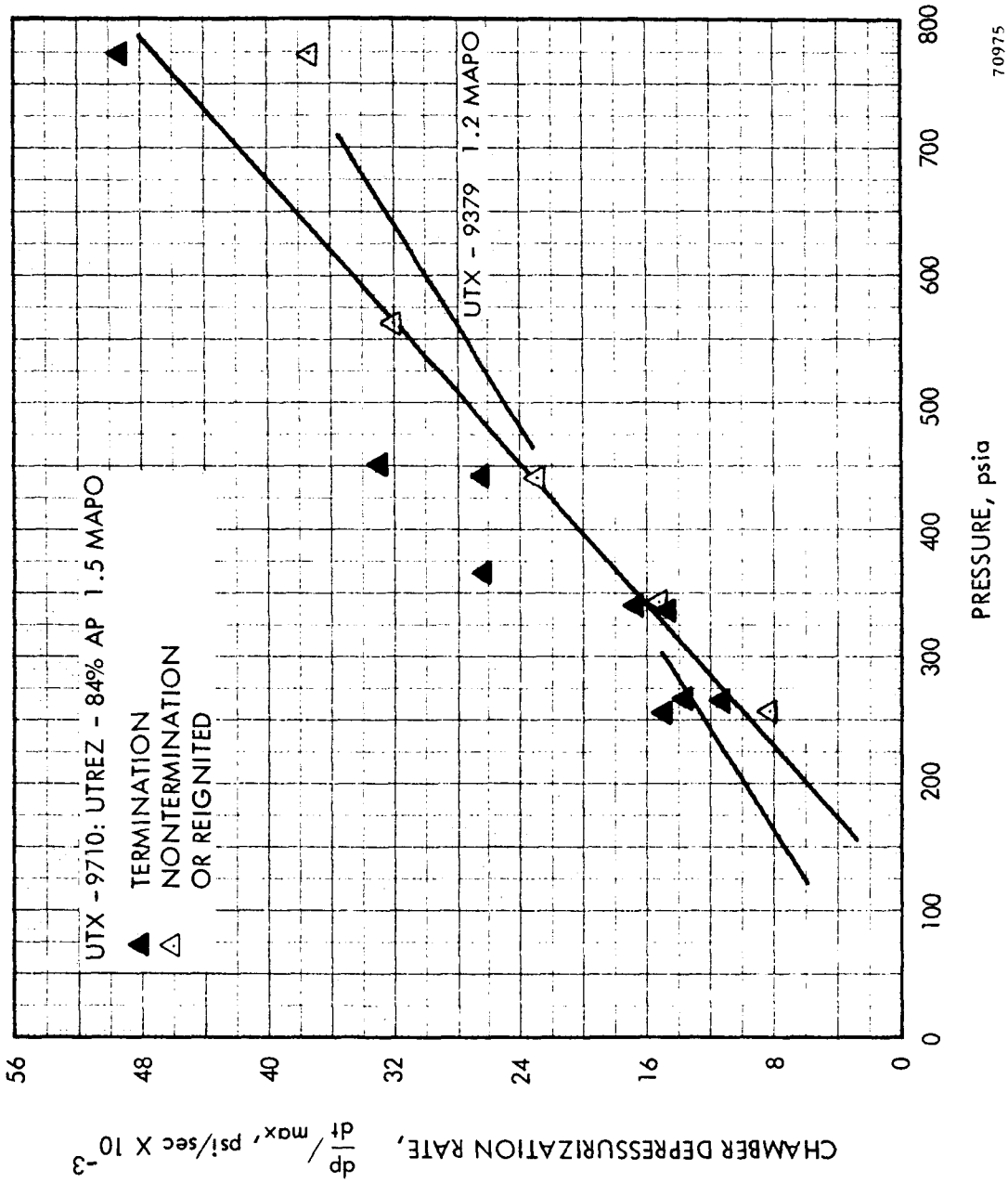

Figure 14. $\dot{P}$ Characteristics of UTX-9710: UTREZ/1.5 MAPO - 84% AP

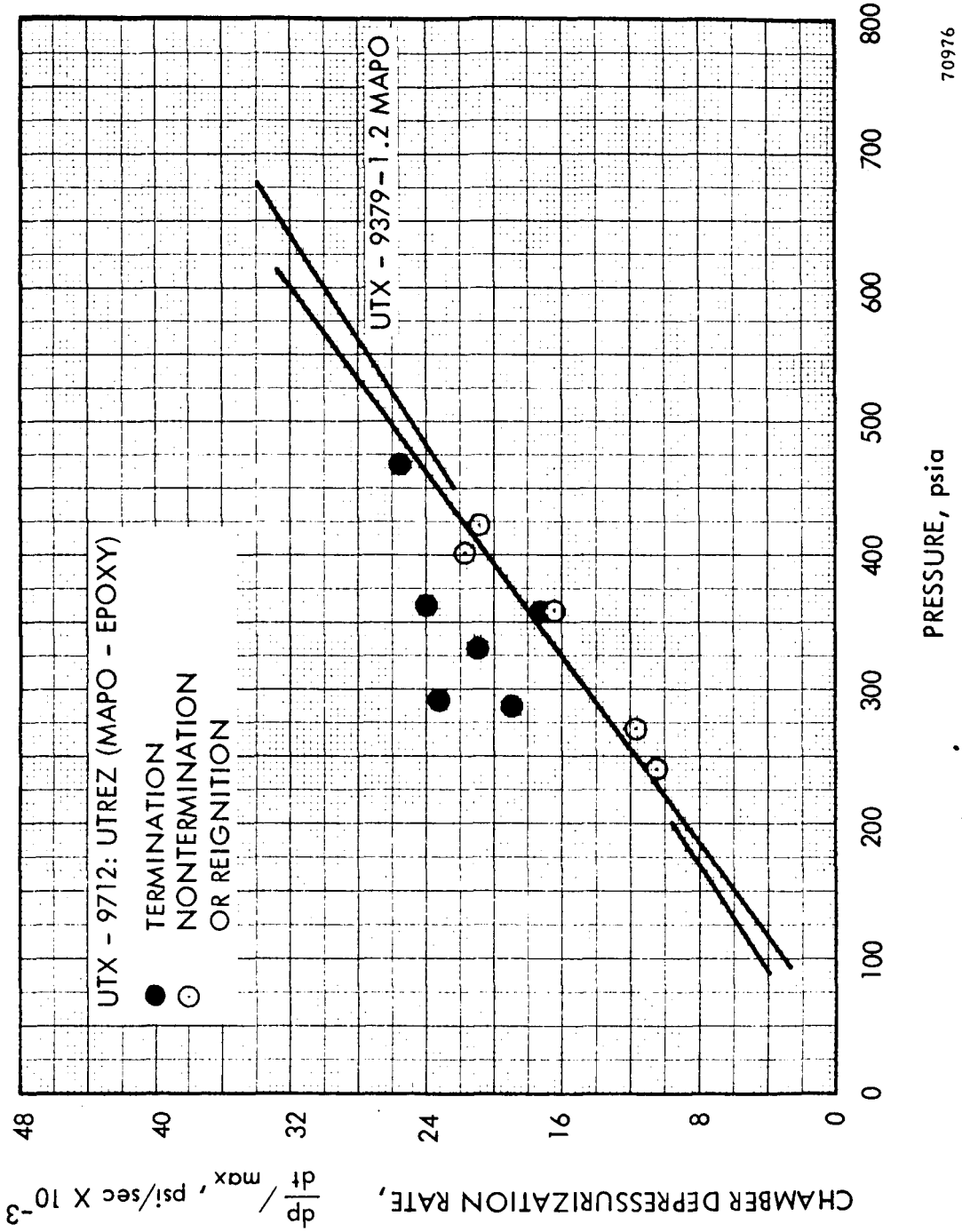

Figure 15. $\dot{P}$ Characteristics of UTX-9712: UTREZ/MAPO/EPOXY - 84% AP

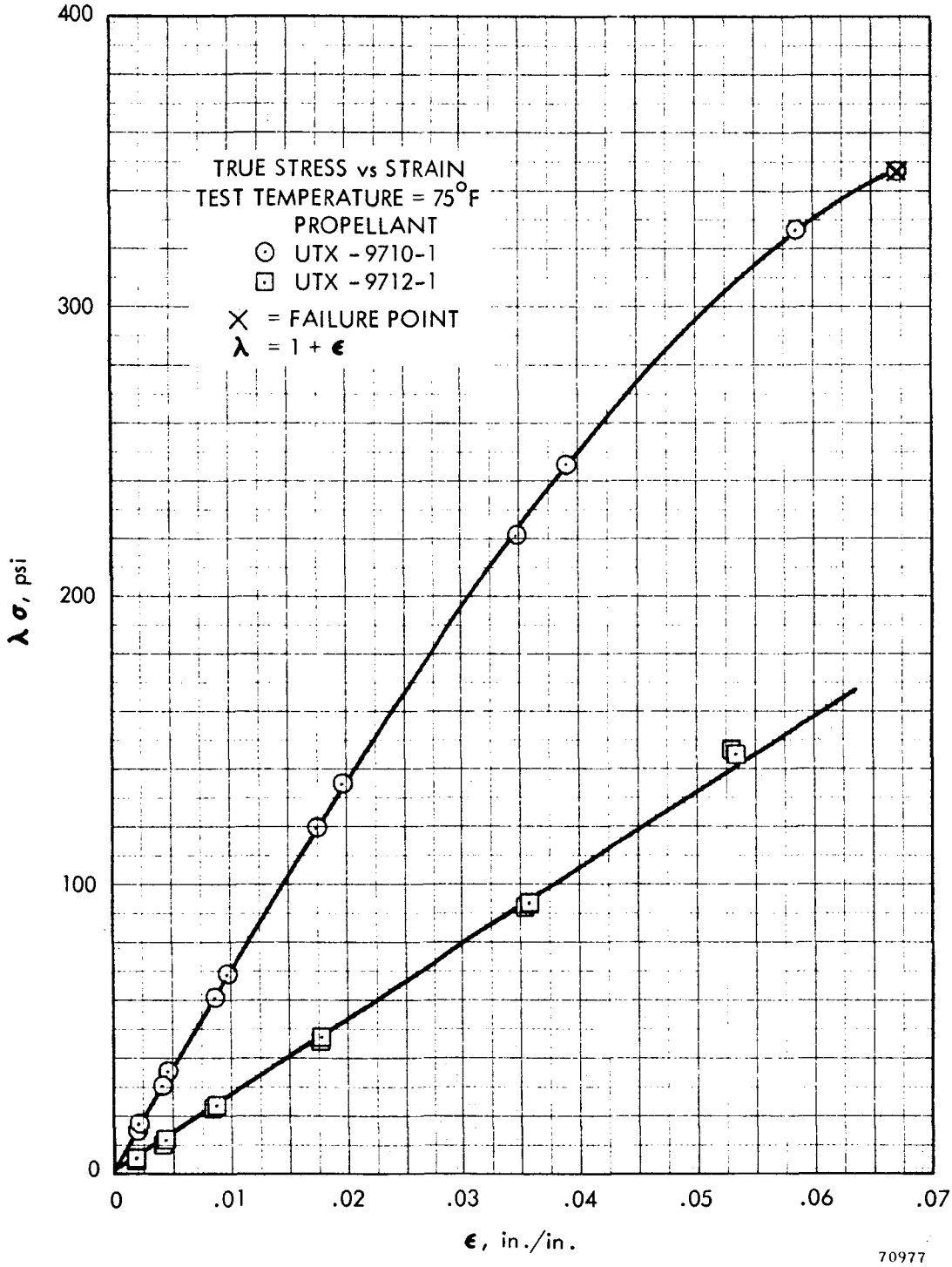

Figure 16. Stress vs Strain Behavior of UTREZ Propellants

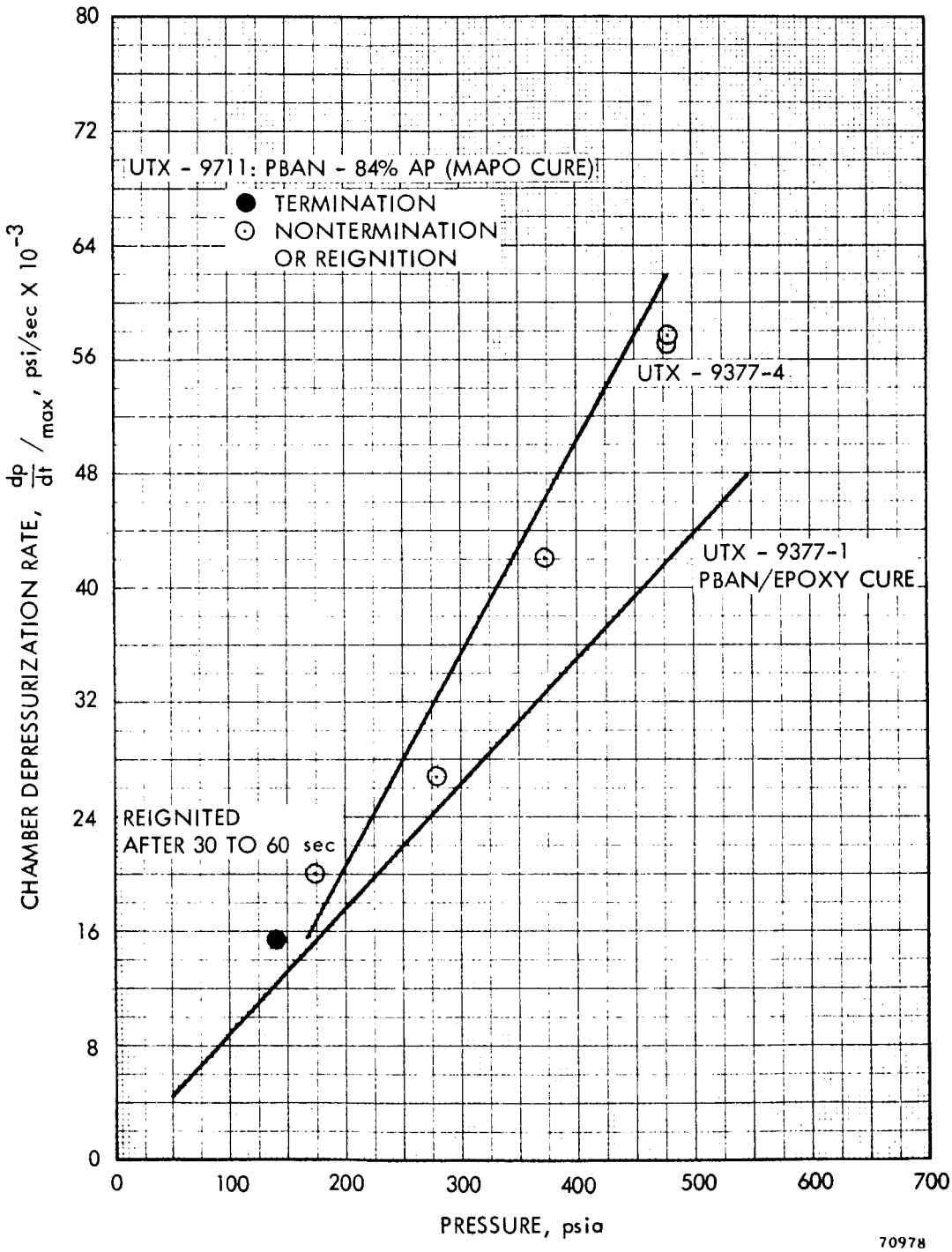

Figure 17. $\dot{P}$ Characteristics of UTX-9711: PBAN/MAPO - 84% AP

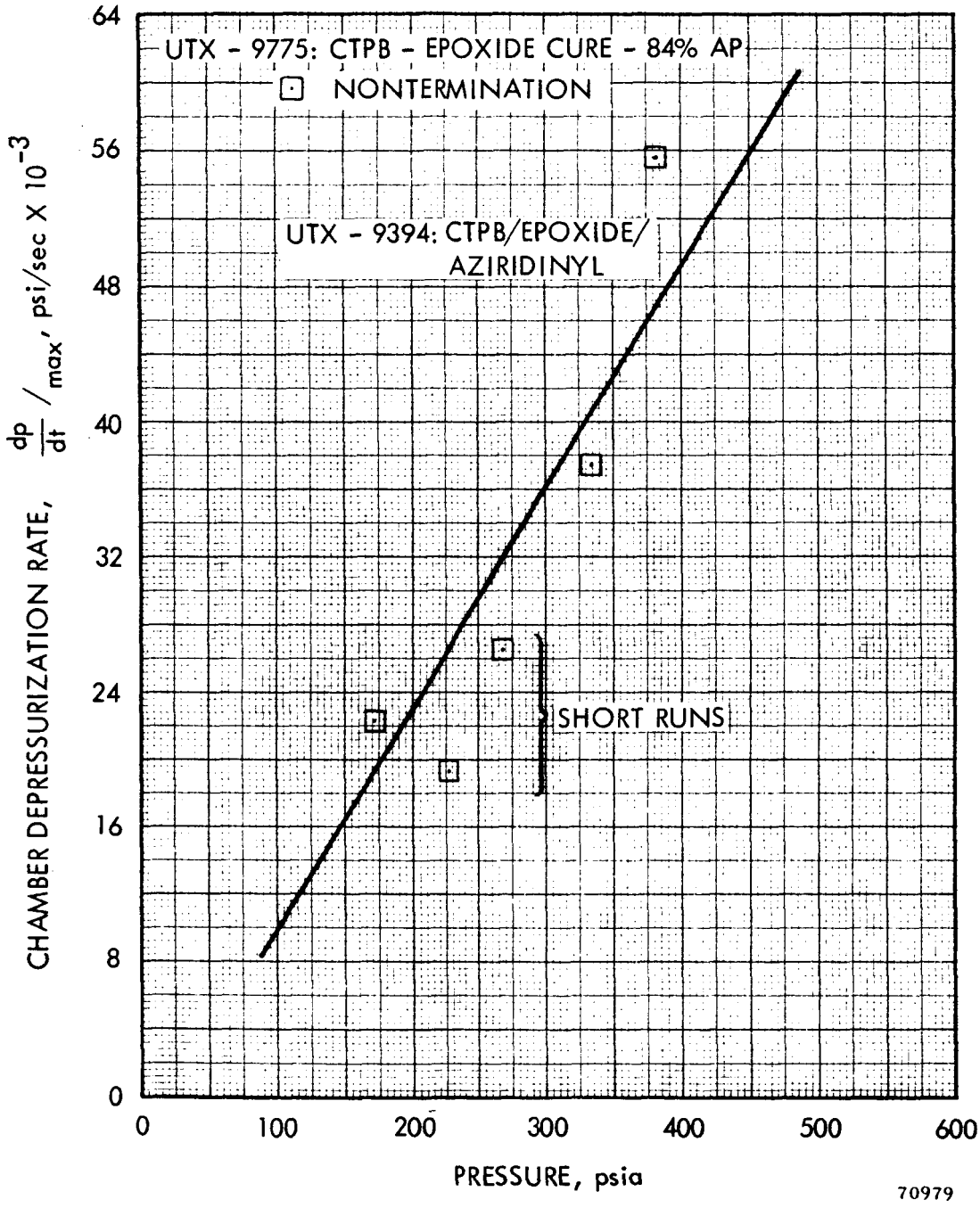

Figure 18. $\dot{P}$ Characteristics of UTX-9775: CTPB/EPOXY - 84% AP

Additive effects: The first three propellants listed in table III were used to study oxidizer (or fuel) loading level, while the other propellants were tested to establish the effect of catalysts, AP particle size and coating, and aluminum addition. These propellants were all formulated with the saturated polymer UTREZ, AP with an 80:30 coarse-to-fine ratio, and an aziridinyl curative (MAPO). UTREZ was chosen for these tests for several reasons. The polymer is a well-defined pure polymer in contrast to such polymers as PBAN or PBAA. It does not present the functionality problems of CTPB and, as far as is known, these tests constitute the first characterization of a chemically saturated binder. Finally, the previously discussed studies with UTX-9379 demonstrated that UTREZ propellants are relatively easily terminated and thus may have application for future controllable solid rocket motors. Strand burning rate data for these propellants, including the reference propellant UTX-9379, are presented in figures 19 and 20.

TABLE III. - COMPOSITIONS OF UTREZ PROPELLANTS

Propellant UTX-	Percent Oxidizer loading (AP)	Additives
9379[a]	84.00	None
9713	80.00	None
9714	76.00	None
9715	83.75	0.25% Iron Oxide
9717	83.50	0.50% Iron Oxide
9718	83.75	0.25% Copper Chromite
9719	83.50	0.50% Copper Chromite
9720	83.87	0.13% Copper Chromite
9754	84.00 (400μ large-diameter AP, 70:30 coarse-to-fine)	None
9757	80.00	Large-particle AP coated with 1.5% Kel-F
9755	80.00	4% H-322 aluminum
9756	76.00	8% H-322 aluminum
9757	68.00	16% H-322 aluminum
9772	68.00	12% H-322 aluminum, 4% aluminum needles

[a] Reference propellant.

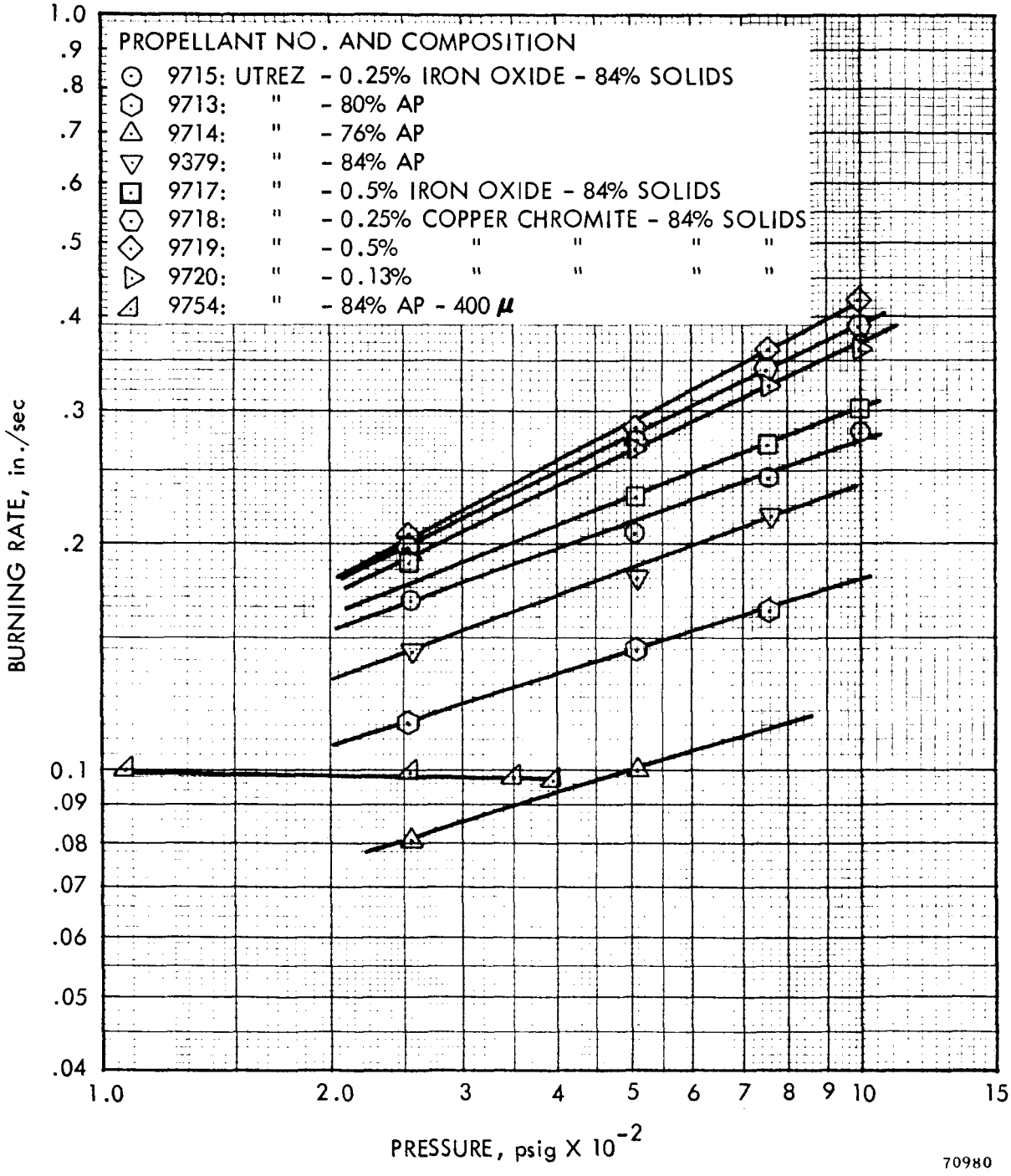

Figure 19. Strand Burning Rate of UTREZ Propellants

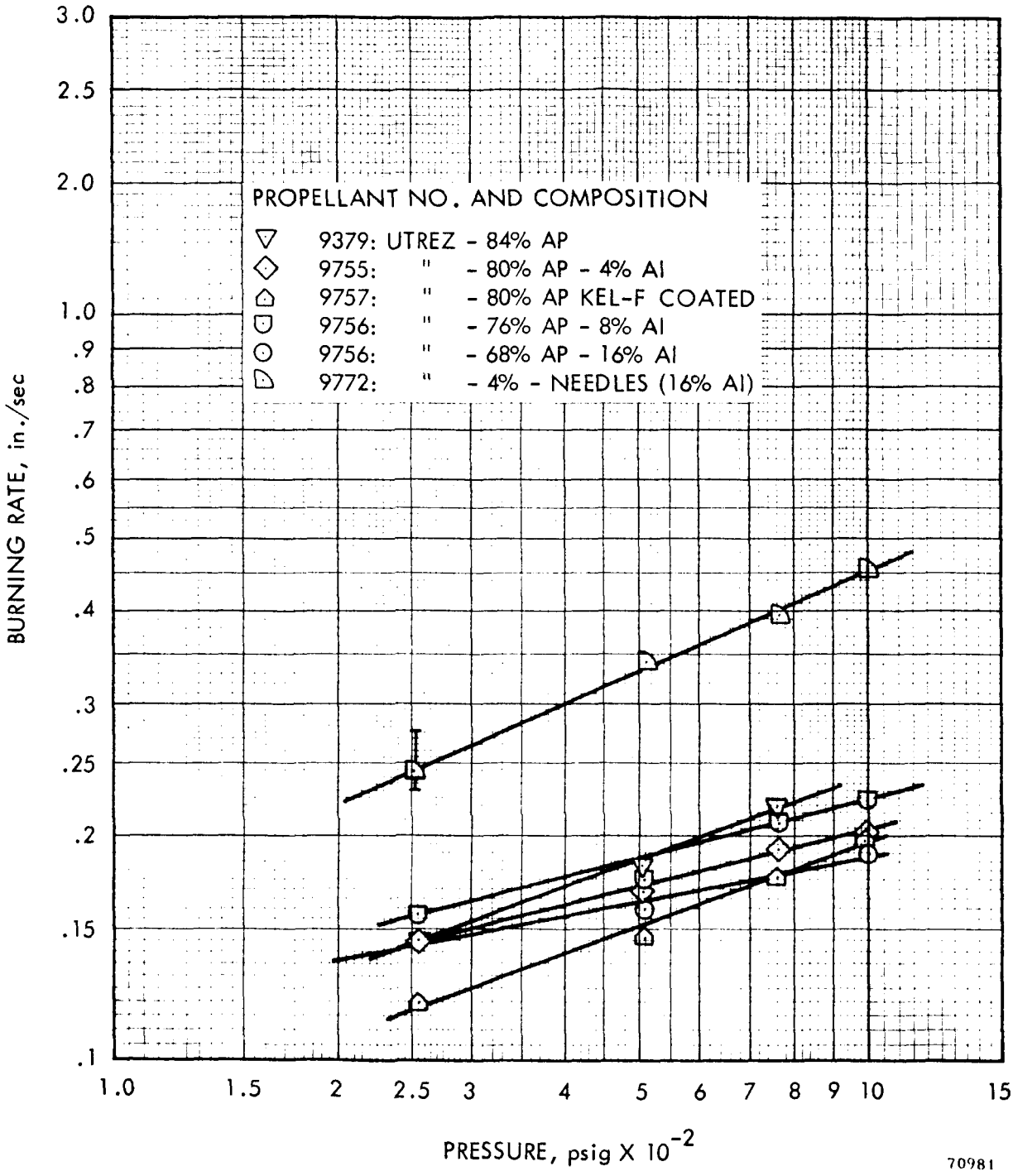

Figure 20. Strand Burning Rate of UTREZ Propellants

Oxidizer loading-level studies: As shown in figure 19, decreasing the oxidizer loading-level resulted in a significant reduction of the propellant burning rates, but had little effect on the burning rate exponents. These propellants also were qualitatively similar in appearance to the more heavily-loaded UTX-9379. Though the strand data for the UTX-9754 show a negative slope, motor data showed a burning rate exponent of 0.18.

Although similar in appearance, these propellants did demonstrate different $\dot{P}$ characteristics. The individual rapid-depressurization test data are shown in figures 21 and 22 and the critical depressurization limit lines are shown in figure 23 in comparison to the line for UTX-9379, the reference propellant. As evidenced in these figures, decreasing the oxidizer loading-level at a given pressure resulted in a significant decrease in the depressurization rates required for termination, the major portion of this decrease occurring in the interval from 84% to 80% AP. Reducing the AP concentration from 84% to 80% reduced the required depressurization rate at 400 psia from 20 000 psi/sec to 9000 psi/sec. Further reduction to 76% AP decreased the rate to 7000 psi/sec. In contrast, the incremental change in burning rate was larger when the AP concentration was reduced from 80% to 76% (0.135 in./sec to 0.095 in./sec) than when the AP concentration was reduced from 84% (0.171 in./sec to 0.135 in./sec).

While it is difficult to quantitatively describe these results, some qualitative interpretation of the effect of decreasing the oxidizer concentration can be made. Both the steady-state combustion and termination behavior are determined by an energy balance at the propellant surface. Increasing the fuel concentration will increase the endothermic contributions to the energy balances for two reasons: (1) increased endothermic thermal decomposition of fuel, and (2) decreased surface area for possible exothermic contributions. Horton, Bruno, and Graesser[12] have demonstrated this mathematically with the aid of a simple but approximate model. As the net heat release at the combusting surface decreases or even becomes more endothermic, the rate of combustion is decreased and the termination requirements are also decreased.

Oxidizer particle size: Data shown in figure 24 indicates that the substitution of 400μ mean diameter coarse AP for the 190μ particles used normally increases the depressurization limits at higher pressures (above 250 psi) and decreases the limits at lower pressures. Strand burning rate data for UTX-9754 shown in figure 19 indicate inclusion of the larger diameter both reduced the burning rate and made the burning rate essentially independent of pressure (i.e., a burning rate exponent of -0.05). This propellant also could not be ignited in strand form at pressures above 400 psi. Pressures realized in the slab motor contradicted the strand burning rate exponent as a value of 0.18 was calculated on the basis of the nozzle sizes required for pressurization.

Oxidizer particle coating: Other workers have suggested the use of halogen flame suppressants[13] for increasing termination susceptibility. The effects of such materials might be three-fold: the halogen-containing material may depreciate the crosslink strength, oxidizer decomposition may be altered, and gas-phase combustion might be inhibited. Any of these

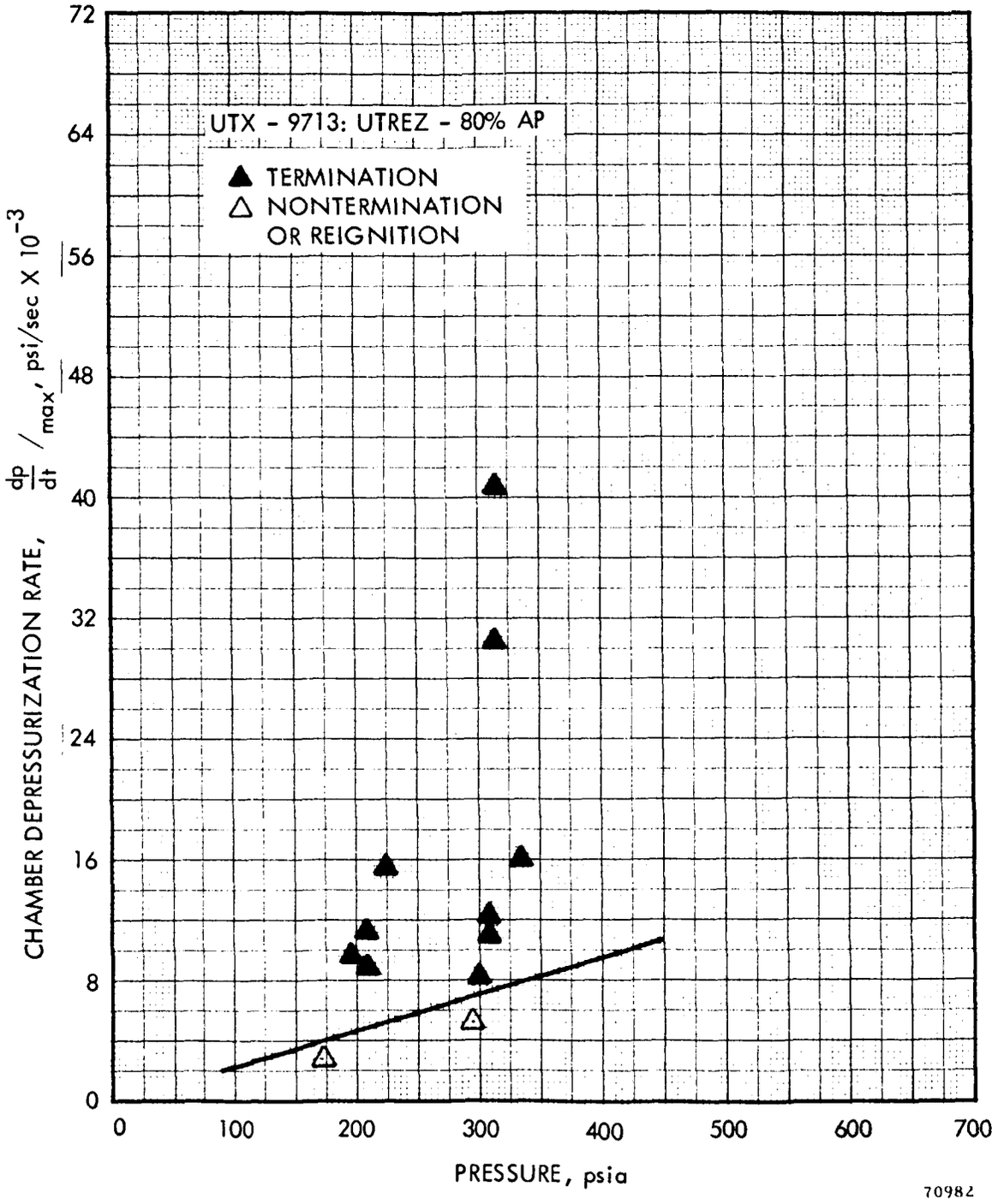

Figure 21. $\dot{P}$ Characteristics of UTX-9713: UTREZ - 80% AP

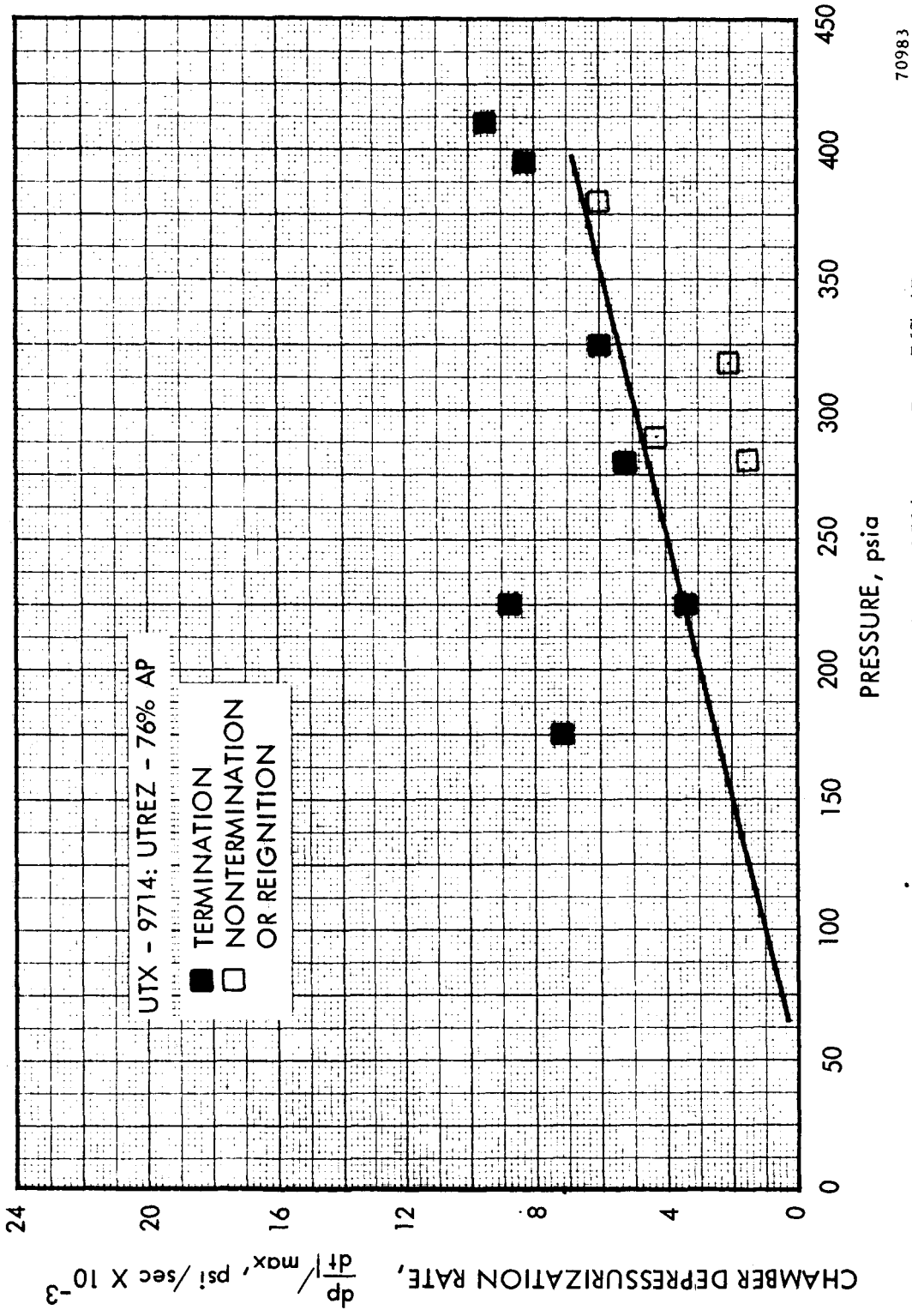

Figure 22. $\dot{P}$ Characteristics of UTX-9714: UTREZ - 76% AP

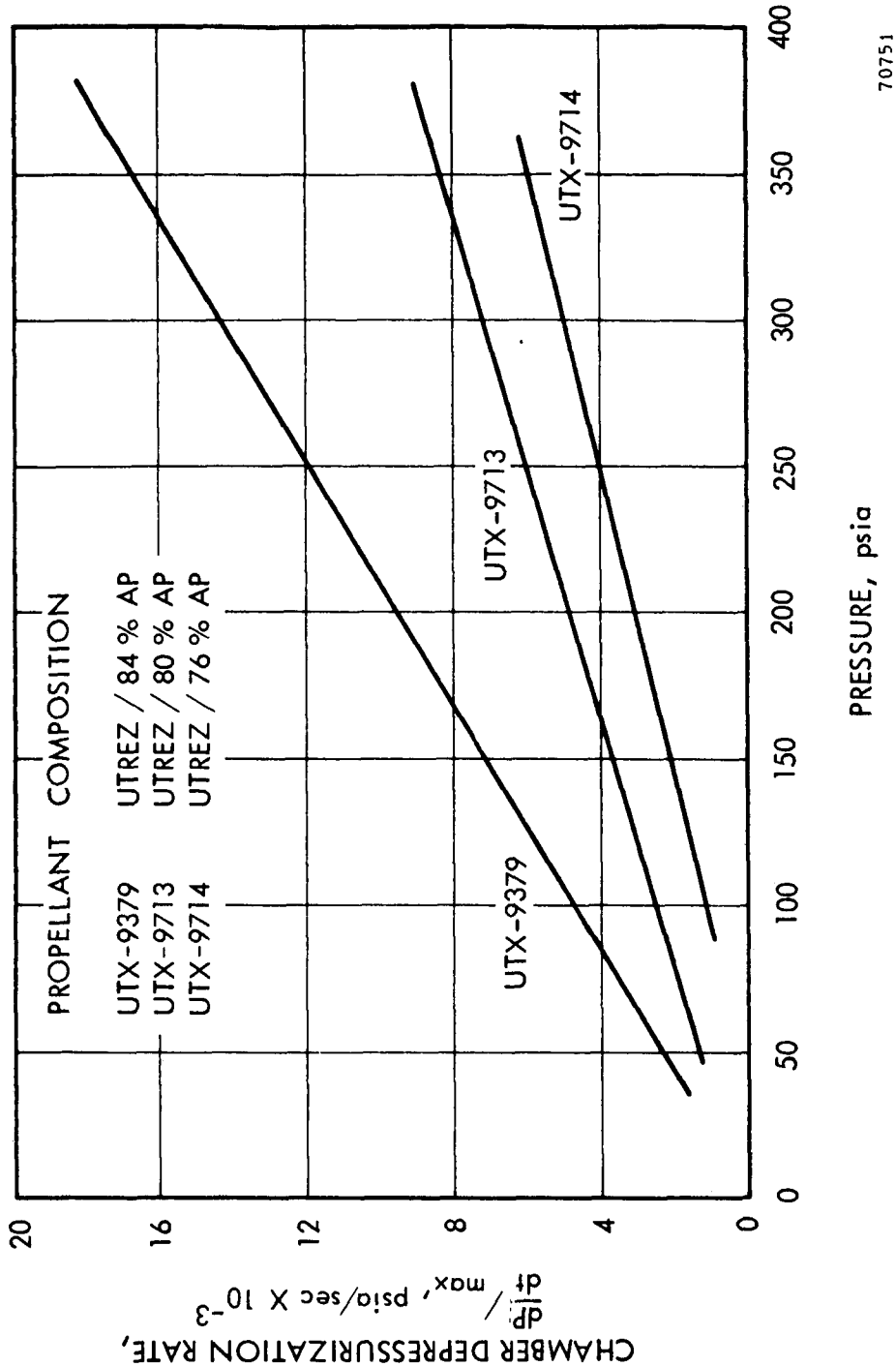

Figure 23. Effect of Oxidizer Loading Level Upon $\dot{P}$ Termination of UTREZ Propellants

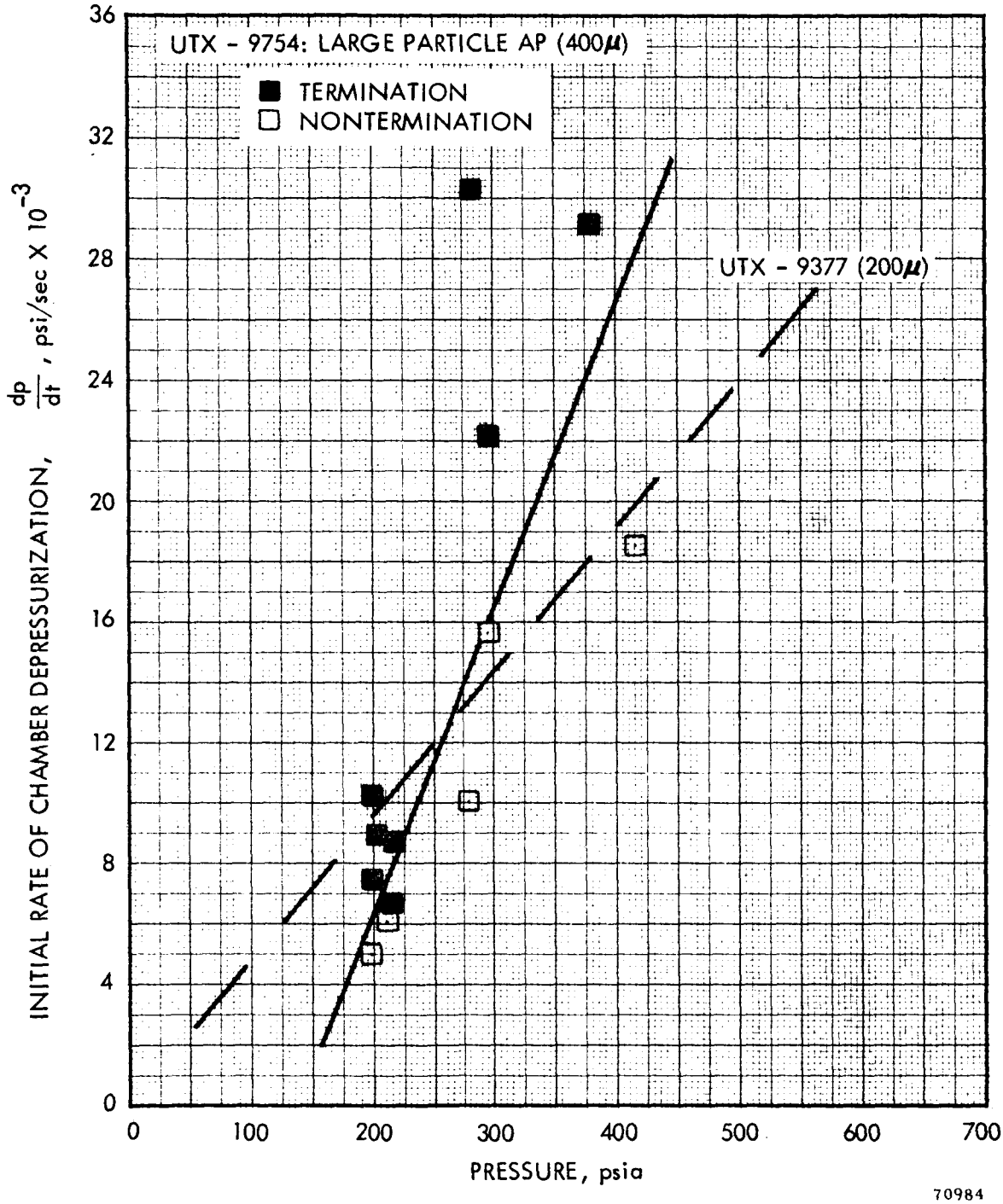

Figure 24. Effect of Oxidizer Particle Size Upon $\dot{P}$ Termination of UTX-9754: UTREZ - 84% AP (400μ Large Diameter Particle, 70:30 Coarse to Fine)

results, particularly the latter two, would result in an increase in termination susceptibility.

The effect of such materials was explored by formulating UTX-9759, in which the large-diameter AP had been coated with 1.5% Kel-F polymer. Since attempts to coat the fine AP resulted in sticky agglomerates, only the coarse AP was coated. Also, because the Kel-F coating impedes the mixing process, only an 80% total solids loading was used. Thus, the Kel-F constituted 0.84% of the total propellant.

Gross comparison of the burning rate data of UTX-9757 and UTX-9713 shown in figures 19 and 20 indicates the Kel-F coating had a negligible effect upon burning rate. The rapid depressurization data for UTX-9757 shown in figure 25 also shows little or no effect upon combustion termination behavior. Whether greater concentrations of Kel-F would yield similar results is open to speculation.

Catalyst studies: The burning rate data presented in figure 19 show that at equal concentrations of catalyst, the copper chromite was a better catalyst than the iron oxide. Both burning rates and burning rate exponents were increased by the addition of copper chromite. Physically, these propellants were similar and were opaque, in contrast to the uncatalyzed UTX-9379.

The depressurization data showing the effect of these catalysts are presented in figures 26 through 30, and the limit lines for all five propellants are compared in figure 31 along with that for UTX-9379, the reference propellant. Within the experimental accuracy of these data, introduction of the iron oxide had no effect upon the termination susceptibility of the two propellants tested, although the burning rates were increased. Use of copper chromite both increased the burning rates and increased the termination requirements. Although the differences are small, they are apparently real. At higher pressures (400 to 600 psi), a particular termination nozzle was sufficient to achieve termination of the noncatalyzed and iron oxide-catalyzed propellants. However, the same nozzle with the UTX-9718 and UTX-9719 propellants generally failed to cause extinguishment and a larger nozzle had to be used. Based on the nozzle throat areas, the copper chromite propellants required up to 15% higher depressurization rates for termination.

Aluminum loading: The effect of aluminum concentration upon rapid depressurization susceptibility was explored using 4%, 8%, and 16% concentration of H-322 powdered aluminum (mean particle diameter = 22μ) with a constant total solids loading of 84%. A fourth propellant, UTX-9772, was formulated with 12% H-322 powdered aluminum and 4% aluminum needles (0.125 in. by 0.004 in. by 0.0045 in.).

Addition of the powdered aluminum demonstrated the usual effect upon the burning rate characteristics. As shown in figure 20, increasing the aluminum concentration tended to both slightly depress the burning rate exponent and the the burning rate. UTX-9759 containing 16% powdered aluminum had a burning rate of 0.16 in./sec at 500 psi and a burning rate exponent of 0.195.

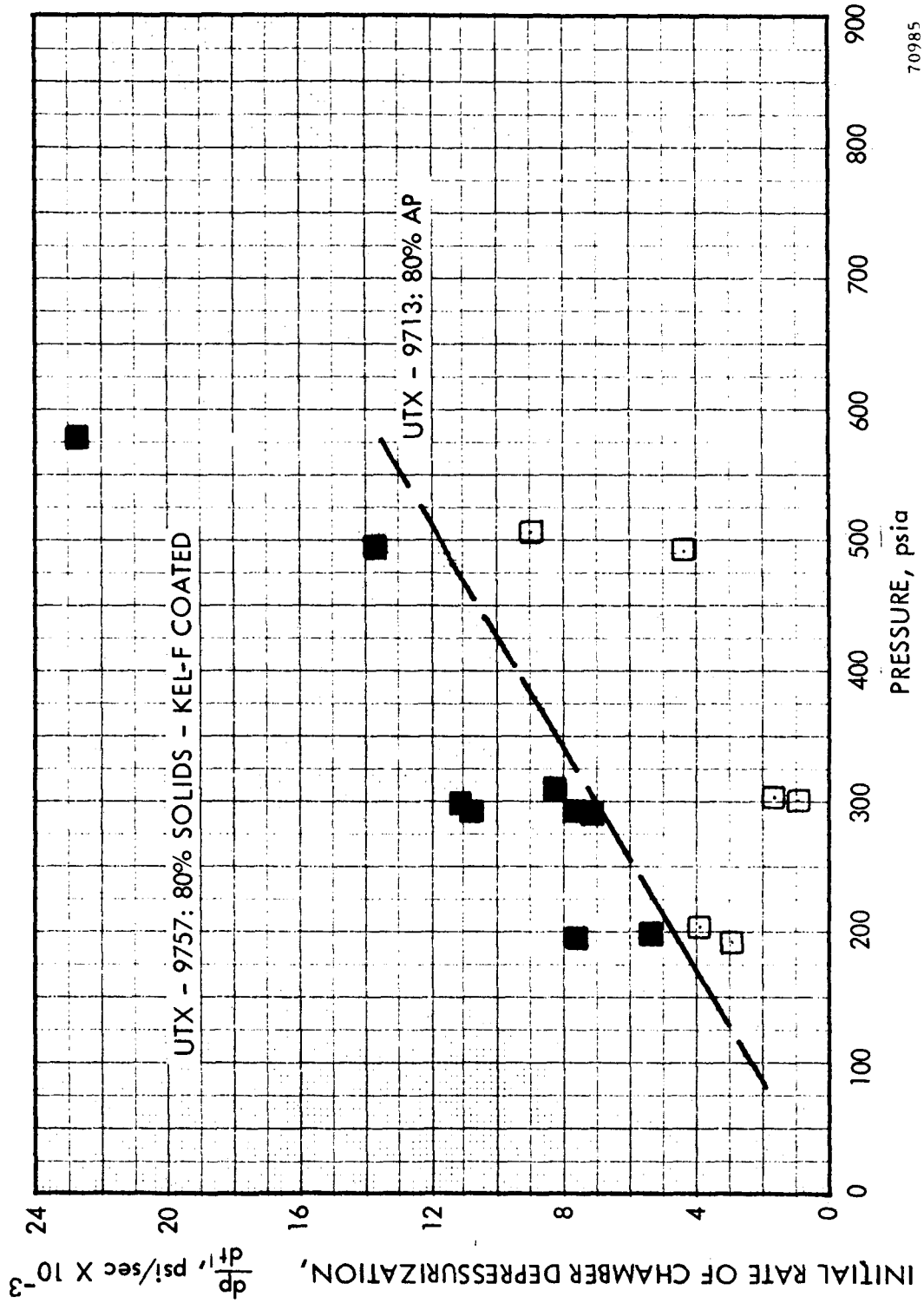

Figure 25. $\dot{P}$ Characteristics of UTX-9757: UTREZ - 80% Solids, Large Diameter Particles Coated with 1.5% Kel-F

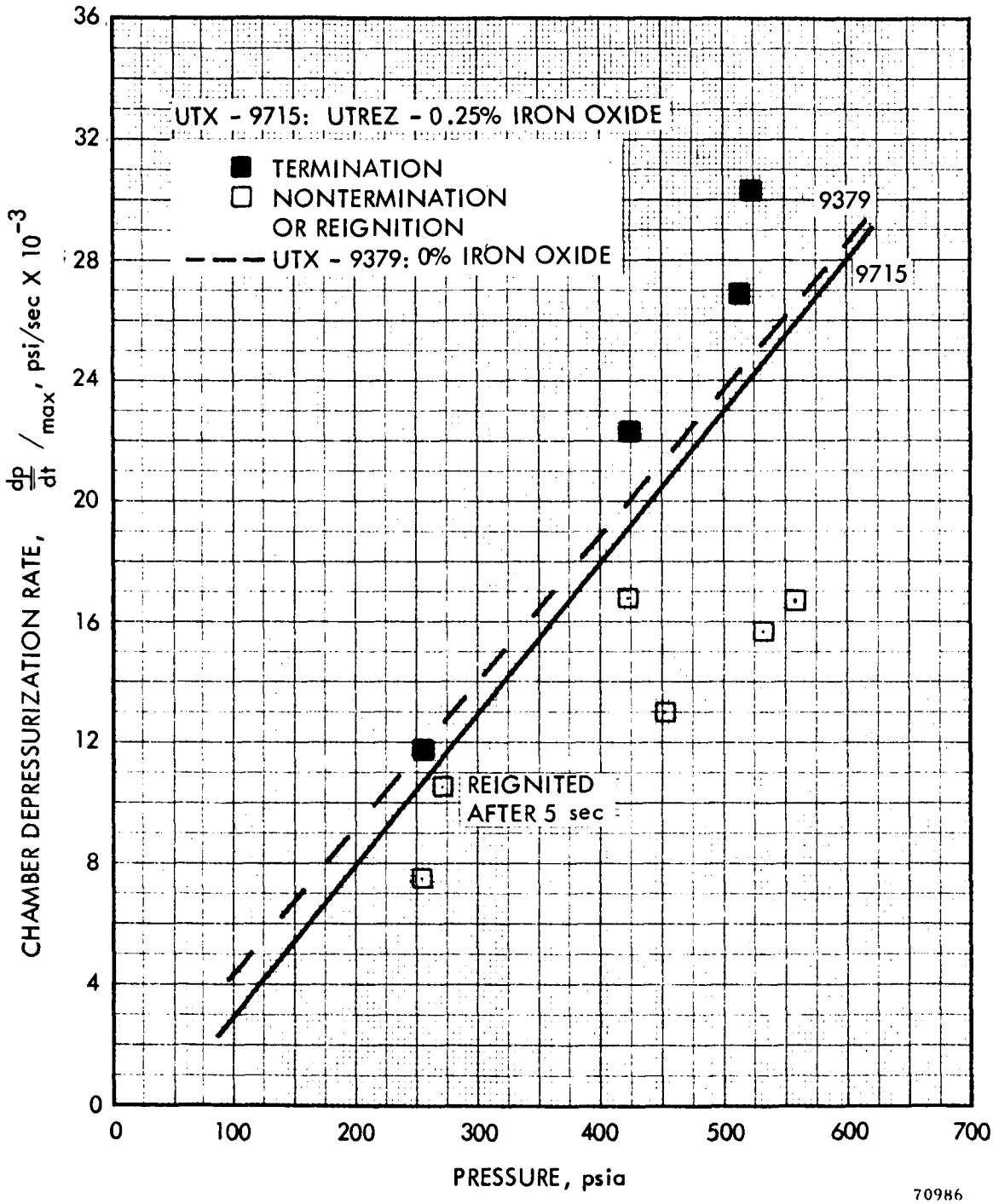

Figure 26. $\dot{P}$ Characteristics of UTX-9715: UTREZ - 84% Solids - 0.25% Iron Oxide

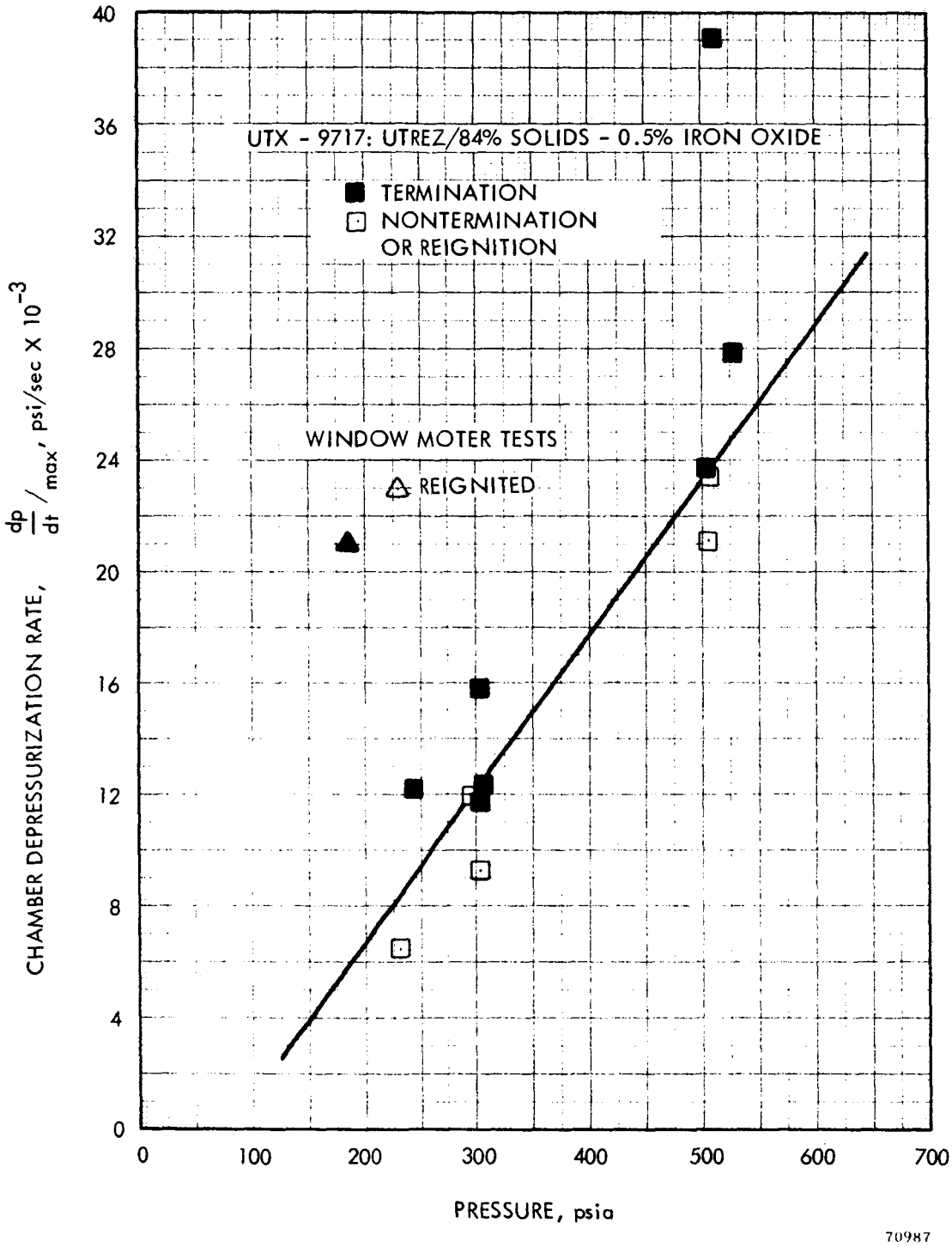

Figure 27. $\dot{P}$ Characteristics of UTX-9717: UTREZ - 84% Solids - 0.5% Iron Oxide

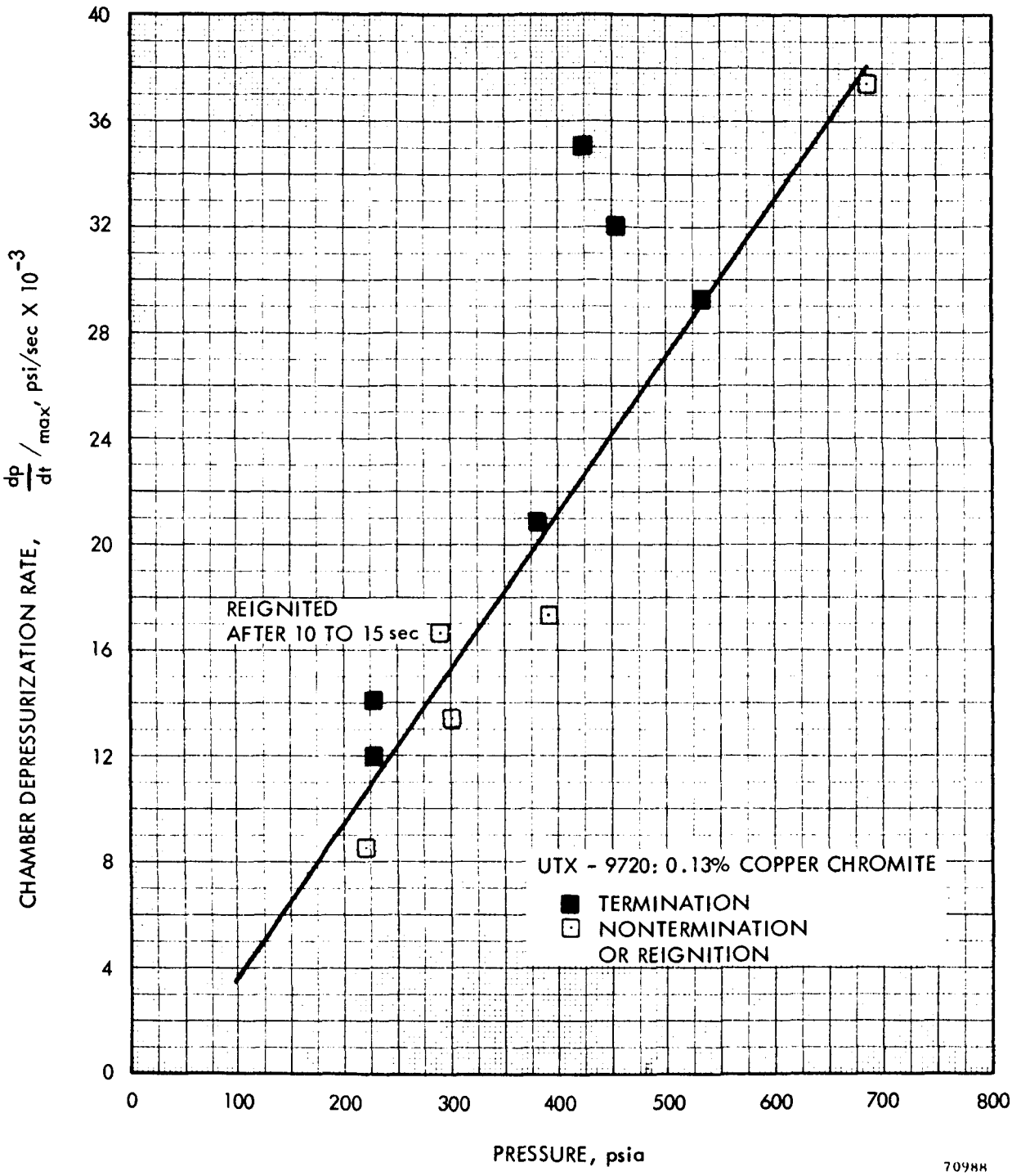

Figure 28. $\dot{P}$ Characteristics of UTX-9720:
UTREZ - 84% Solids - 0.13% Copper Chromite

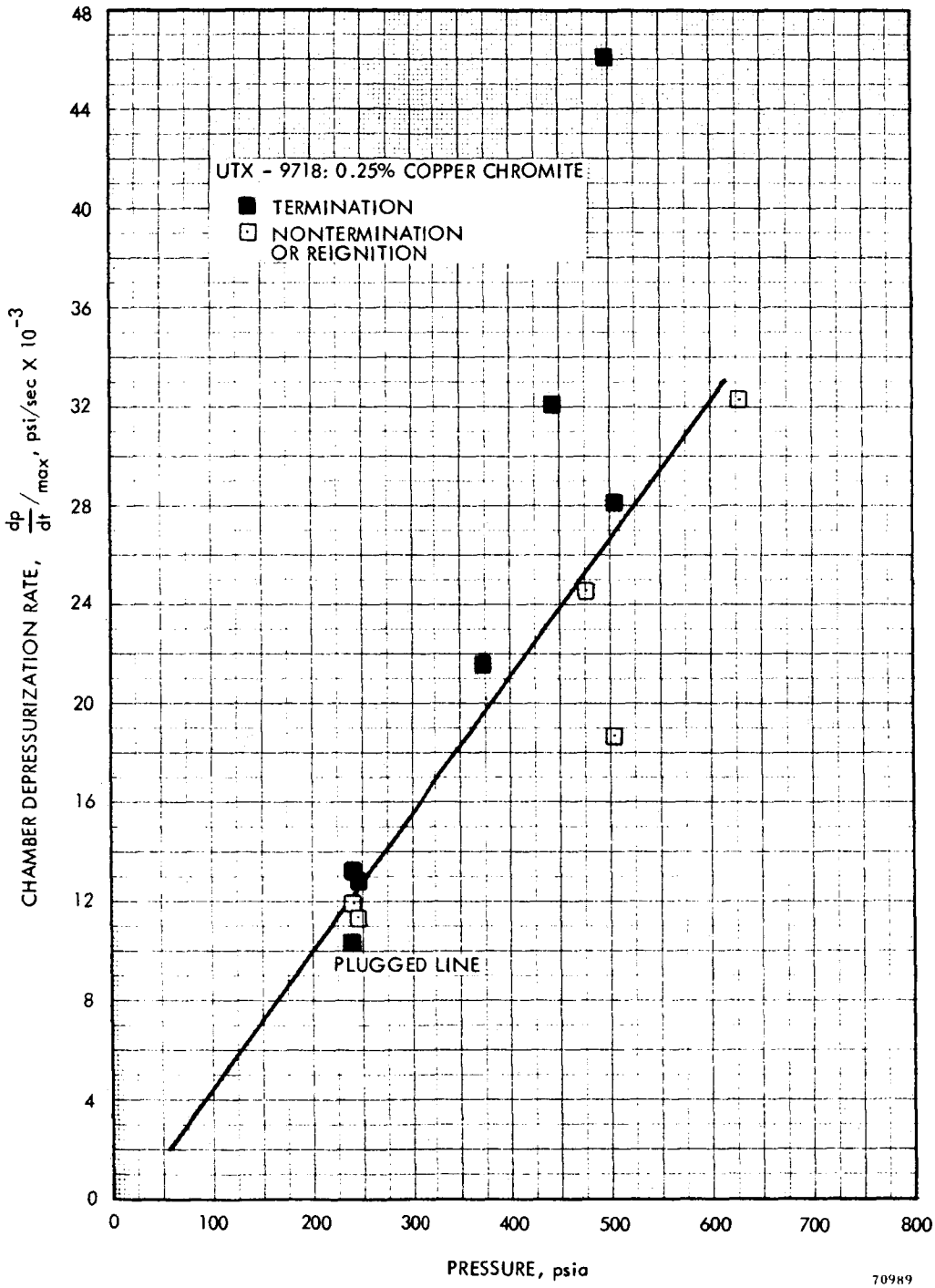

Figure 29. $\dot{P}$ Characteristics of UTX-9718: UTREZ - 84% Solids - 0.25% Copper Chromite

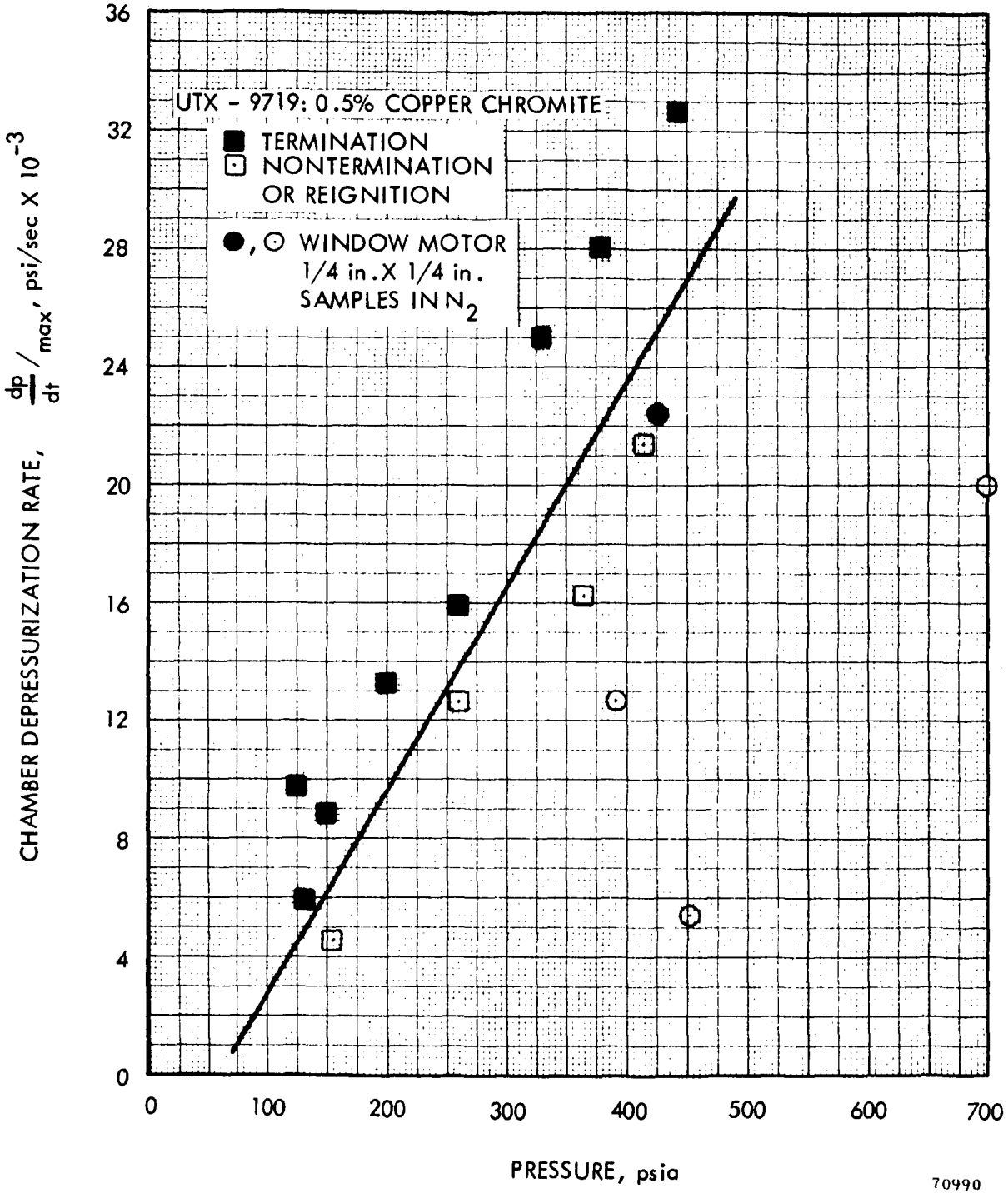

Figure 30. $\dot{P}$ Characteristics of UTX-9719: UTREZ - 84% Solids - 0.5% Copper Chromite

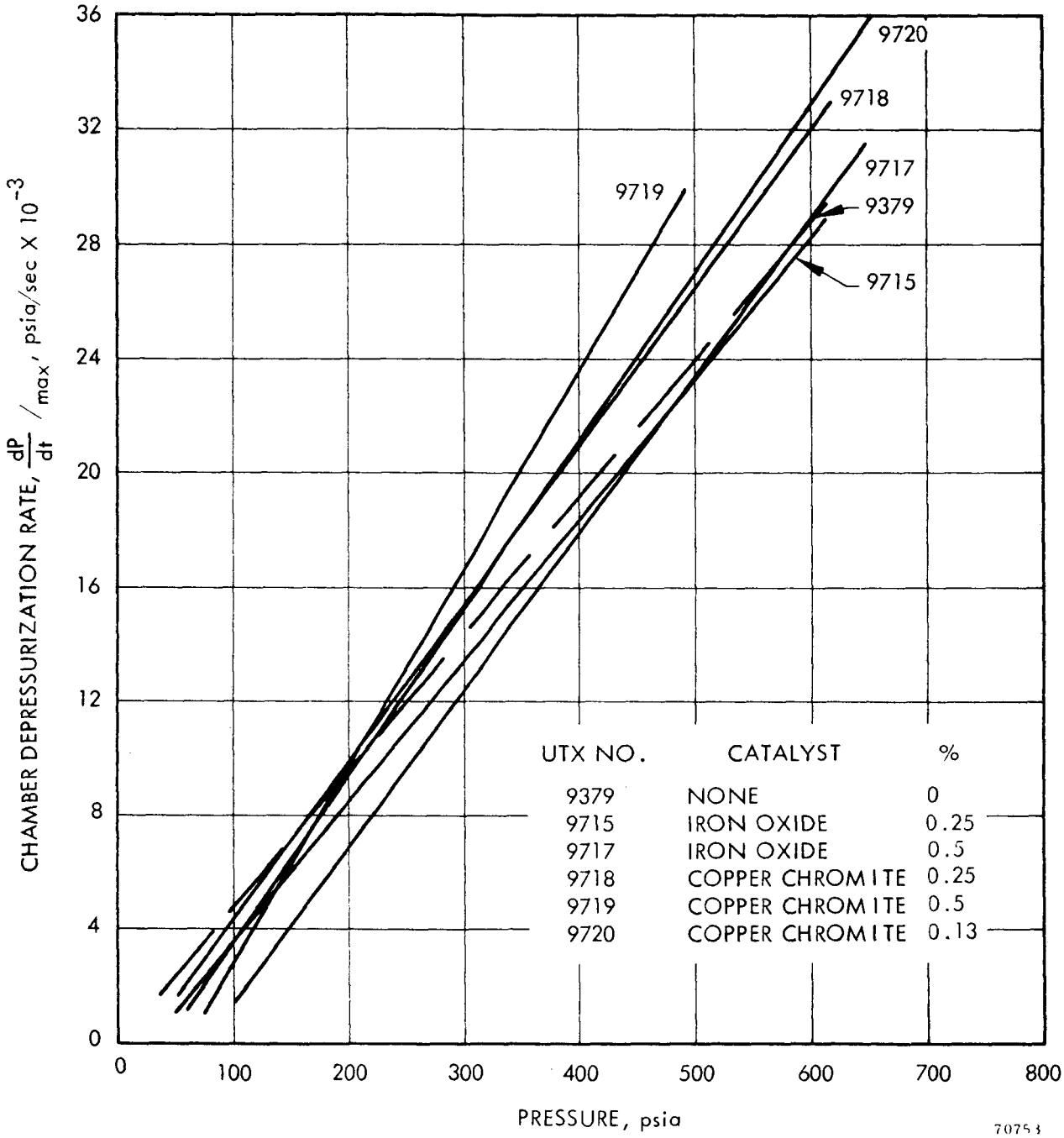

Figure 31. Comparison of Critical Depressurization Limits as a Function of Catalyst - UTREZ Binder - 84% Solids

Shown in figures 32, 33, and 34 are the rapid depressurization characteristics determined using the three concentrations of powdered aluminum. Giving consideration to the experimental precision of the data, it can only be concluded that substitution of aluminum for AP at a constant fuel loading has little or no effect upon the termination susceptibility of UTREZ propellants. Examination of figures 32 and 33 shows the initial depressurization limit lines for the aluminized propellants to agree with that for UTX-9379 containing 0% aluminum, although there is some difference at lower pressures where the addition of the aluminum has reduced the termination requirements slightly. Comparison of the limit lines for the aluminized propellants with those for propellants containing equal AP concentrations but higher fuel loading shows the aluminized propellants to have significantly higher termination requirements.

As shown in figures 34 and 35, the substitution of 4% aluminum needles for aluminum powder, while maintaining a 16% aluminum concentration, results in a large increase in the rates of depressurization required for termination. In fact, UTX-9772, containing 4% needles, could not be terminated in the 1-lb. slab motor.

High-speed film tests. - High-speed film studies were performed in conjunction with the slab-motor characterization studies to provide a supplemental means of determining precise termination conditions and to provide visual observation of environmental factors such as gas flow patterns and the effect of propellant inhibitors. The window motor was constructed as a dual-nozzle, self-pressurized motor in order to avoid the problems encountered by other investigators[14] using externally-pressurized depressurization motors. Most studies were performed using free-standing, end-burning grains inhibited on the sides with clear Tygon paint. In these tests, the propellant samples were 1-3/8-in. in diameter by 0.3-in. to 0.4-in. in length, with ignition being achieved by the use of a thin nichrome wire and a layer of propellant filings taped to the sample face. The wire was electrically heated, causing ignition of the face and pressurization of the motor. Filming, at the rate of 500 frames per second, was initiated immediately prior to ignition of the sample and stopped 500 to 1000 msec after chamber depressurization. A major portion of the photographic studies were devoted to developing and refining the filming techniques. Most of this work was performed using the camera and lighting setup as described in the section entitled "Window Motor." More recent studies included the use of smaller propellant samples burning in the motor pressurized with nitrogen, higher framing speeds (2000 frames per second), and Schlieren studies.

In the first studies, a number of filming problems were encountered. In some instances vapor condensed on the Pyrex windows during ignition of the sample. The vapor appeared to be due only to the ignition process and (in most cases) cleared up during steady-state combustion. During other tests, smoke obscured the sample. To alleviate these problems, tests were conducted with a nitrogen window-flush, while in other instances a thin

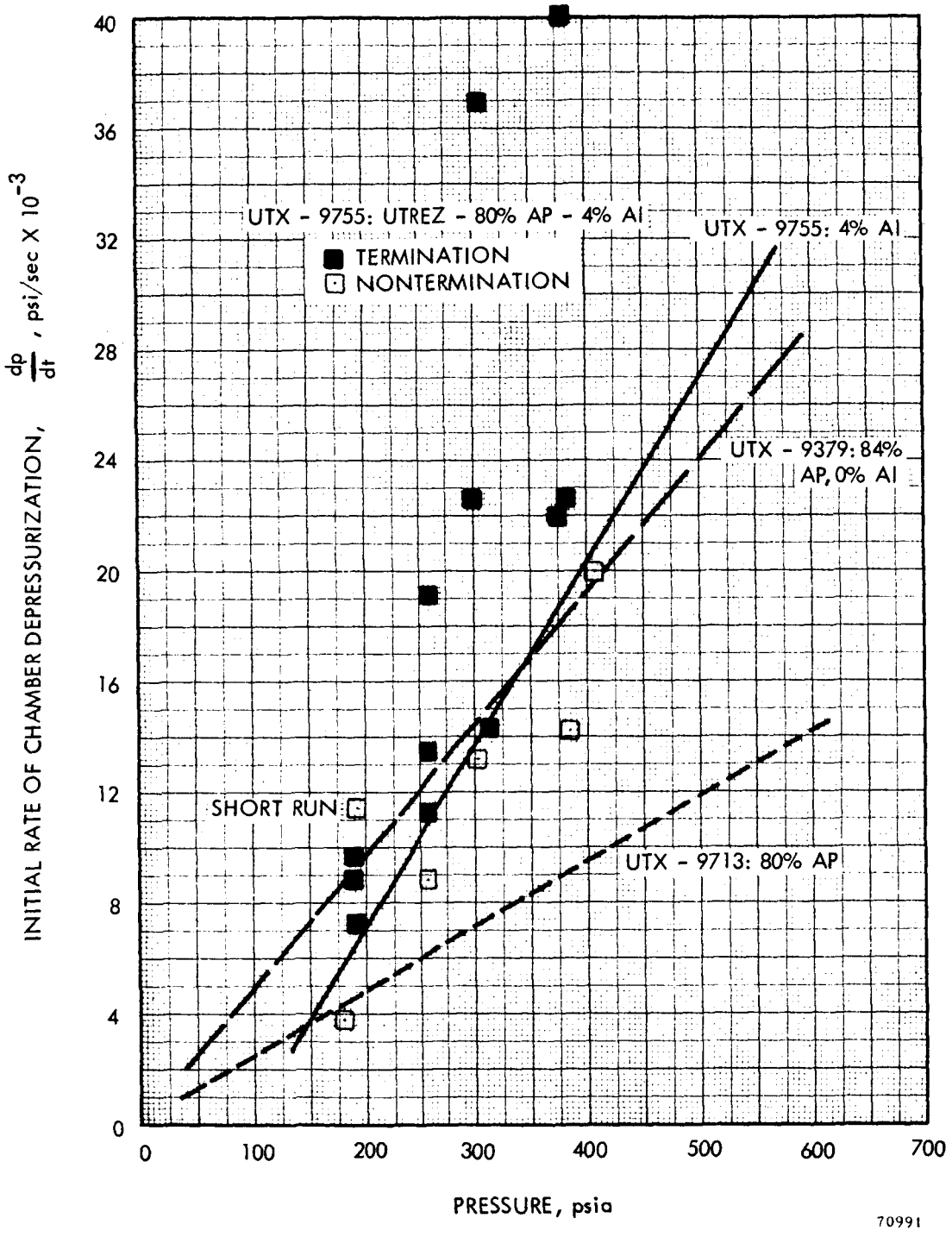

Figure 32. $\dot{P}$ Characteristics of UTX-9755: UTREZ - 80% AP - 4% Aluminum

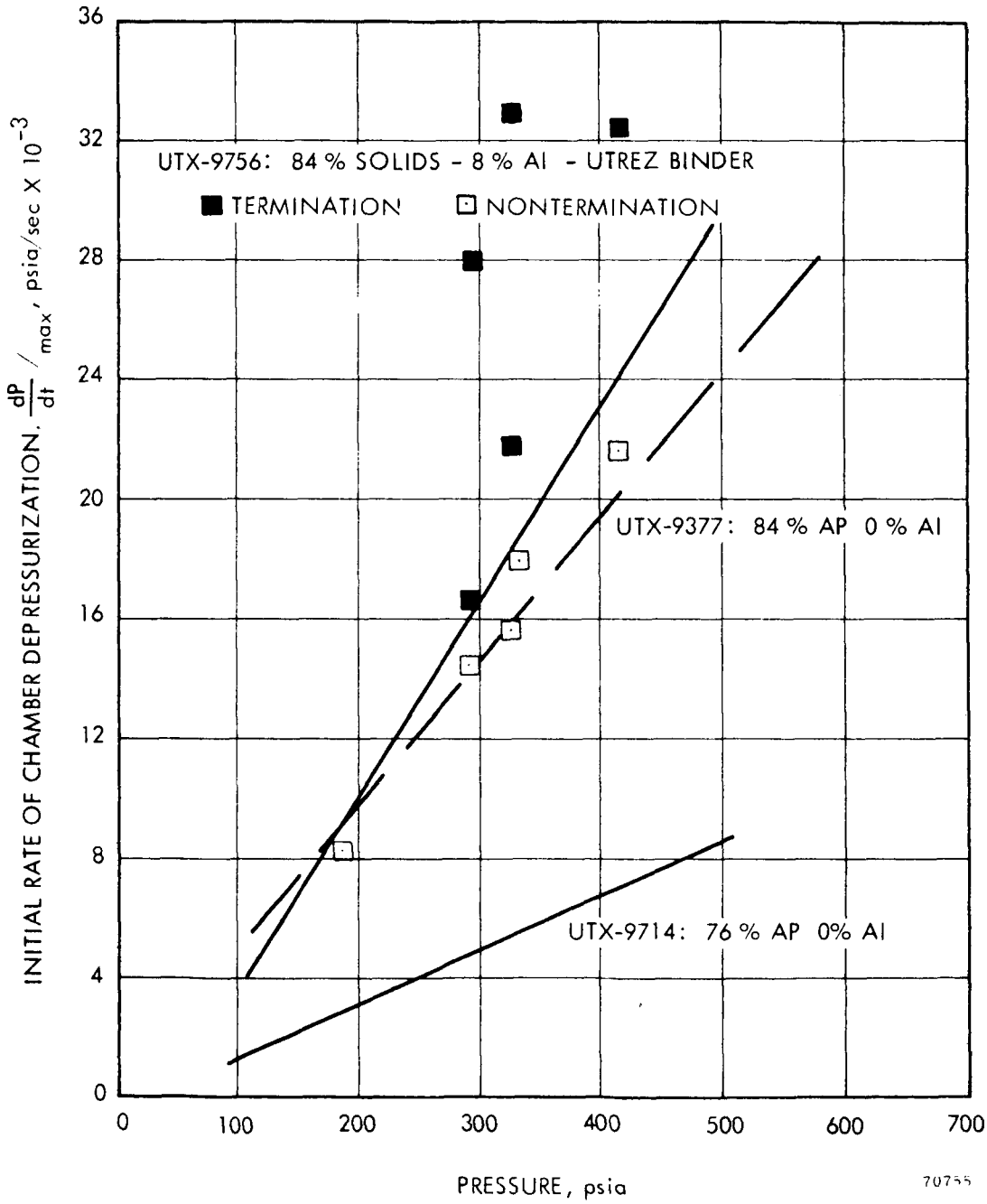

Figure 33. $\dot{P}$ Characteristics of UTX-9756: UTREZ - 76% AP - 8% Aluminum

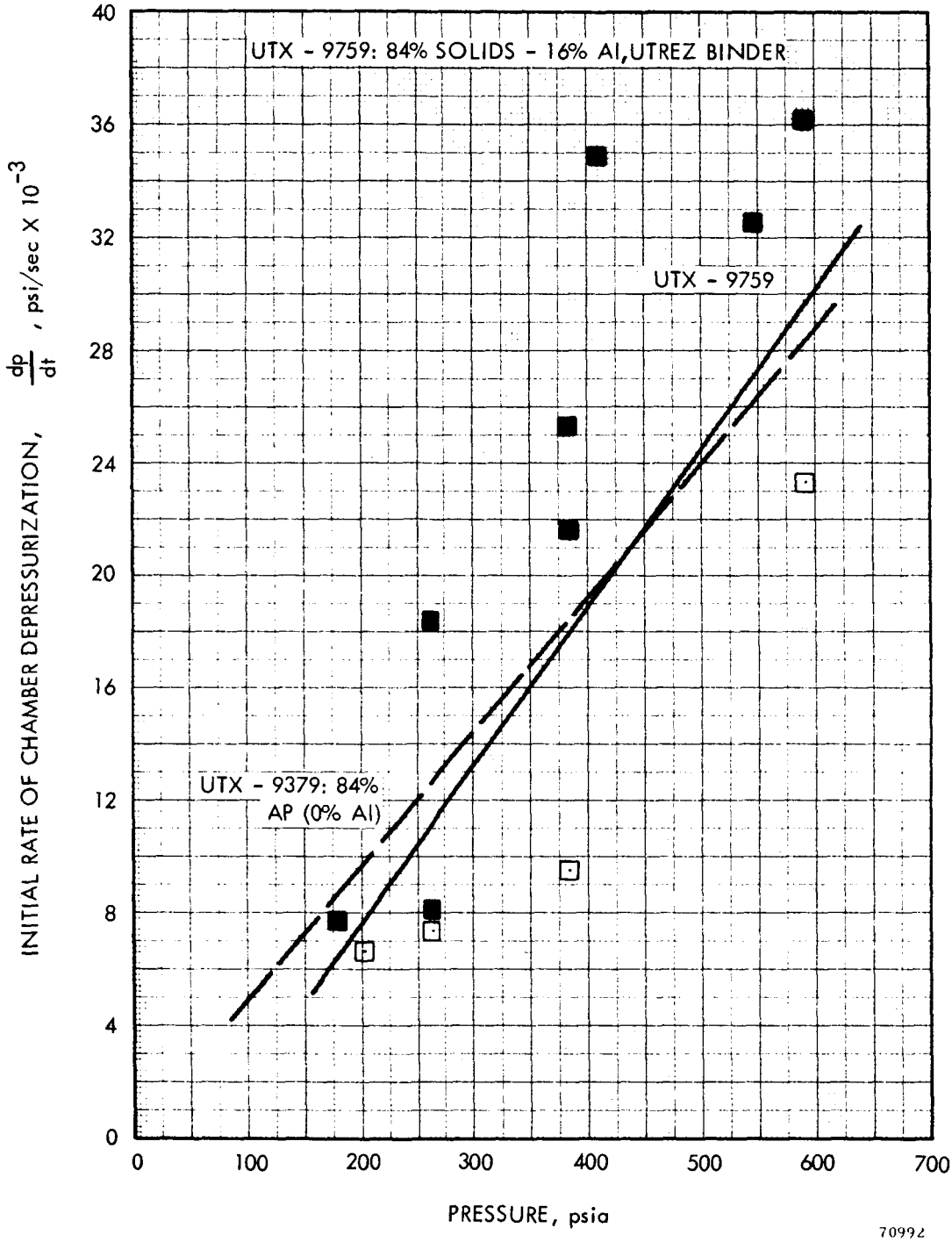

Figure 34. $\dot{P}$ Characteristics of UTX-9759: 68% AP - 16% Aluminum

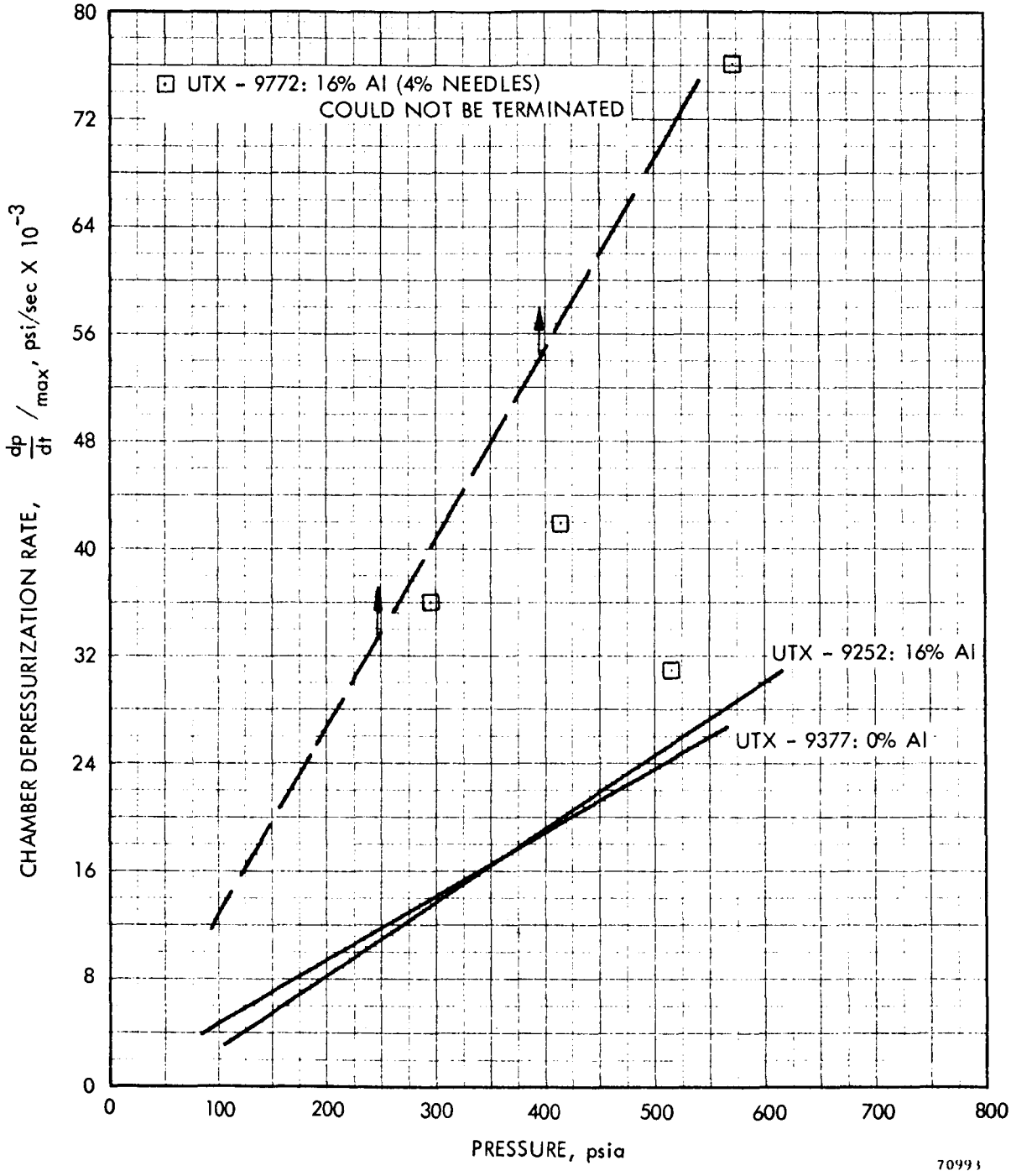

Figure 35. $\dot{P}$ Characteristics of UTX-9772: UTREZ - 16% Al (4% Needles)

film of glycerine or a commercial antifog compound was spread on the windows. Use of the antifogging compound and the nitrogen flush did alleviate the problem of vapor deposition; however, in some tests, the nitrogen flush caused an increase in the amount of smoke swirl in the viewing area. By using only the antifogging compound, vapor deposition was reduced and reasonable picture quality was achieved. Attempts to eliminate the smoke entirely by the use of a versamid inhibitor rather than the Tygon inhibitor only resulted in a larger amount of smoke which completely obscured the sample. Best results were achieved using grains uninhibited on the sides, though this technique resulted in a progressive-regressive burning-rate trace.

Although extensive analysis of the film sequences was not performed, several significant points concerning the mechanisms of termination and nontermination or reignition were noted. In those instances where the rate of chamber depressurization was significantly above the rate necessary for termination, combustion extinction was achieved shortly after initiation of chamber venting and at a pressure level above the exhaust or ambient pressure level. In those cases in which the rate of chamber depressurization was much less than that needed for extinction, there was no discernible pause in the combustion of the grain although there was an adjustment of the burning rate to the imposed pressure change. At rates near the critical depressurization rate, the grain appeared to be completely extinguished though reignition may have occurred several seconds later. These points are best illustrated by the data shown in table IV.

TABLE IV. - HIGH-SPEED FILM TEST RESULTS

Test no.	Propellant UTX-	P_c psi	dP/dt psi/sec	dP/dt/critical psi/sec	msec	P_{ex} psig
3-27-1	9379	205	-10 600	-10 200	47	27
3-27-2	9379	235	-23 300	-11 200	16.7	27
3-27-4[a]	9389	305	-18 000	-18 000	16.7	36
3-27-5[a]	9395	601	-84 000	-96 000	20	21
2-22-5[b]	9395	270	-78 000	-32 000	9	24
2-22-4[a]	9394	155	-24 000	-14 000	13.5	17

[a]Grain reignited.

[b]Grain face was terminated, but reignition occurred in crack between the back of the sample and the sample holder.

The time for combustion extinction, τ, was not always easily determined by visual examination of the filmstrips. τ was measured by counting the number of frames of film from the apparent point of depressurization to the first frame where combustion of the surface could not be noted. Cross-examination of the data trace was then used to determine the pressure, P_{ex}, at the point of extinction. Visual determination of the point or time of extinction was necessarily a qualitative judgment. In several instances, material was still flowing from the sample, though for all intensive

purposes, combustion had been terminated, Generally, the flow of extraneous smoke obscured the exact frame showing combustion extinction.

The source or point of reignition in the instance where extinguishment was not complete was not always apparent, although in two tests, reignition sources were observed which could be encountered in motor environments. In one test, the combustion face of the end-burning grain was completely extinguished; however, during steady-state combustion prior to termination, a crack developed between the propellant and the sample holder. Although the rate of depressurization was sufficient to cause termination of combustion on the front surface, combustion in the crack was not extinguished and acted as a source of reignition for the grain. In the second instance, reignition occurred several seconds after venting, although the rate of chamber venting was sufficient to completely extinguish the combusting surface. In the last few frames of the film sequence (filming was stopped just after the venting process) two glowing hotspots could be seen at the interface between the propellant surface and the inhibitor used to prevent combustion down the sides of the grain. The film sequence does not show reignition of the grain, but in all likelihood, reignition was the result of the local hotspots. Such interfaces, which are likely to be encountered in working motors, must necessarily be considered in the design of any termination system.

In an attempt to achieve better picture quality, small samples (1/4-in. by 1/4-in. on the face) were burned in a prepressurized nitrogen environment. While picture quality during steady-state combustion conditions was improved, depressurization of the motor caused a fog (probably condensed hydrogen chloride and water) to form, which often completely obscured the sample face. Examination of the pressure trace also showed pressure oscillations occurring in the motor during the pressure transient. Finally, the use of either the nitrogen environment or small propellant samples caused a significant lowering of the propellant termination requirements. This is shown in figure 36 where, in the case of the UTX-9759 containing 16% aluminum, the critical depressurization limit was halved.

Results obtained using the higher framing rates or the Schlieren system were less than satisfactory. Framing rates of 2000 frames per second filming were used with a 2-sec high-intensity flash bulb as a backlight and with no forelight. Smoke from the sample, and the lack of a forelight, caused both a shadowgraph effect and the combusting face to be obscured. Any future tests would require a high-intensity forelamp and probably a nitrogen flush flowing about the sample. Several Schlieren tests were also tried. Though the rough surfaces on the glass windows caused some problems, the early portions of the films during ignition were successful. But as smoke and hot gases started swirling toward the windows, the picture quality quickly deteriorated and nothing could be observed. From these tests it is expected that quality pictures would require a nitrogen flush and optically-ground windows.

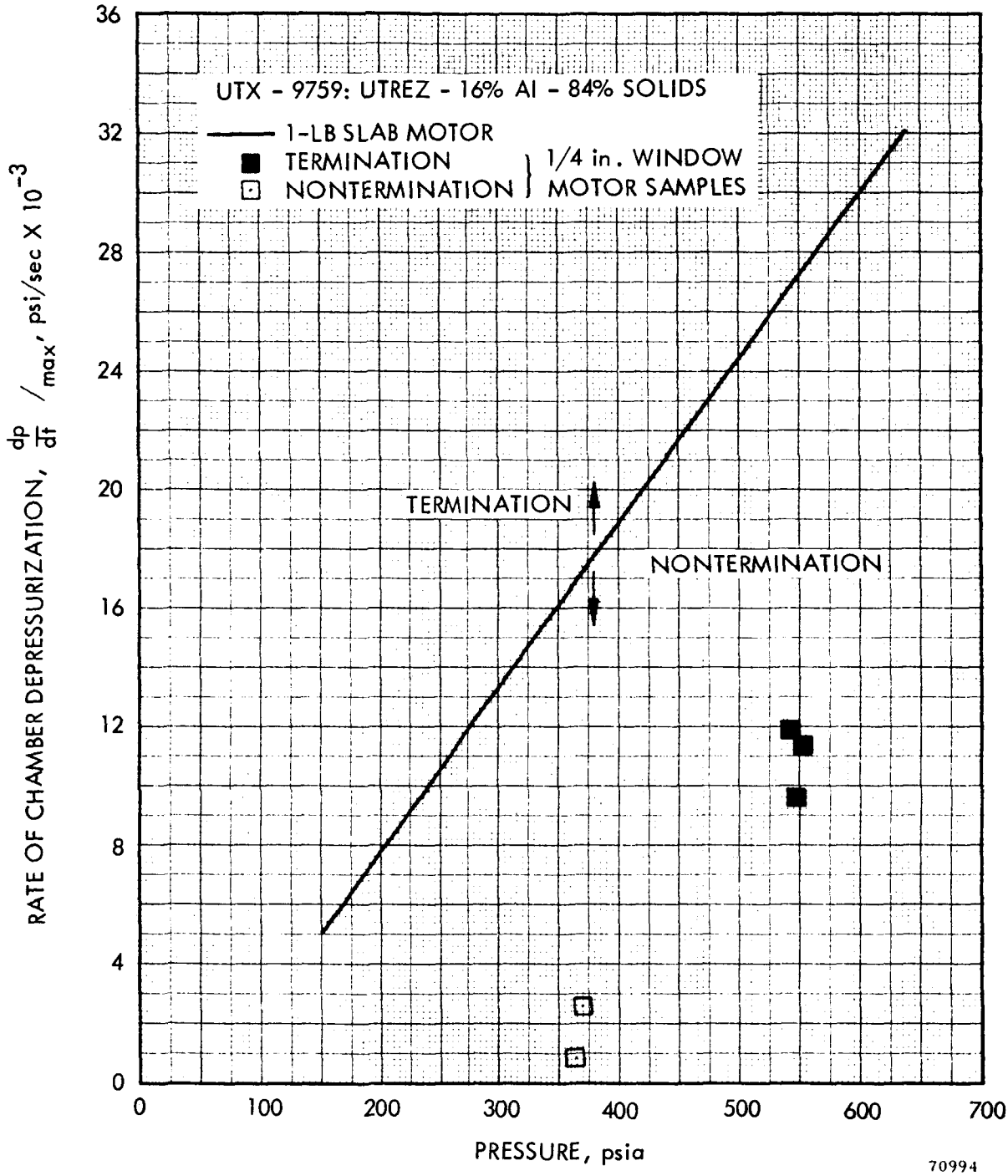

Figure 36. Effect of Grain Size and Environmental Conditions upon Combustion Termination

Photomicrographs of some of the 1/4-in. by 1/4-in. x 1-in. samples terminated in a nitrogen atmosphere were taken in order to determine if any significant differences of the propellant surfaces could be noted. The photographs shown in figure 37 were taken at a magnification of about 45X; however, development of the film resulted in a slightly greater magnification. For reference purposes, a 500μ dimension has been included on the pictures. The surface of the CTPB propellant containing no catalyst or aluminum has the appearance of once being molten. The outer perimeters of the large-particle AP are very smooth and glassy while the center portions of the crystal protrude slightly. Although not shown in these figures, the PU propellant had the appearance of aggregate concrete with rounded lumps of larger particle AP protruding above the surface. There was no division between the small AP/polymer matrix and the larger AP perimeters, and there was no evidence of the melted AP surfaces observed with the CTPB and UTREZ propellants.

As mentioned, the UTREZ formulations with no catalyst or aluminum showed evidence of melting and flowing of the large-particle AP. These particles have frosty or glassy blistered centers which protrude slightly. The large-particle perimeters of the 84% AP formulation have the appearance of having flowed over the polymer/small AP matrix below. Figure 37-B for the similar appearing 80% AP formulation shows small white balls on a portion of the large AP particles. Both the 80% and 84% AP formulations are lightly flecked with what appears to be charred polymer.

Introduction of 0.5% copper chromite resulted in the formation of two or three small green balls on the surfaces of the large AP, as shown in figure 37-C. In figure 37-D, the tops of the large-particle AP of the UTX-9717 containing iron oxide are capped with a coating of iron oxide. The perimeters of these particles are smooth and glassy appearing. At the intersection of some of the iron oxide-covered caps and the smooth melted perimeters are dark round beads of approximate 40μ diameter.

The surface of the UTX-9755 shown in figure 37-E has a thin filigree of sintered aluminum balls. The balls range in size from 20 μ to 100 μ indicating melting and agglomeration of the balls. In contrast to the other UTREZ propellants, the surface of the AP particles shows little evidence of melting.

The surface of the 16% aluminum formulation shows a much larger network of sintered aluminum balls. As shown in figure 37-F, the network extends out from the surface of the propellant with the lower ends of the networks being composed of the smaller aluminum balls and with the upper ends often culminating in much larger aluminum balls. Again, there is little evidence of melting on the AP surfaces though many of the aluminum ball networks contain clear glassy balls approximately 100 μ in diameter.

L* studies. - This portion of the program was conducted using the window motor used for the high-speed film tests. The necessary modifications to the motor and the experimental procedures employed are discussed in the following section, while the experimental results obtained are presented in the section entitled, "Experimental Results."

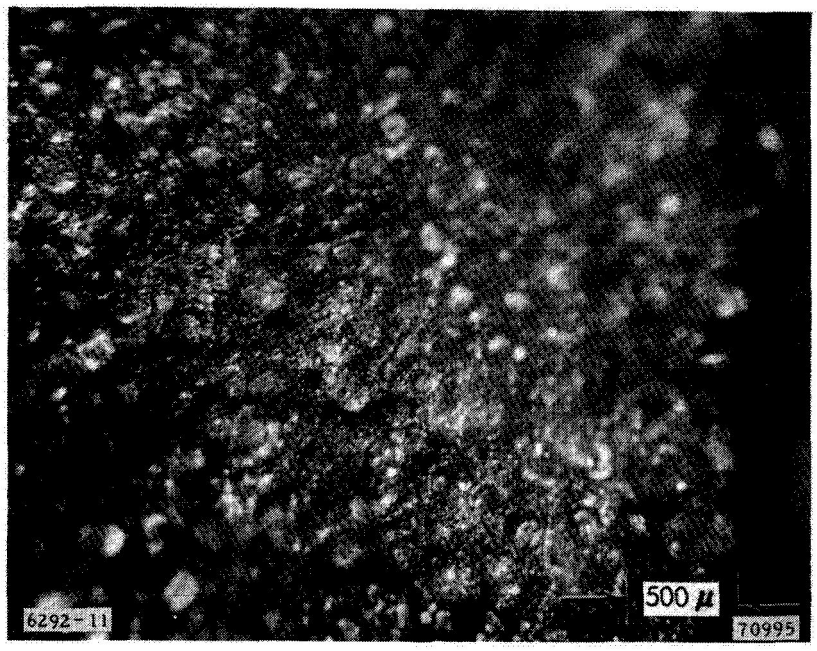

Figure 37-A. UTX-9775: CTPB - 84% AP

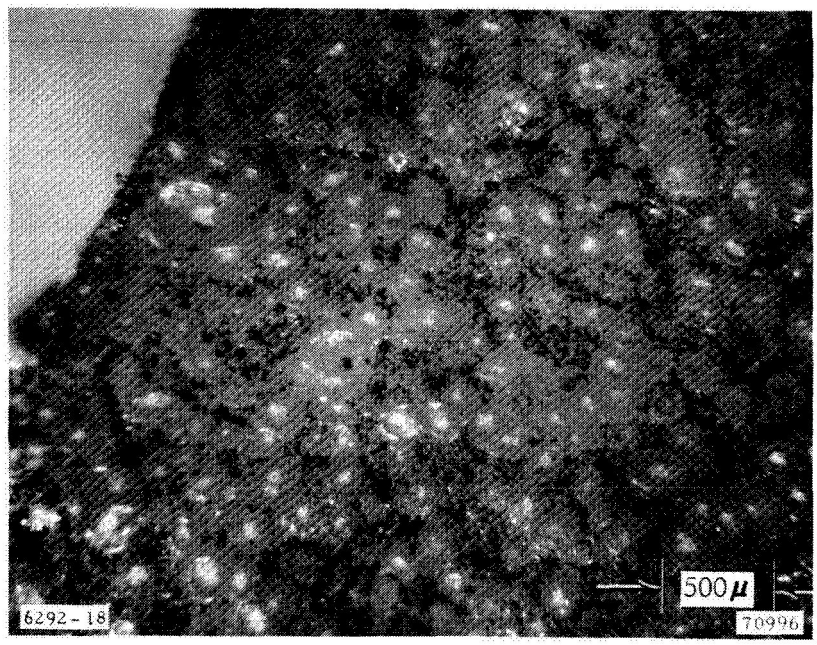

Figure 37-B. UTX-9757: UTREZ - 80% AP

Figure 37. Photomicrographs of $\dot{P}$ Terminated Propellant Surfaces

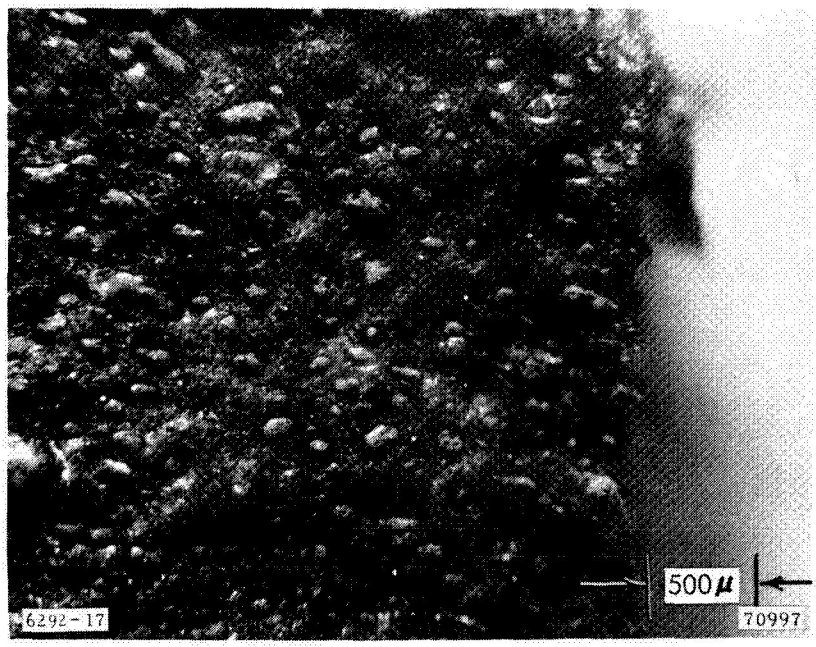

Figure 37-C. UTX-9717: UTREZ - 0.5% Iron Oxide

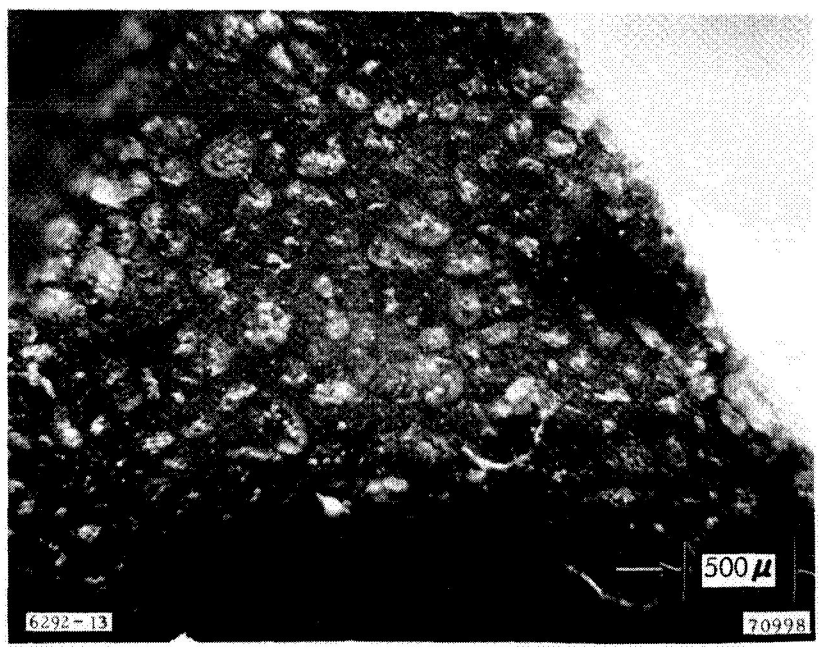

Figure 37-D. UTX-9719: UTREZ - 0.5% Copper Chromite

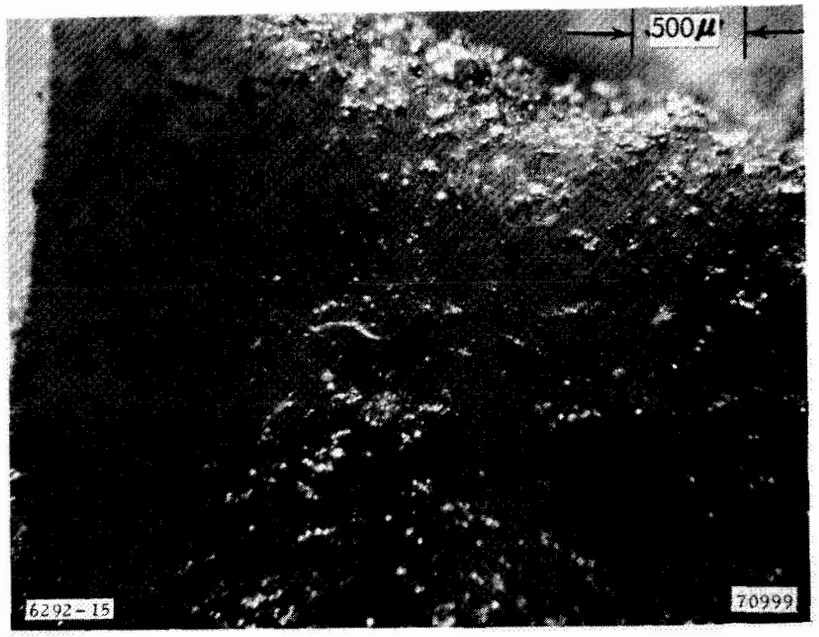

Figure 37-E. UTX-9755: UTREZ - 4% Al

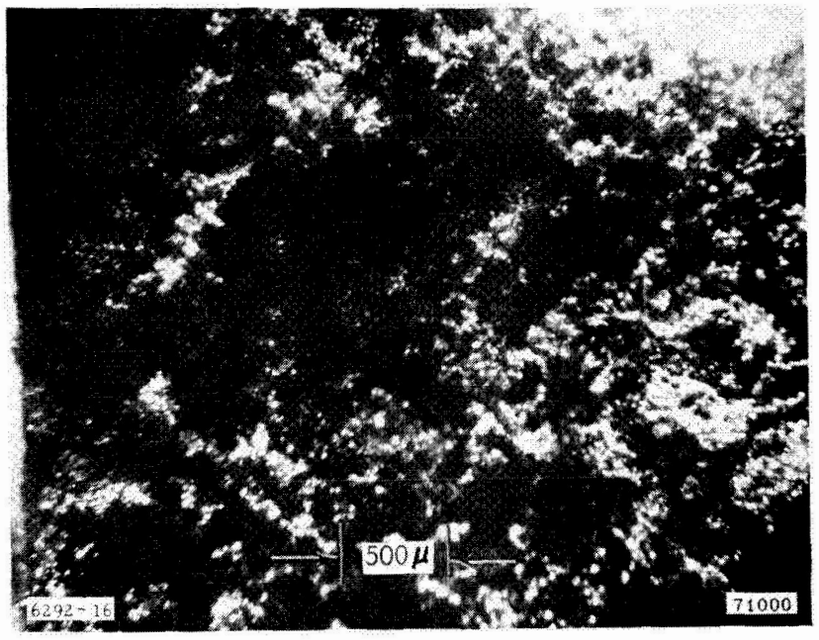

Figure 37-F. UTX-9759: UTREZ - 46% Al

Equipment: L* tests were conducted using the window motor with the termination nozzle as the steady-state nozzle and with the other nozzle plugged. In contrast to the film studies, the windows were removed and the window ports plugged to reduce the motor volume. The motor was connected to a 1000-liter vacuum tank and evacuated to less than 0.007 atm prior to firing (the minimum ignition pressure of the propellants tested was 0.05 atm), rather than firing into the atmosphere as was done with the $\mathring{P}$ tests.

In conducting the tests, the L* of the motor was varied by selection of the nozzle throat area. Regressive grains were then selected to give a 2 to 5-sec burn period following ignition. By using longer grains with the larger diameter nozzles, it was generally possible to achieve 100 in. or less L* values. Significant further reduction of the motor L* could have been obtained only by reducing the volume of the motor. Since Barrére[15] found the L* extinction pressure to be a function of both L* and volume, the L* testing was conducted with a constant volume to provide a better evaluation of propellant differences. (In actuality, the final volume changes slightly from test to test because of differences in web thickness at termination. In these tests, this variation was less than 10% of the total motor volume and was thereby considered of no importance.) A reliable pyrotechnic igniter system was developed which would produce pressures above the minimum ignition pressure within the combustion chamber as well as quickly ignite all the grain surfaces. Initially, the nozzle was blocked by a mylar disc so that the pressure in the motor would rise to a higher level. However, when the disc burst, the depressurization which followed terminated the grain. After discarding the disc, successful ignitions were then achieved by using a boron-potassium-nitrate bag igniter and by spreading a thin layer of propellant dust on the grain surface. By using this technique, sufficient pressure over a long enough period of time for ignition could be obtained.

Chamber pressure was monitored with a 0 to 100-psia Statham strain-gage transducer whose output was recorded on a Consolidated Electrodynamics Corporation 124 oscillograph at a chart-speed of 16 in./sec. The lowest frequency response element in the instrumentation system was a CEC 7-319 galvanometer which had a flat frequency response (5%) to 350 cycles/sec and a natural frequency of 585 cycles/sec. Two Texas Instrument LS223 light sensors were used to follow the visible and near-infrared radiation output. The response of these units was not as good as desired due to radiation attenuation by the deposition of pyrotechnic and propellant combustion products. However, the cessation of radiation emission could be determined in most instances.

Experimental results: A representation of a typical data recording with both a light sensor and the pressure trace is shown in figure 38. Except at higher L*s (400 in.), low-frequency instability was noted prior to termination and, in general, there were two to three full cycles detected. Three pressures are noted in figure 38: (1) P_f, the pressure at which low-frequency instability began; (2) P_c, the normally recorded L* extinction pressure; and (3) P_L, the pressure at which the light sensor trace and pressure trace indicated combustion ceased. In table V are noted typical values of these parameters, the frequency of oscillations, and the test conditions for some of the L* tests.

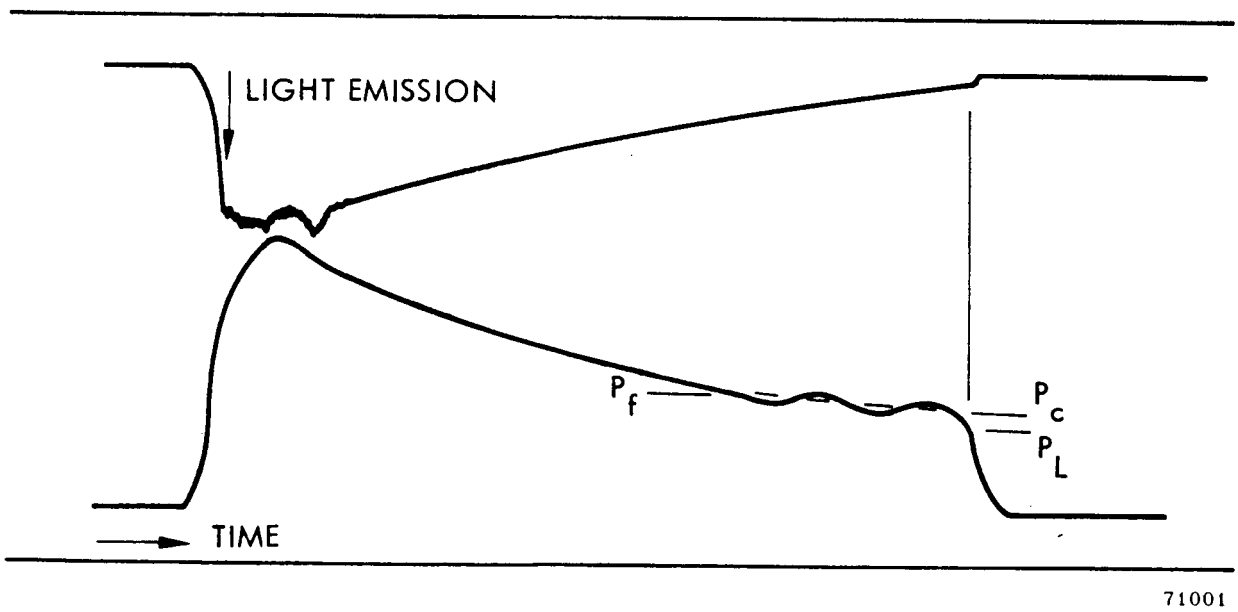

Figure 38. Representative L* Data Trace

TABLE V. - L* TEST DATA

Propellant UTX-	L* in.	P_c psia	P_L psia	P_f psia	Frequency cycles/sec
9715	440	10.7	9.9	not observable	
9717	208	18.2	16.2	28.7	5.5
9713	209	17.4	15.4	21.8	5.5
9715	212	19.6	15.8	28.7	5
9717	96.6	31.5	28.0	36.5	15
9715	97	25.8	22.8	30.0	10
9718	98	22.9	19.0	25.8	10
9713	436	29.7	25.4	not observable	
9713	436	27.8	23.8	not observable	
9717	440	10.3	9.6	not observable	

Examination of these data shows a rough correspondence between the motor L* and the frequency of oscillation. As the L* is decreased, the frequency is increased. The exact cause of the instability is open to question at this time.

In the course of the L* test program, the effect of the polymer or binder was studied as were the effects of oxidizer loading level, burning-rate catalysts, oxidizer coatings, and aluminum-loading level. In all cases the propellants studied were of the same formulation as those used in the $\dot{P}$ program and, where possible, the propellant samples were obtained from the same batches of propellant.

The L* termination characteristics of those propellants formulated with different binders are presented in figures 39 and 40. These data are plotted in the normal manner of ln L* versus ln P_c. As may be noted, the more easily $\dot{P}$-terminated UTREZ and PU propellants are also more easily terminated by L* techniques. That is, these propellants extinguish at higher pressures than do the CTPB and PEP propellants. Because the vacuum tank pressure rose during firing to 1.5 to 2.5 psia, it was impossible to even determine the L* pressure levels of the PBAN propellant. Point A noted on figure 40 indicates that the backpressure level may be important, at least for the PU propellant. Inadvertent use of a larger grain caused both a higher backpressure and a higher termination pressure.

Data obtained by reducing the AP concentration in a series of UTREZ propellants are shown in figure 41. Substitution of fuel for AP was found to increase the L* pressure levels just as the $\dot{P}$ requirements were reduced. Addition of burning rate catalysts which had a slight or negligible effect upon the $\dot{P}$ limits of the basic UTREZ propellants also had no effect upon the L* termination behavior, as shown in figure 42. Similar observations were found for the Kel-F-coated AP propellant, UTX 9757. Comparison with the L* data of figure 43 for the uncoated AP propellant with data for propellants with the same AP loading shows no effect of coating. This pattern was not found to hold with the aluminized UTREZ propellants. While the substitution

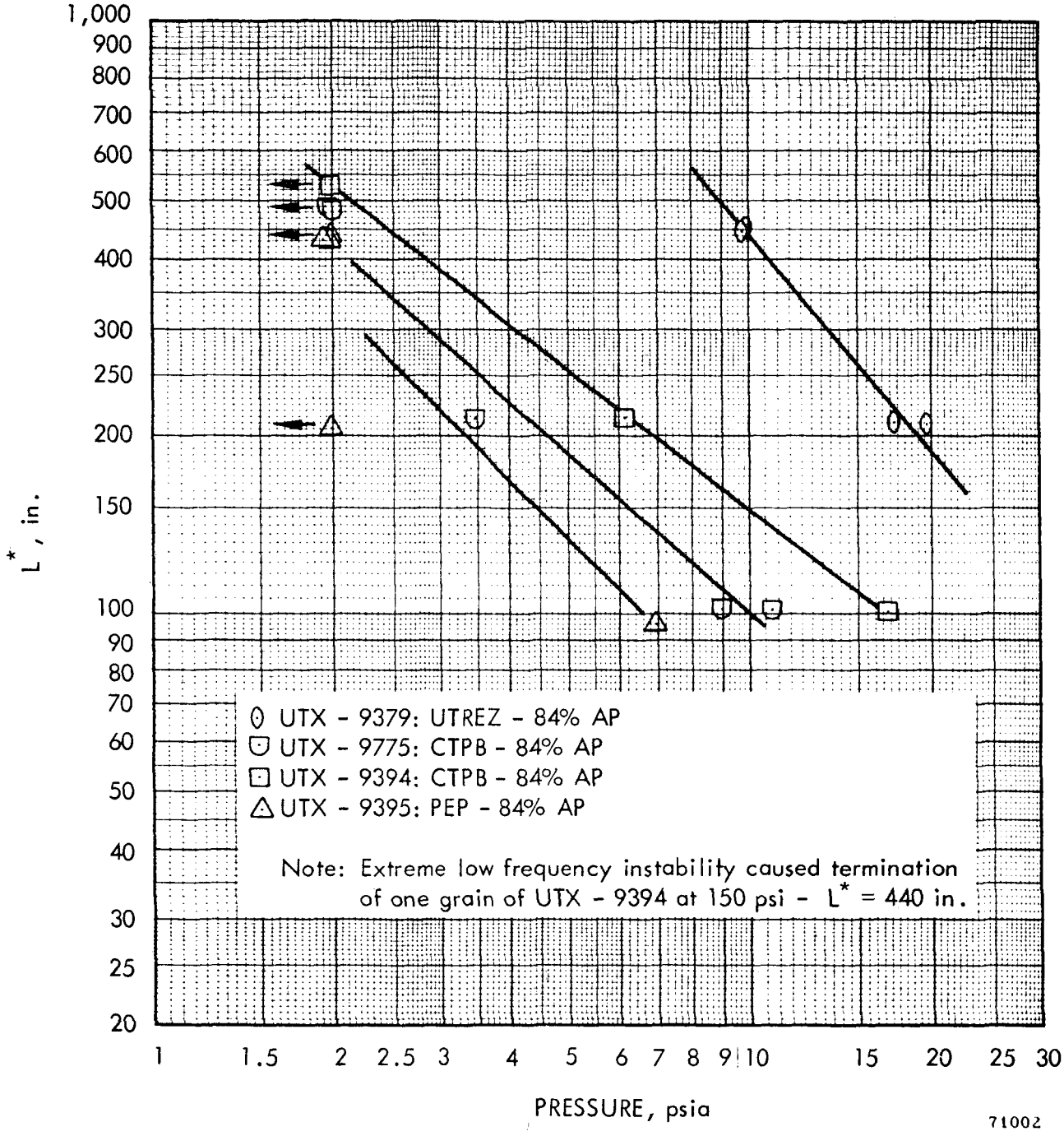

Figure 39. L* Termination Characteristics of UTREZ, CTPB, and PEP Propellants - 84% AP

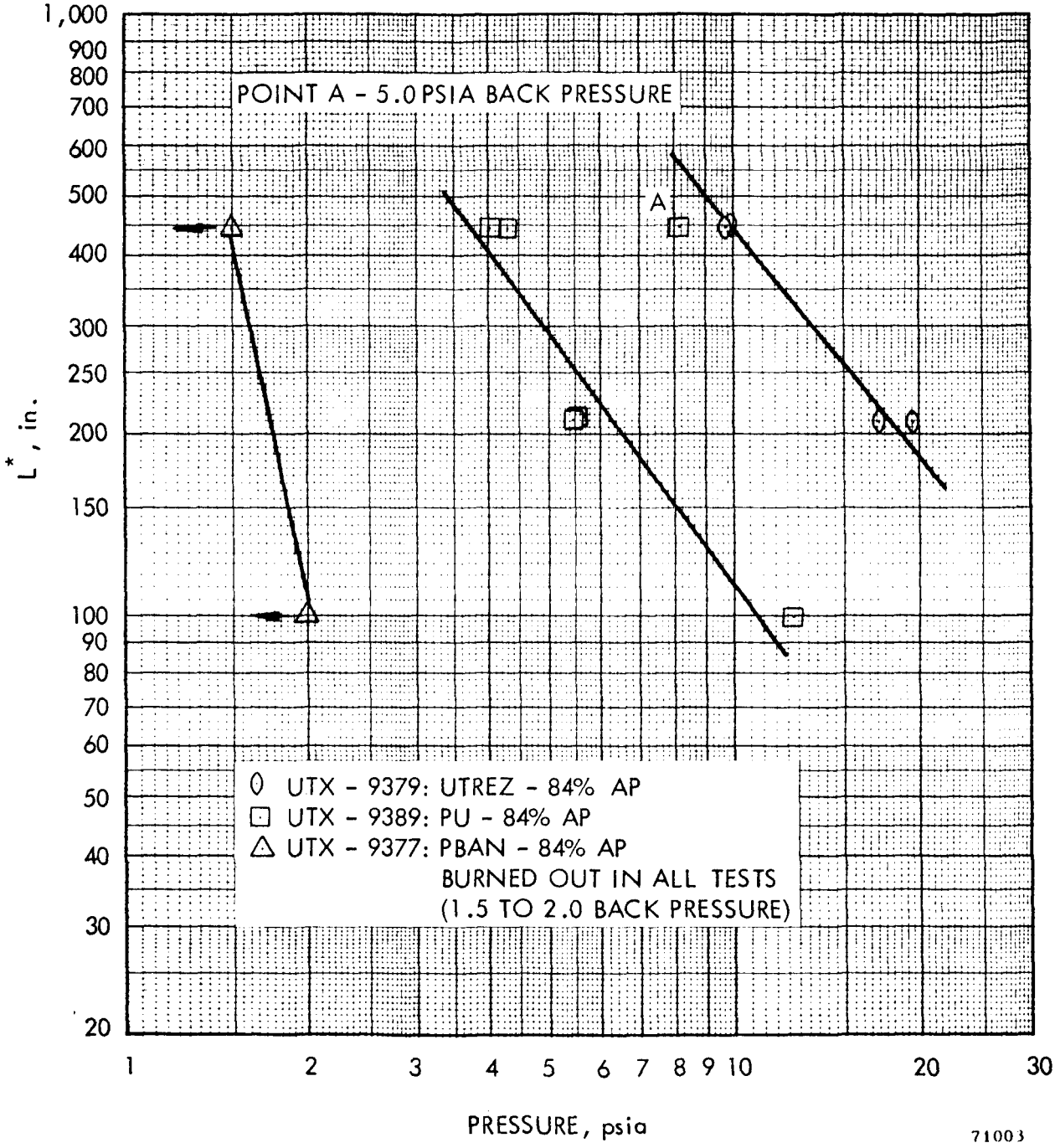

Figure 40. L* Termination Characteristics of Polyurethane, PBAN, and UTREZ Propellants - 84% AP

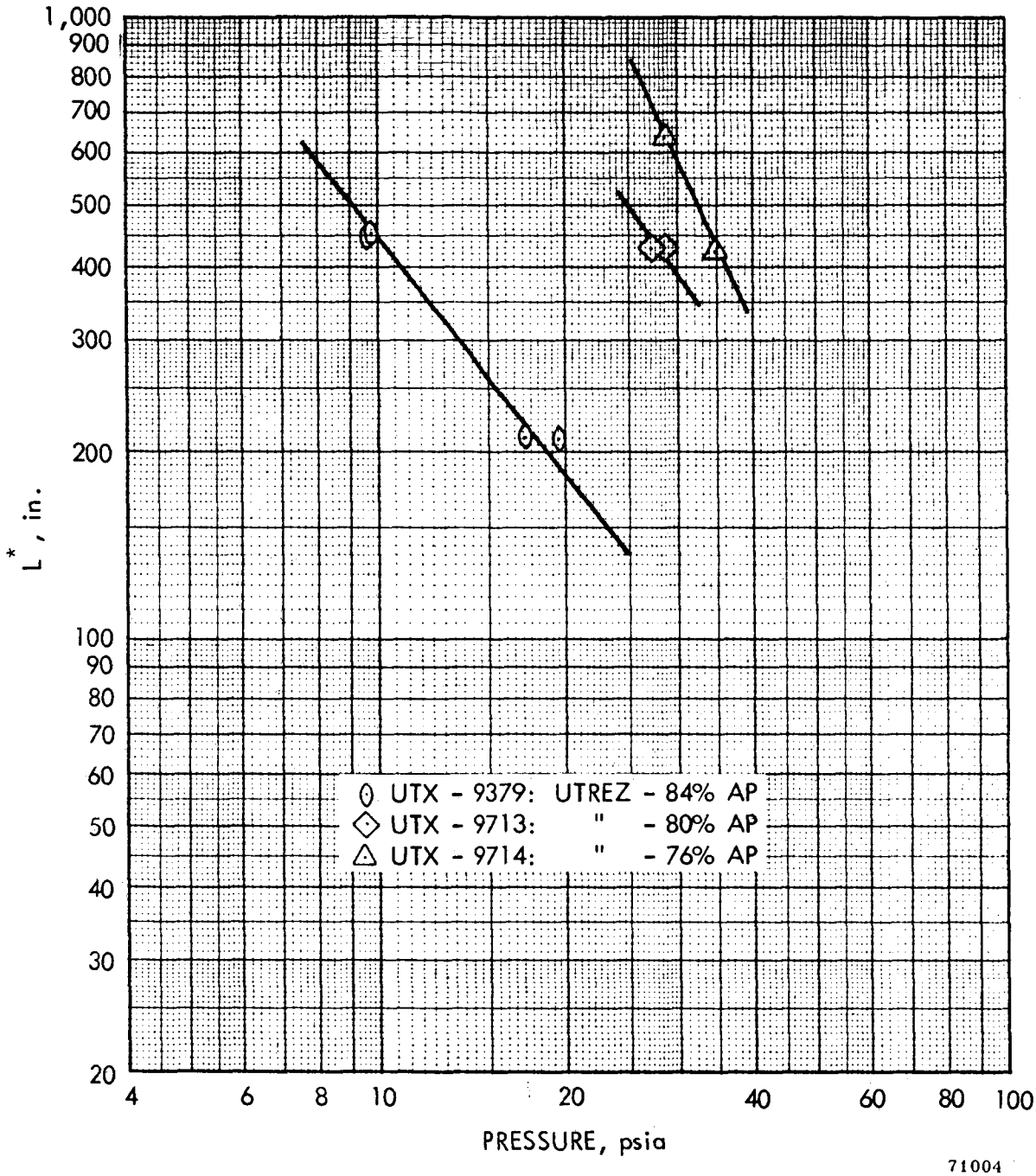

Figure 41. Effect of Oxidizer Loading Level Upon L* Behavior of UTREZ Propellants

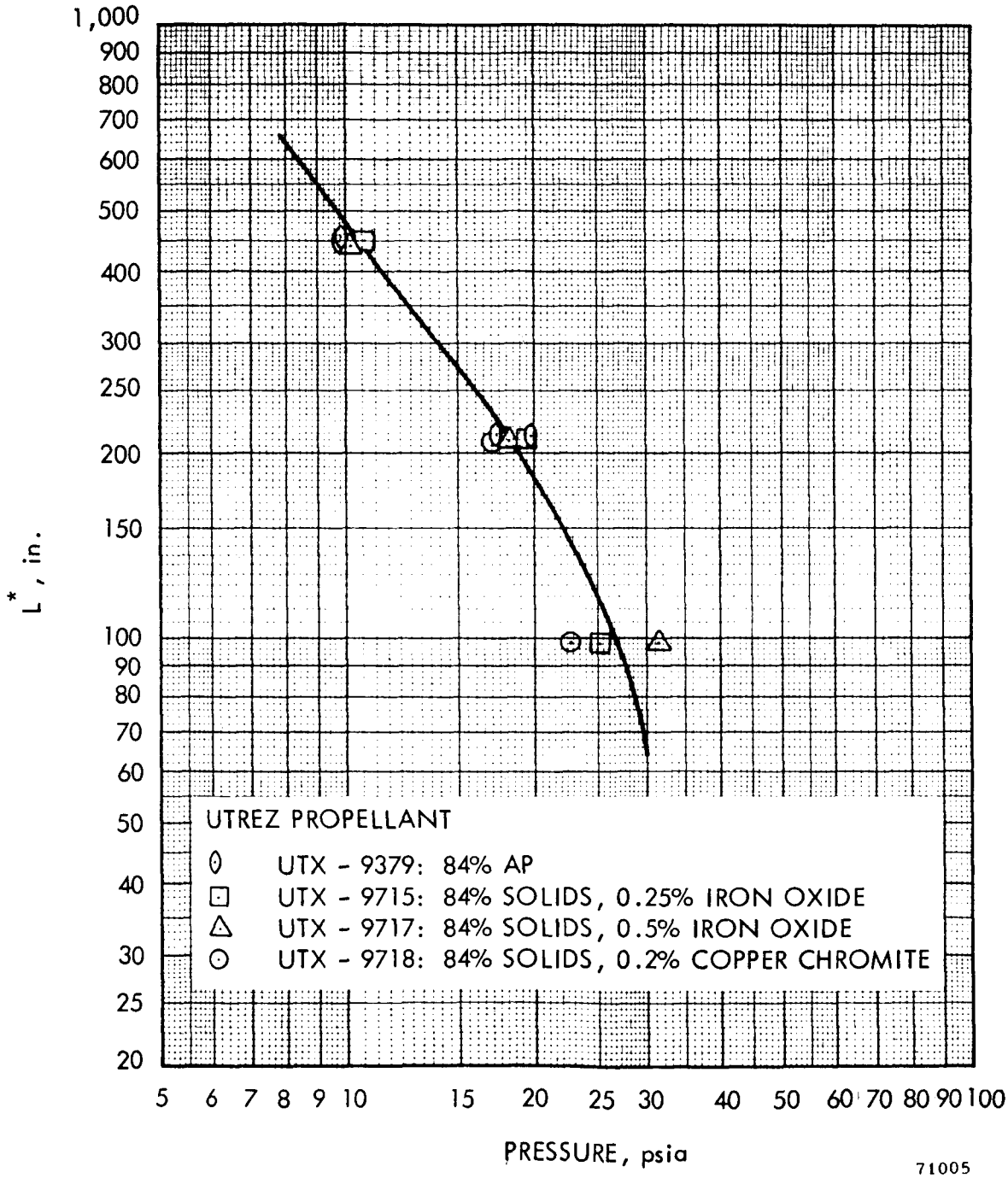

Figure 42. Effect of Catalyst Upon L* Behavior of UTREZ Propellants

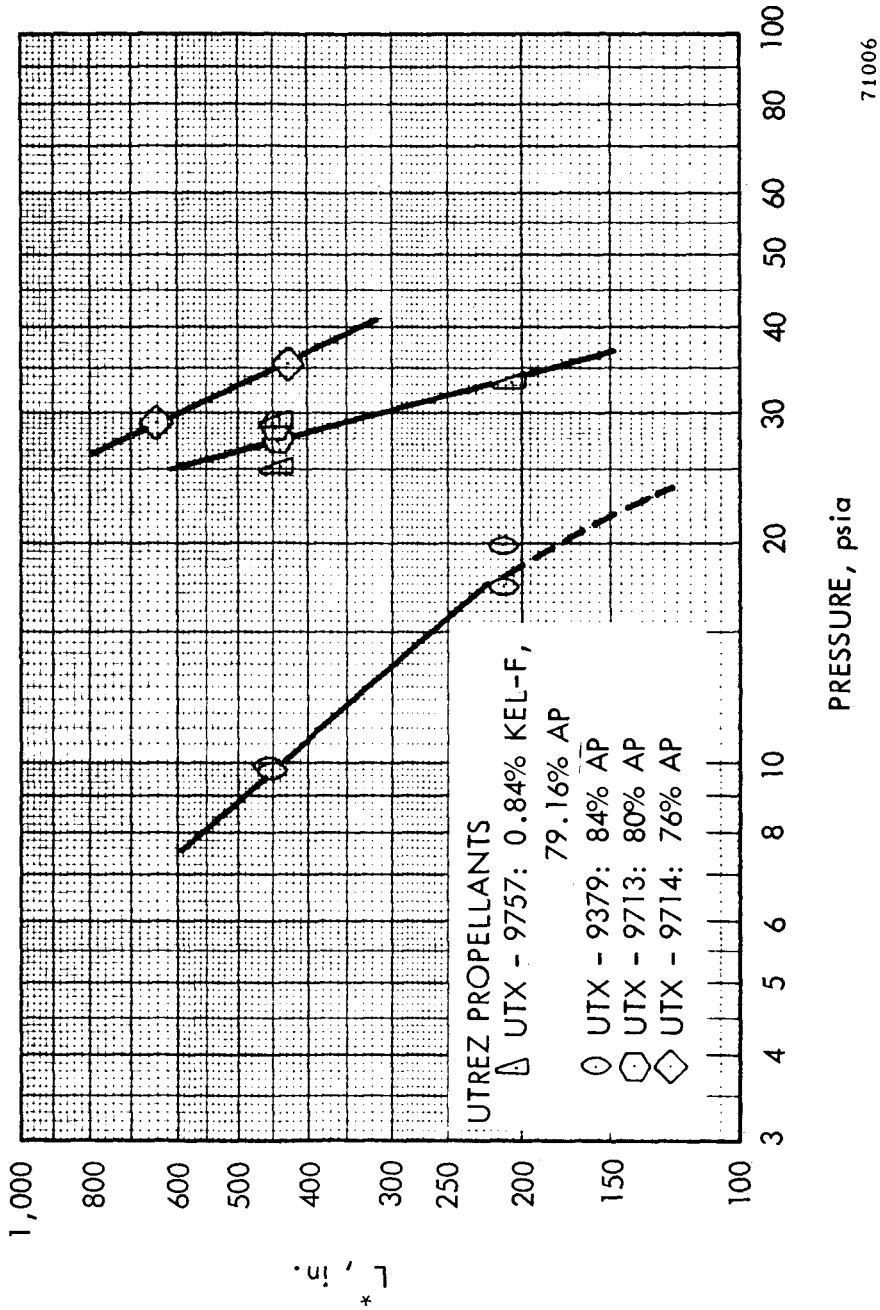

Figure 43. Effect of Kel-F Coating of AP Particles

of aluminum powder for AP resulted in little or no increase of the $\dot{P}$ requirements, a definite increase in the L* pressures resulted as shown in figure 44.

Photomicrographs of the terminated L* grains also yielded some interesting results. All the UTREZ propellant surfaces showed considerable evidence of melting while the aluminized grains showed evidence of aluminum melting and agglomeration. As shown in figure 45-A, the surface of UTX-9714 containing 76% AP and no catalyst or aluminum is covered with a profusion of glassy balls. The surface of the UTX-9379, which is not shown here, was found to be similar to that of the UTX-9714. Milky white to clear balls of what appeared to have once been molten material appeared on about one third of the large AP crystals. The balls were lightly fused at their bases to the large-particle AP surfaces and ranged in diameter from 50 μ to 150 μ. These masses were not all round in shape but ranged from frosty blisters to fully formed balls. Dark flecks of apparently charred polymer could be seen around the outside of the large AP crystals.

The PEP propellant surface shown in figure 45-B also is covered with white balls and globules, but which are attached to the small AP/polymer matrix rather than to the larger AP crystals. The material around the AP crystals is dark as though charred.

The inclusion of 0.5% iron oxide in the UTREZ formulation produced the dark balls depicted in figure 45-C. With the exception of these balls, the surface of the propellant is exceptionally smooth with no large AP crystals protruding from the surface. The glassy hard balls are lightly attached to the surface and easily removed. Less prevalent on the surface are milky white globules of about one-tenth of the diameter of the coarse AP. The majority of the coarse AP is covered with a lacy red network of what could be polymer and iron oxide.

In contrast, the surfaces of copper chromite-containing UTREZ formulation were covered with semitransparent to dark-green glassy balls. The propellant surface was not as smooth as that of the iron-oxide formulations and the coarse AP protrued slightly and was relatively clean.

The PU propellant surface shown in figure 45-D shows the coarse AP protruding from the propellant surface and no evidence of once-molten balls or globules. This type of surface was also observed on the CTPB propellants with the exception that the coarse AP crystals were smooth and clean while the coarse AP on the PU propellants was covered with a white flaky-appearing material which was distinct from the glassy material seen on the UTREZ and PEP propellant surfaces.

A number of the balls were collected from the surfaces of the uncatalyzed UTREZ grains and examined in an attempt to define their composition. As may be noted in figure 45-A, the balls ranged in appearance from transparent uncolored to opaque white. Examination of these balls was performed by placing groups of the balls on the heating element of a hot-stage microscope and observing their behavior as the temperature of the stage was increased slowly. Heating the balls had no effect until the heating element reached 600° to 640°C, at which temperature the transparent balls melted and fused together.

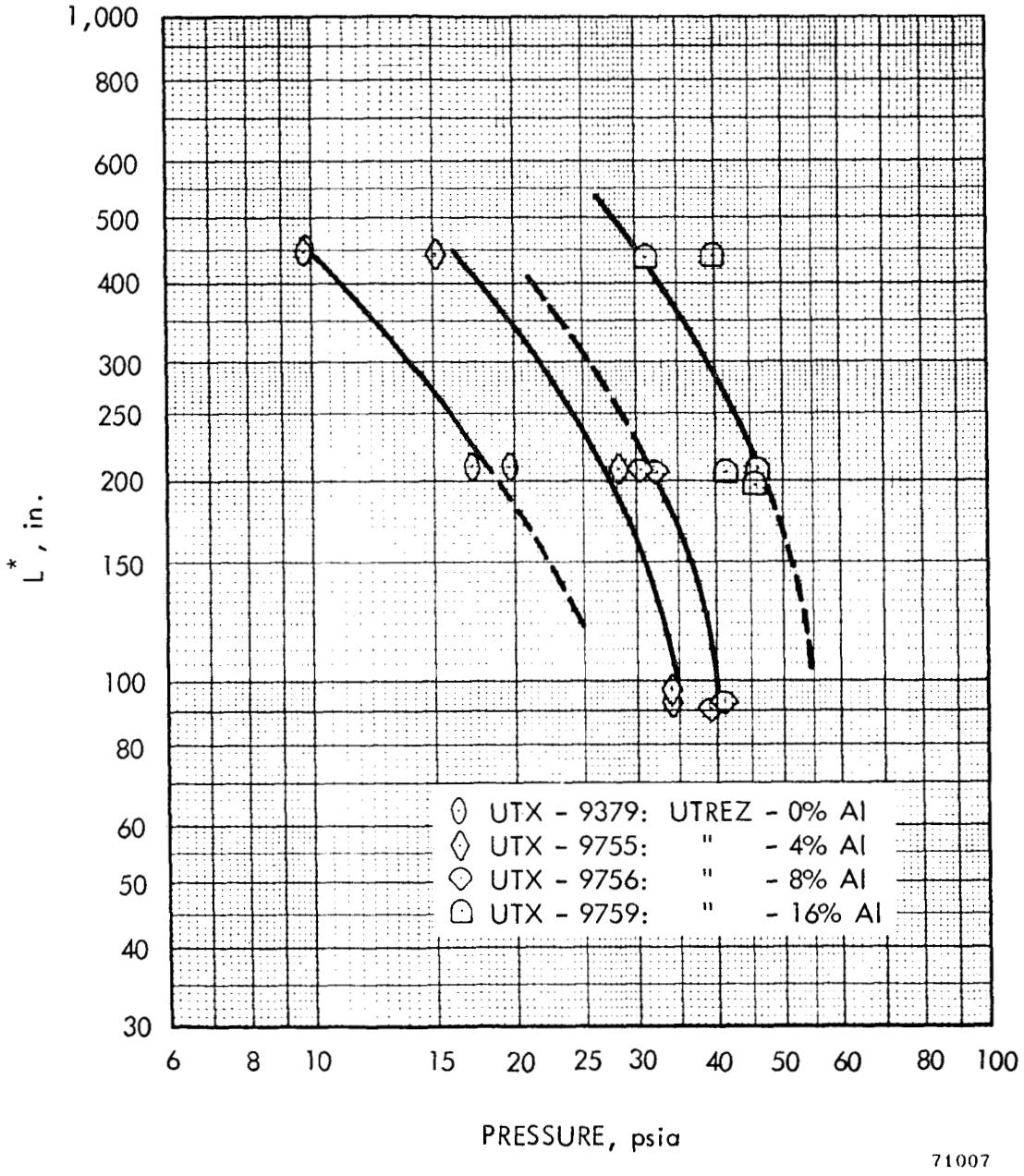

Figure 44. Effect of Aluminum Concentration Upon L* Behavior of UTREZ Propellants

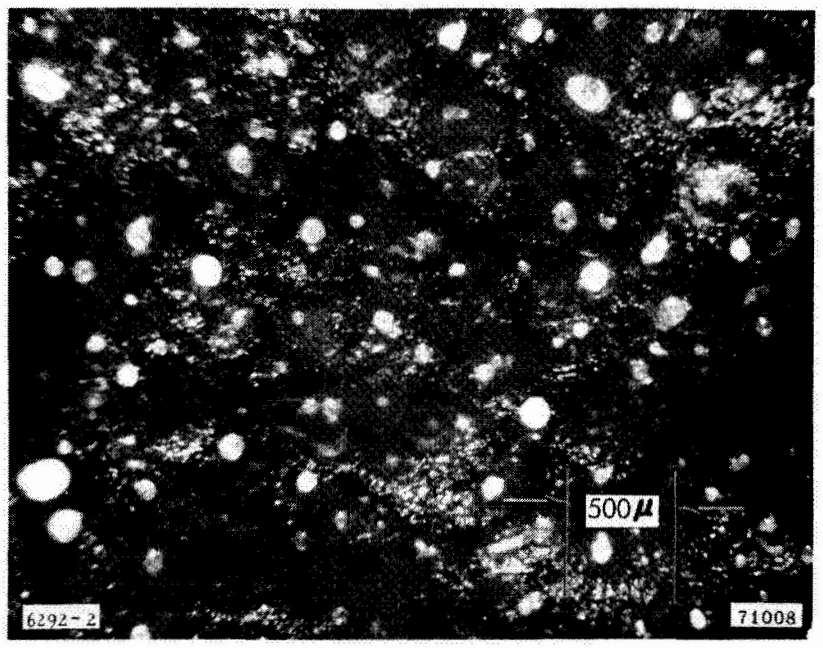

Figure 45-A. UTX-9714: UTREZ - 76% AP

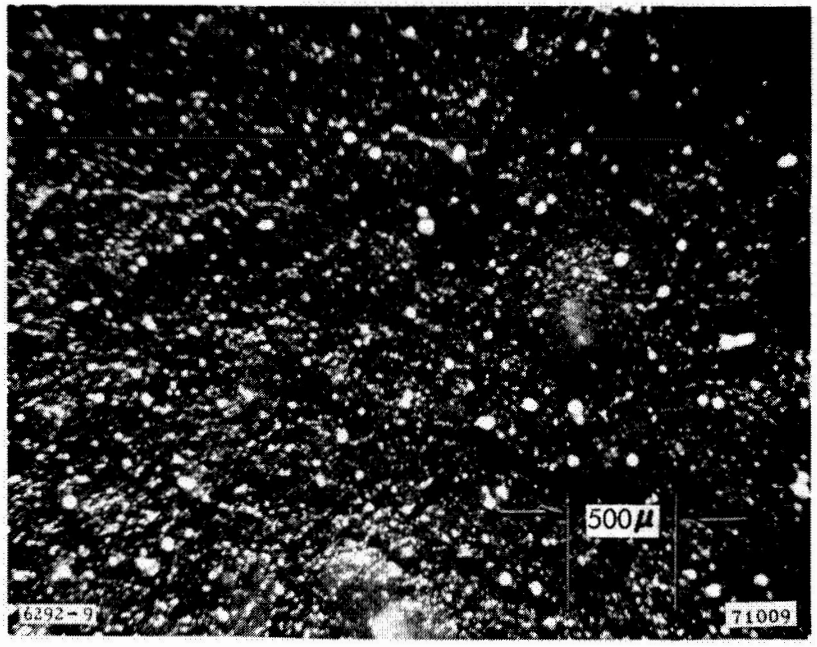

Figure 45-B. UTX-9395: PEP - 84% AP

Figure 45. Photomicrographs of L* Terminated Propellants

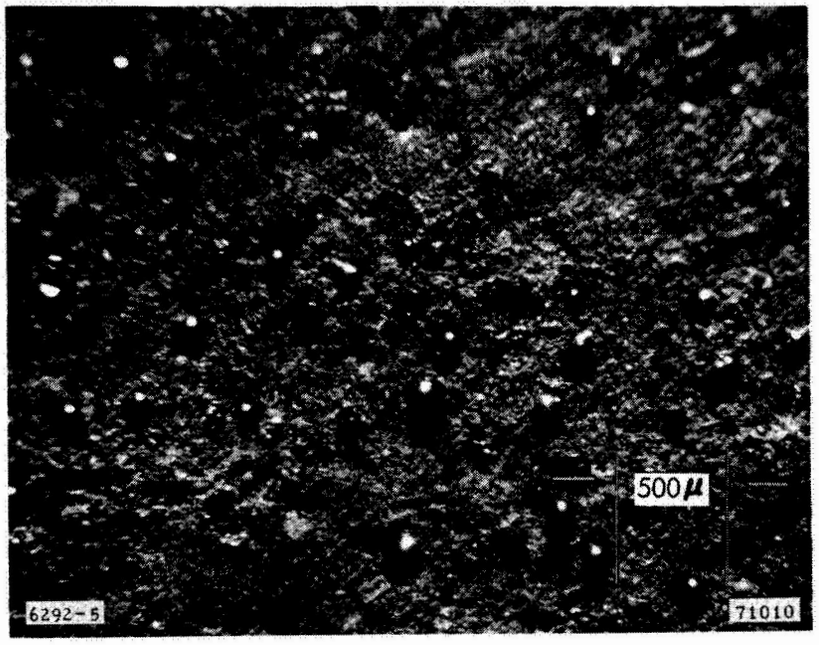

Figure 45-C. UTX-9717: UTREZ - 0.5% Iron Oxide

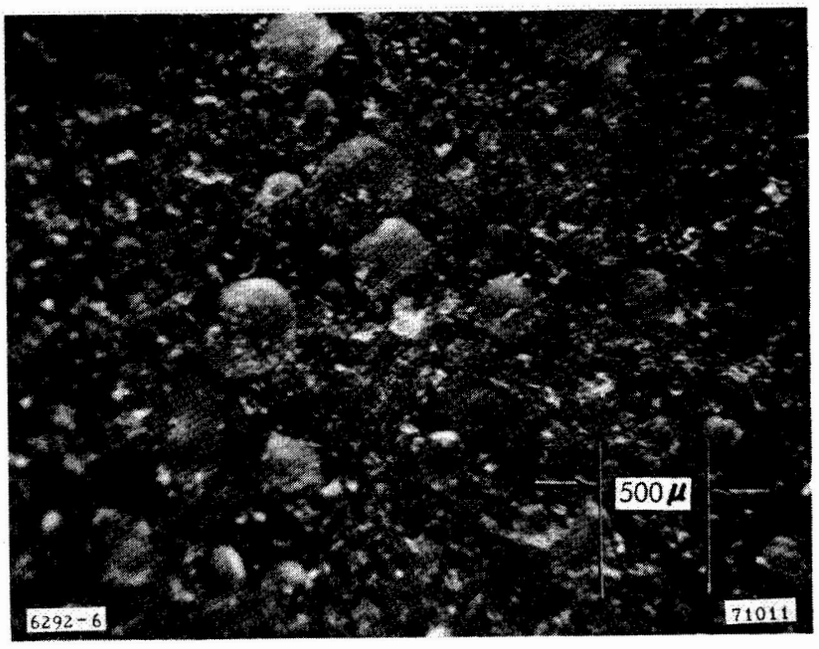

Figure 45-D. UTX-9389: PU - 84% AP

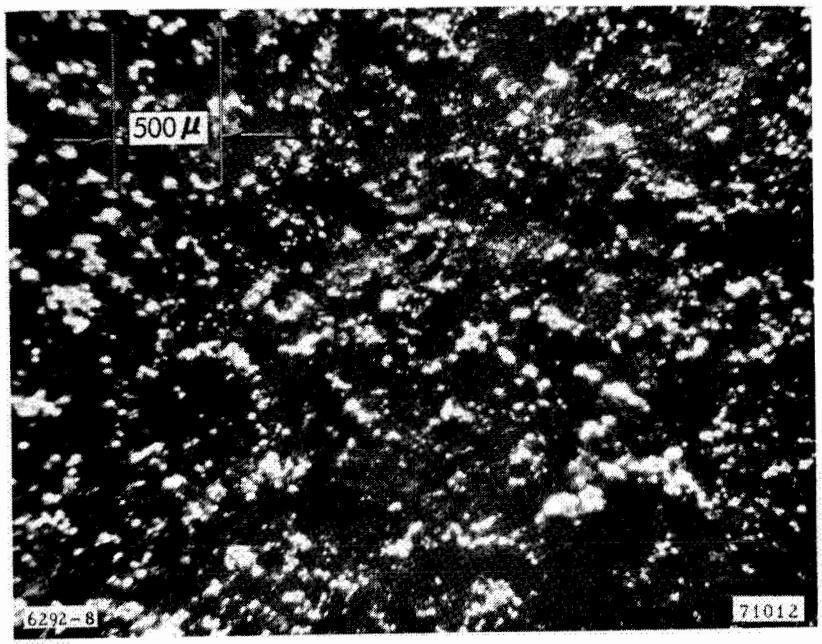

Figure 45-E. UTX-9755: UTREZ - 4% Al

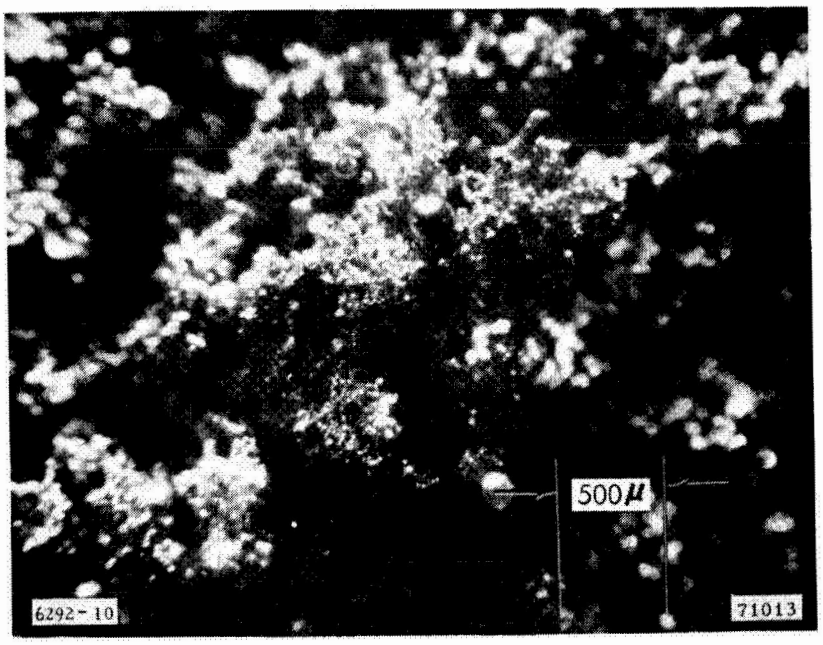

Figure 45-F. UTX-9759: UTREZ - 16% Al

Further heating caused the molten mass to begin boiling and to regress slightly (approximately 20% reduction in volume), but had no effect upon the originally opaque balls. After several minutes of heating at 700°C, no further regression was noted and all the remaining material had the same opaque white coloration. When touched with a scalpel point, the originally opaque balls were easily crumpled, in contrast to their hard structure at room temperature. At 750°C, the surfaces of this type of ball showed melting; however, further heating to 800°C, the upper limit of the hot stage, caused no observable regression or decomposition.

The high-temperature stability of the majority of the ball material indicated that balls were not composed of AP, but must consist primarily of inorganic impurities present in the AP. The major impurity in the AP used in this program was 0.2% tricalcium phosphate (m.p. 1620°C) which is added to prevent caking and agglomeration of the AP crystals. Other minor contaminants are sodium chlorate (.002 wt.%, m.p. 248-261°C), ammonium chloride (.014%, s. 335°C), and sodium bromate (.001%, m.p. 381°C).

When some of the high-temperature residue was placed in a high-temperature gas flame along with a small amount of tricalcium phosphate, both materials melted nearly at the same time and had the same general appearance. A phosphomolybdate analysis was then run using a fraction of milligram of the collected balls. The test results showed a positive indication of phosphate ions.

Based on these results and other observations, it is concluded that the balls found on both the $\dot{P}$- and L*-terminated grains are composed primarily of tricalcium phosphate with lesser amounts of other contaminants and possibly once molten AP. Tests to show whether the balls also contained significant amounts or any AP were inconclusive. A few milligrams of the balls were collected and analyzed using a differential scanning calorimeter. The data trace showed a 240°C endotherm and higher temperature exotherms indicative of AP. After having been heated to 500°C, the upper limit of the unit, the sample was weighed and found to have lost 0.4 mg or 15% of the original material. It is impossible, however, to state whether the lost material was originally an integral part of the balls or was merely fine AP which was picked up with the balls when they were collected. The hot stage studies did not indicate any AP present, but decomposition of 15% of the total mass over several hundred degrees of heating would not be readily discernible.

Any catalysts present were evidently picked up in the molten balls and globules; resulting in the dark balls seen on the iron-oxide catalyzed propellant surfaces and the glassy green balls seen on the copper-chromite catalyzed propellant surfaces. What effect this phenomenon or the molten material itself has upon steady-state or transient combustion phenomena is open to speculation. It is possible that if the melt is extensive it may have significant effect upon oscillatory combustion behavior. Also, the fact that the melt absorbs combustion catalysts or products of the catalysts might indicate that the melt may influence both steady-state combustion behavior and the propellant termination requirements.

As with the $\dot{P}$-terminated grains, the UTREZ propellants containing aluminum were found to be covered with a network of small sintered aluminum balls, much

larger aluminum balls, and glassy balls enmeshed in the aluminum network. As can be seen in figures 45-E and F, these networks are much more extensive than those in the $\dot{P}$ grains. In the case of 16% aluminum concentration, the sintered networks extend 0.05 to 0.1 in. above the propellant surface. At the point of focus on figure 45-F is a large aluminum ball at the top of the network. To the right and below on the picture are two glassy balls connected to another portion of the network. The aluminum evidently melted on or near the surface, followed by sintering into networks of aluminum balls. This process then culminated by further melting and the formation of the large balls of aluminum.

DISCUSSION AND ANALYSIS

To provide both insight into the mechanisms of combustion termination and a basis for engineering correlations for the design of controllable solid propellant motors, it is desirable to develop a model of the processes occurring during combustion termination. As noted by Coates,[16] there are several analyses of termination behavior of varying degrees of complexity,[1,2,4,17,18] but perhaps the most useful is the Von Elbe[1] analysis or modified versions developed by Paul[2] and Summerfield and Parker.[18] Though developed from different premises, all three models yield a common expression for the transient burning rate during rapid depressurization

$$\dot{r} = \bar{r}\left(1 + \frac{1}{\lambda}\,\frac{n\,\alpha}{\bar{r}^{\,2}}\,\frac{1}{P}\,\frac{dP}{dt}\right) \qquad (1)$$

where $\dot{r}$ is the transient burning rate, $\bar{r}$ is the steady-state burning rate at pressure, P, and is related to pressure by $\bar{r} = aP^n$; α is the propellant thermal diffusivity, and λ is a constant with a value of one-half for the Von Elbe model, 1 for the Paul model, and 2 for the Summerfield model. At the point of extinction, $\dot{r}$ is zero and the criteria for extinction is given by

$$\frac{dP}{dt} = -\lambda\,\frac{\bar{r}^{\,2}}{n\,\alpha}\,.\,P \qquad (2)$$

To evaluate the utility of equation (2), the data in table VI were prepared for all the propellants studied during the course of this program. While equation (2) is based on the pressure, rate of depressurization, and burning rate at the point of extinguishment, it is difficult to establish this information exactly from experiment. Thus the data of table VI were prepared using the burning rate at 500 psi and a pressure of 500 psi. α was calculated assuming for the nonaluminized propellants

$$k = 8 \times 10^{-4}\ \text{cal/cm-sec°K},\ \rho = 1.65\ \text{g/cm}^3,\ \text{and}\ C_p = 0.3\ \text{cal/g°K}$$

In calculating the value of α for the aluminized propellants, these values were increased slightly to accomodate the higher thermal conductivity and density of the aluminum. Using these values, the values of $P\bar{r}^{\,2}/n\alpha$ were calculated. These and the experimentally measured rates of depressurization required for extinction are compared in figure 46. Examination of figure 46 reveals that the predicted rates of depressurization ($-P\bar{r}^{\,2}/n\alpha$) are 4 to 10 times the magnitudes actually required. The experimental data for the polybutadiene propellants agree more closely with the predicted values than do

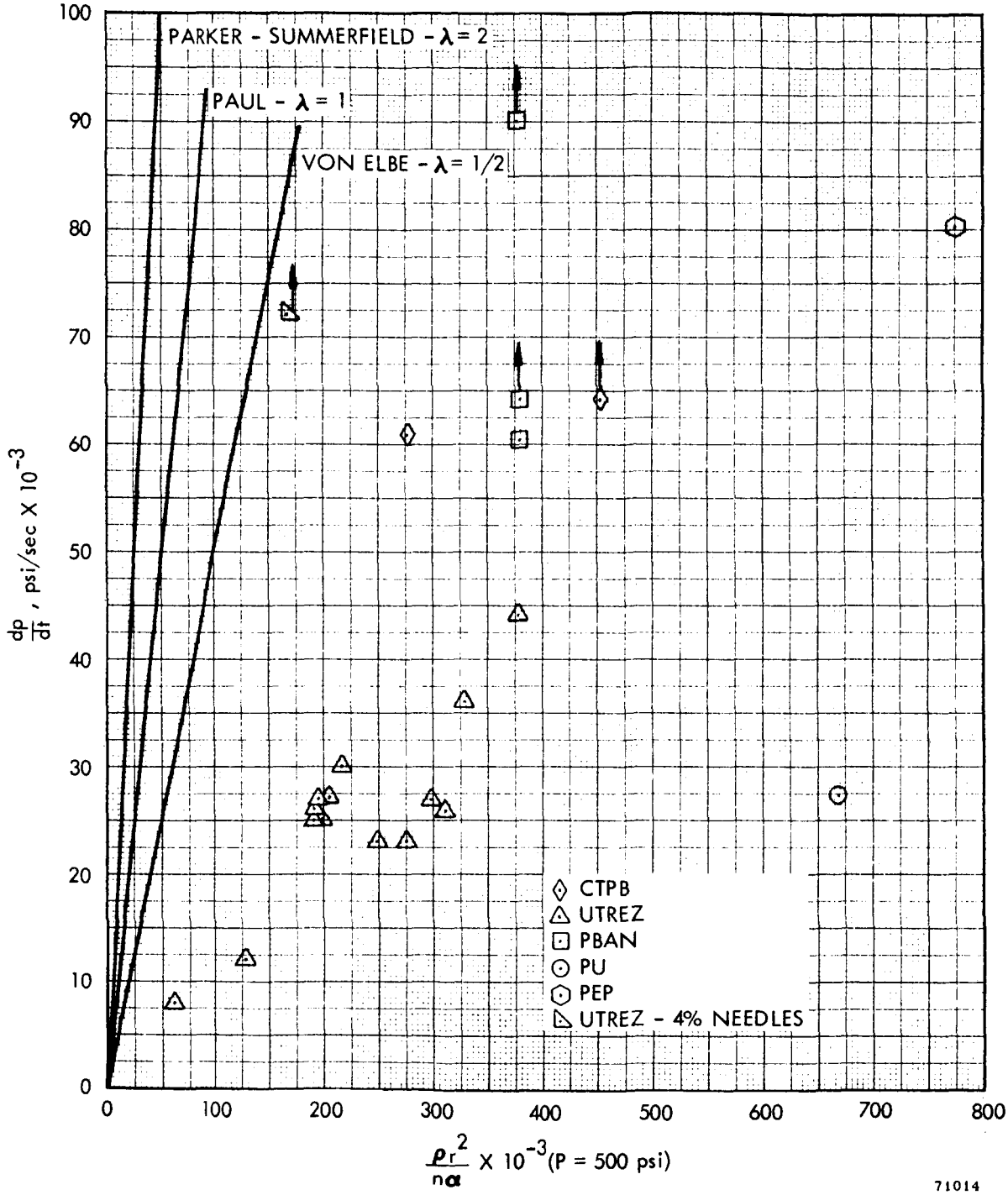

Figure 46. Predicted Termination Requirement vs Experimental Results (500 psi)

the UTREZ, PEP, and PU propellants. This is in agreement with results obtained by other workers[19] using PBAA propellants.

TABLE VI. - PREDICTED AND EXPERIMENTAL DEPRESSURIZATION RATES (500 psi)

Propellant UTX-	Binder	$\dot{r}$ at 500 psi	n	$-P\dot{r}^2/n\alpha$	Experimental -dP/dt at 500 psi
9377-1	PBAN	0.270	0.384	380 000	44 000
9377-2	PBAN	0.270	0.384	380 000	>90 000
9379	UTREZ	0.185	0.364	192 000	25 000
9389	PU	0.255	0.195	670 000	27 000
9394	CTPB	0.230	0.384	280 000	61 000
9395	PEP	0.301	0.231	780 000	80 000
9710	UTREZ	0.180	0.325	197 000	27 000
9711	PBAN	0.255	0.384	340 000	>60 000
9712	UTREZ	0.187	0.364	192 000	26 000
9713	UTREZ - 80% AP	0.145	0.325	129 000	12 000
9714	UTREZ - 76% AP	0.10	0.325	62 000	8 000
9715	UTREZ	0.213	0.364	250 000	23 000
9717	UTREZ	0.230	0.384	276 000	23 000
9718	UTREZ	0.276	0.488	312 000	26 000
9719	UTREZ	0.290	0.510	330 000	36 000
9720	UTREZ	0.265	0.467	300 000	27 000
9775	CTPB	0.280	0.345	455 000	>64 000
9379-4	PBAN	0.270	0.384	380 000	64 000
9755	UTREZ - 4% Al	0.17	0.25	207 000	27 000
9756	UTREZ - 8% Al	0.185	0.26	218 000	30 000
9759	UTREZ - 16% Al	0.163	0.195	198 000	25 000
9772	UTREZ - 4% ndls	0.33	0.445	170 000	>72 000
9754	UTREZ - 400μ AP	0.1	0.18	111 000	36 000

It should be pointed out, however, that combustion is not terminated immediately upon depressurization, but at a lower pressure and lower rate of depressurization. According to the Von Elbe type of analysis, the depressurization rate upon extinction is related to pressure by

$$\frac{dP}{dt} \propto P^{2n+1} \tag{3}$$

while, to a good approximation, the actual depressurization rate of the motor at any time is directly related to pressure. Thus, though the initial rates of motor depressurization are far less than the predicted, depressurization rates ($P\dot{r}^2/n\alpha$) based on the initial chamber pressure; there will be more agreement as the pressure in the motor falls. If it is assumed that extinction actually occurs at 100 psi, then the predicted critical rates of depressurization would be much less and would more closely approach the

experimental depressurization rates. This is shown in table VII and figure 47, where dP/dt_{pred} was scaled down from the 500 psi values of table VI by the ratio of $(100/500)^{2n+1}$ and the experimental rates were scaled down by the ratio of (100/500). Though better agreement between the predicted rates and the experimental rates is shown, there is still a divergence and a difference between the different binder systems. If the exact pressures and depressurization rates at extinction could be used for comparison, perhaps these differences would not be as great. This point certainly deserves more attention in future studies. That the difference between binder systems is real is illustrated by examining the burning rate data of figure 6. Over the

TABLE VII. - PREDICTED AND EXPERIMENTAL DEPRESSURIZATION RATES (100 psi)

Propellant binder	n	$\left(\frac{100}{500}\right)^{2n}$	$\left(\frac{P\bar{r}^2}{n\,\alpha}\right)\left(\frac{100}{500}\right)^{2n+1}$	$\frac{dP}{dt}\Big/_{exp} \cdot \frac{100}{500}$
PBAN	0.384	0.29	14 400	8 800
PBAN	0.384	0.29	14 400	>18 000
UTREZ	0.364	0.31	11 900	5 000
PU	0.195	0.534	71 500	5 400
CTPB	0.384	0.29	16 200	12 200
PEP	0.231	0.475	74 000	16 000
UTREZ	0.325	0.35	13 800	5 400
PBAN	0.384	0.29	19 700	>12 000
UTREZ	0.364	0.31	11 900	5 200
UTREZ - 80% AP	0.325	0.35	9 100	2 400
UTREZ - 76% AP	0.325	0.35	4 300	1 600
UTREZ	0.364	0.31	15 500	4 600
UTREZ	0.384	0.29	16 000	4 600
UTREZ	0.488	0.208	13 000	5 200
UTREZ	0.510	0.194	12 800	7 200
UTREZ	0.467	0.225	13 400	5 400
CTPB	0.345	0.33	30 000	>12 800
PBAN	0.384	0.29	22 000	12 800
UTREZ - 4% Al	0.250	0.448	18 500	5 400
UTREZ - 8% Al	0.260	0.433	18 900	6 000
UTREZ -16% Al	0.195	0.534	21 200	5 000
UTREZ - 4% ndls	0.445	0.24	8 200	>14 400
UTREZ - 400μ AP	0.18	0.56	12 400	7 200

pressure range of 250 to 500 psi, the PU and polybutadiene propellants have nearly identical burning rates. Thus, use of the Von Elbe model would predict nearly identical depressurization rates, though this was not found to be true. Though the PU propellant burning rates are much higher than the UTREZ propellant burning rates, these propellants have similar termination characteristics. Furthermore, the addition of burning rate catalysts to the basic UTREZ propellant caused large increases in the burning rates. Thus, increased termination requirements would be predicted though little difference was noted experimentally.

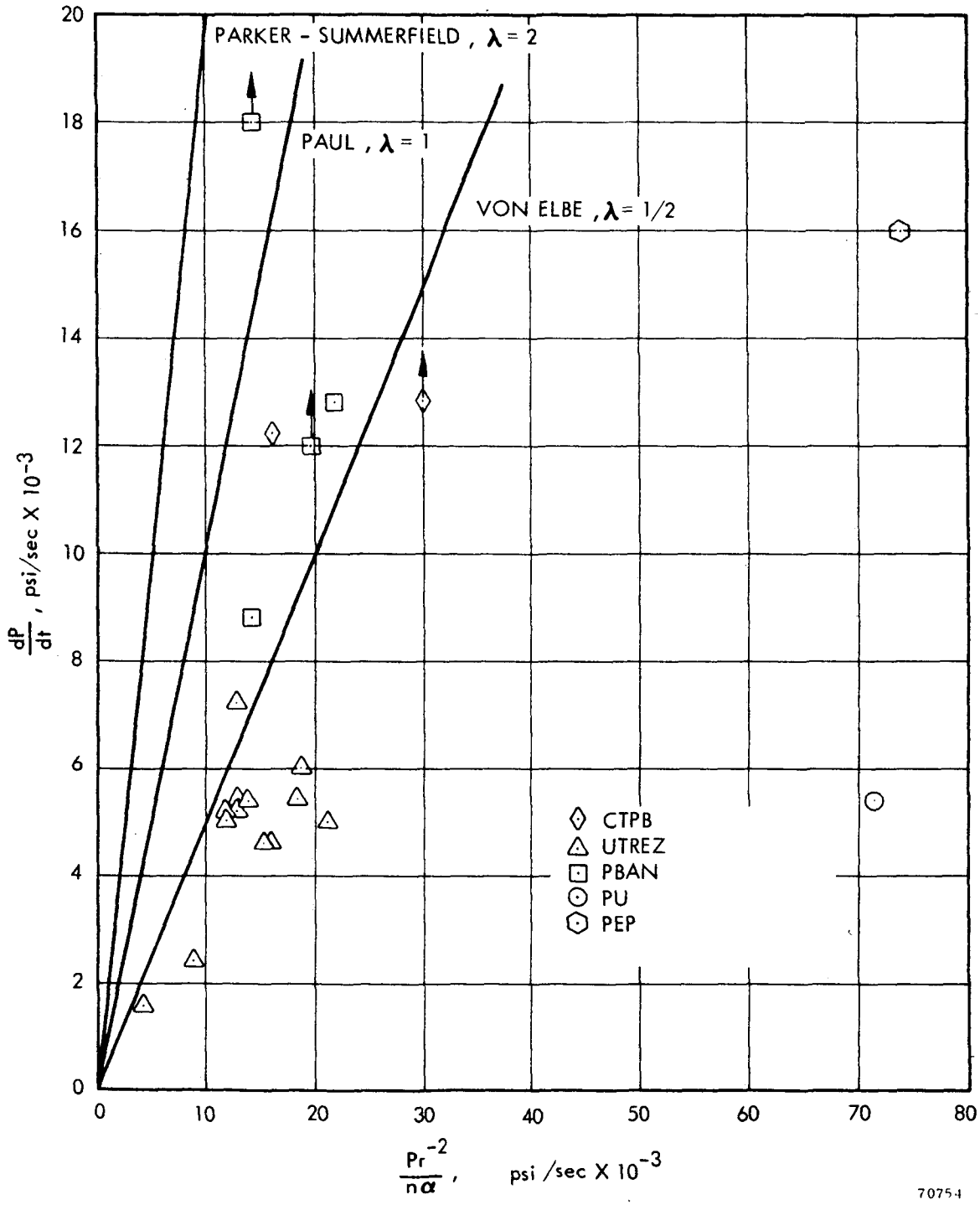

Figure 47. Predicted Termination Requirement vs Experimental Requirements (100 psi)

The difference between the binder systems is not unexpected. The major differences between the tested formulations are the oxidative and thermal degradative properties of the binders. There is a paucity of quantitative information concerning the degradation and combustion of the five polymer systems; however, the available information[20,21,22,23] indicates that the more easily terminated PU and UTREZ formulations are less subject to exothermic (oxidative) degradation of the polymer and are more easily degraded by endothermic thermal decomposition. Contrarily, the CTPB and PBAN polymers should show greater susceptibility to oxidative degradation and less to thermal degradation.

In addition to the polybutadiene polymers being more reactive than polyurethane, Reed, et al,[24] have noted that the heat of combustion of polybutadiene polymer is greater than that of polyurethane or polyether polymers. In a more speculative vein, it also was postulated that the emissivity of the carbonaceous pryolyzed binder species of oxygenated binder systems is much higher. Thus, propellants formulated with polybutadiene should have lower minimum P_{dl}s, as demonstrated by Reed, and should be less readily extinguished by rapid depressurization or L* techniques as was found to be true in the course of this program.

The lower P_{dl} limits found by Reed for the polybutadiene propellants do, in fact, correspond with reduced L* extinction requirements shown in the section entitled "L* Studies." The minimum deflagration pressure, as it is generally determined, is the L* extinction pressure for a motor of essentially infinite L*. Whether or not the minimum deflagration pressure is the minimum ignition pressure is a question which has not been resolved, since there is experimental evidence to support both viewpoints. If these pressures are different, it would be expected that P* would be the higher pressure.

Reed and coworkers have also found that aluminized propellants containing 11% to 12% of hydroxyl or carboxyl terminated saturated binder (hydrogenated polybutadiene) had higher P_{dl}s than similar CTPB propellants. Since the heats of combustion are essentially the same, these differences may be due to the greater susceptibility to oxidative and thermal degradation of unsaturated CTPB binder. This difference in P_{dl} indicates that propellants formulated with the hydroxyl and carboxyl saturated binders should be more easily terminated by rapid depressurization of L* techniques. As shown in the previous sections, this was also found to be true for the saturated polymer, polyisobutylene, with terminal carboxyl groups.

Comparison of the termination characteristics with concurrent ignition studies[11] being conducted at UTC shows the ease of combustion termination to be inversely related to the ease of propellant ignition. These studies, substantiated by other investigators,[4] show those propellants with high ignition pressures (or minimum P_{dl}s) are more easily terminated by $\dot{P}$ and L* techniques than those propellants with lower ignition pressures. Data[11] presented in figure 48 shows the more easily terminated PU and UTREZ propellants containing AP to have higher minimum ignition pressures than do those propellants formulated with CTPB and PBAN binders. (The effect of flux level upon ignition delay at different pressure levels is shown for the UTREZ propellant in

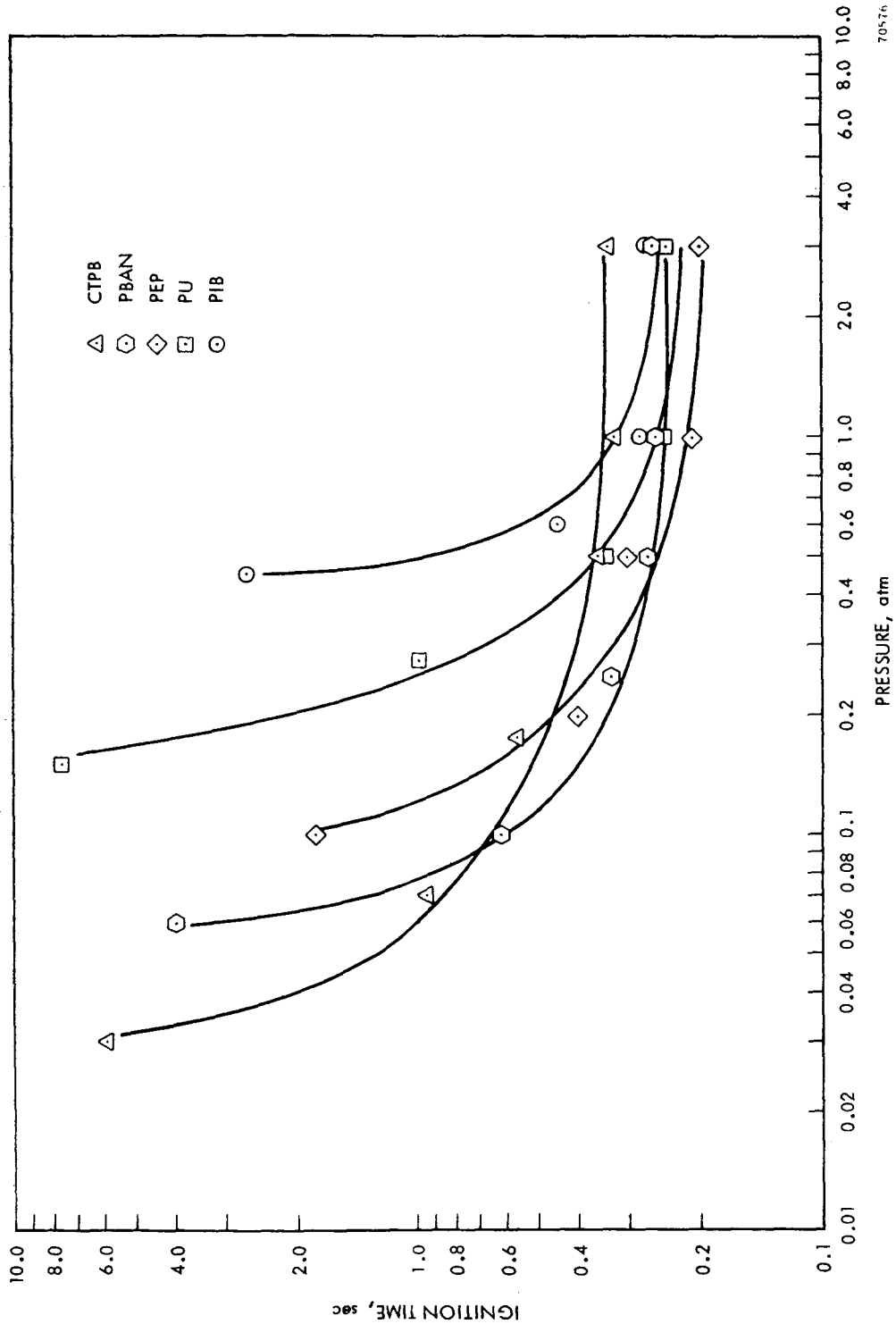

Figure 48. Effect of Polymer in Arc-Image Furnace Delays as a Function of Environmental Pressure (N_2) for a Constant Flux Level

figure 49.) The data shown in figures 48 and 49 are for essentially the same propellant formulations as were tested in the course of this program, with the exception that the ignition study propellants contained 0.25% iron oxide. Ignition studies showed, however, that catalysts have little effect upon ignition behavior.

The ignition studies also showed that the effect of binder differences upon ignition behavior is most pronounced in the range of P* to 1.0 atm. Since these differences can be related primarily to the oxidative and thermal degradation characteristics of the binder, termination characterization studies conducted at exhaust pressures in this range might also show greater differences in binder effects, thereby permitting greater discrimination of combustion termination mechanisms. This was partially demonstrated by SRI studies[4] where the exhaust pressure was shown to significantly affect combustion termination behavior. Since many potential controllable solid rocket motors would be operating at altitudes where the exhaust pressure is in the range of the ignition pressure, the effect of exhaust pressure deserves study from both design and mechanistic viewpoints.

As was noted in the section entitled "Additive Effects," increasing the binder content of an AP/PIB formulation reduces the depressurization rates required for combustion termination. These data show that at 500 psi, the depressurization rate required for extinguishment was reduced from -20 000 psi/sec for 84% AP to -9000 psi/sec for an 80% AP formulation. Increasing the oxidizer concentration in the propellant formulation has the potential of increasing the concentration of reactive species. Hence, the contribution of surface and subsurface reactions to the overall process may be increased, making the propellant less susceptible to extinction. Increasing the oxidizer concentration would also increase the heat of combustion, thereby possibly increasing the heat feedback to the propellant surface and making combustion termination more difficult. More importantly, however, the lesser fuel concentration on the propellant surface and subsequent reduced endothermic pyrolysis would also tend to increase the termination requirements.

Additive Effects: Iron oxide and copper chromite burning rate catalysts were selected for study because of their demonstrated effects as burning rate promoters, AP decomposition catalysts, and polymer degradation catalysts. While both agents function to increase propellant burning rate, they do not function necessarily in the same manner.[25] In fact, there are six possible reaction mechanisms which can be influenced in different ways by these catalysts as follows:

1. AP solid phase decomposition (exothermic above 300 mm Hg)
2. AP decomposition to gaseous species
3. Exothermic oxidation of fuel prior to pyrolysis
4. Endothermic fuel pyrolysis

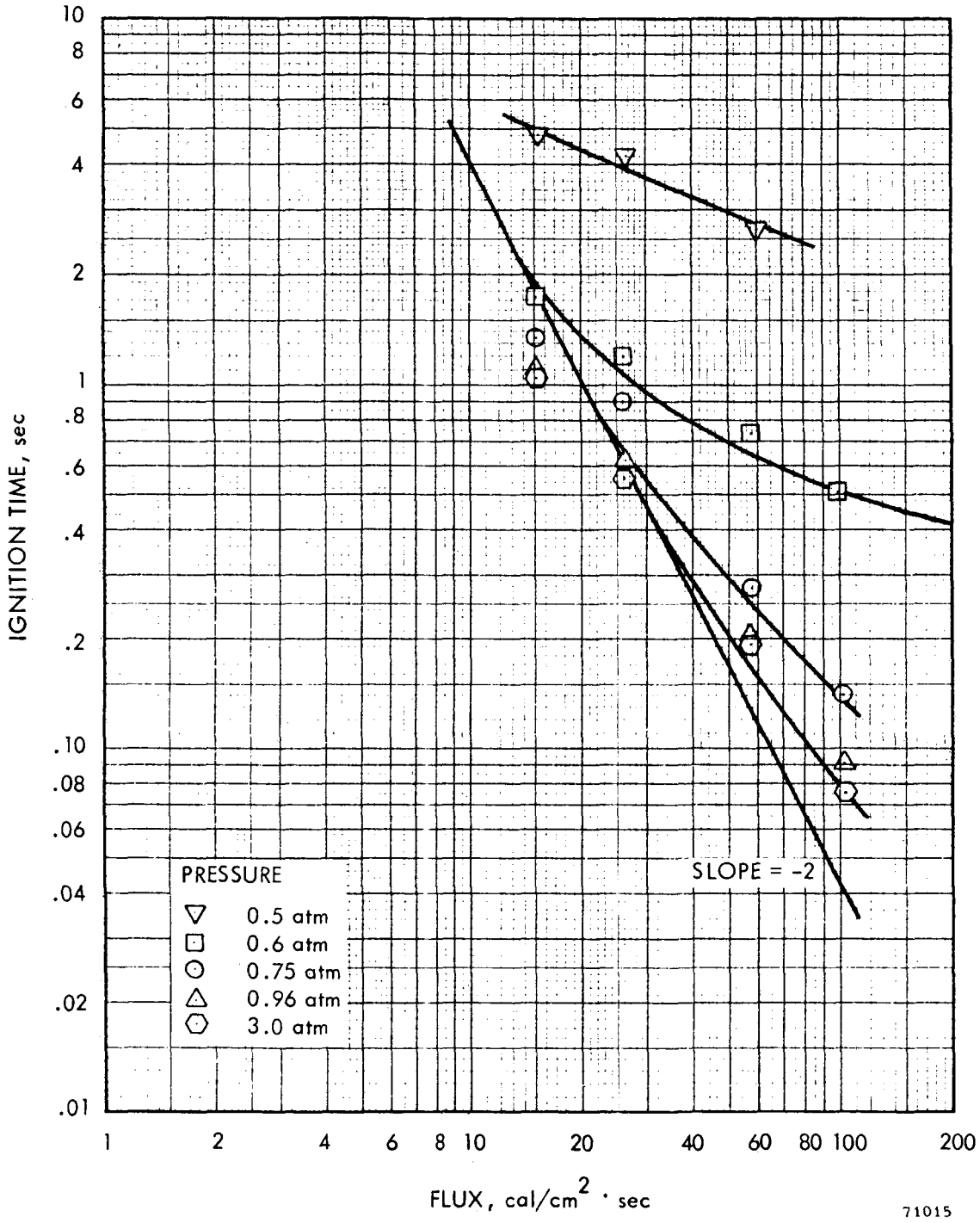

Figure 49. Effect of Flux Upon Ignition Delay of UTREZ Propellants for Different Environmental Pressures (N_2)

5. Combustion of oxidizer-derived ammonia and perchloric acid (exothermic)

6. Combustion of oxidizing gases and fuel species (exothermic).

In the catalytic AP thermal decomposition studies published to date,[25] it has been found that copper, manganese, and zinc compounds are better catalysts for AP decomposition than iron-containing materials. Less extensive data also indicate that copper is a better promoter of fuel oxidative degradation.[23] Complicating the understanding of the net effects of these two catalysts is recent data obtained by Waesche[26] which show the thermal decomposition of the AP and organic binder together as a composite propellant to be increased in the same manner by copper chromite and iron oxide.

The effect of subsurface reaction or decomposition upon termination of the PIB propellants is probably minimal. Addition of the iron oxide and copper chromite catalysts which might be expected to increase subsurface decomposition had little or no effect upon $\dot{P}$ or L* termination. Also, the substitution of 400 μ large-particle AP for the standard 190 μ increased $\dot{P}$ termination requirements slightly, though there was a significant[19] reduction of subsurface interfacial area. AP particle size was found to have little effect upon PBAA composite propellants containing no catalysts. However, when 2% copper chromite was included, the $\dot{P}$ termination requirements were increased when the average particle size was increased. Baer's studies also showed that the introduction of copper chromite in the basic PBAA propellant increased the termination requirements. Thus, it is possible that endothermic thermal decomposition of isobutylene propellants is a dominant factor while the more easily oxidized unsaturated binders such as PBAA are affected by both exothermic oxidative and endothermic thermal decomposition and would be more affected by the inclusion of burning rate catalysts.

The contradictory effect of aluminum on $\dot{P}$ and L* termination behavior is presently unexplainable. It would be expected that the presence of hot aluminum on the propellant surface would act as a heat source, making $\dot{P}$ and L* extinction more difficult and causing reignition in marginal depressurization situations. In addition, combustion of the aluminum particles will increase the heat of combustion, thereby increasing gas-phase heat feedback. Also, the aluminum combustion products in the gas phase will cause increased radiation heat feedback. The apparent difference between the negligible effect shown upon $\dot{P}$ termination and the marked effect upon L* termination deserves greater attention in future studies. It was found, however, in the course of the AFOSR ignition studies[11] that, if surface absorbtivity differences are compensated for, addition of aluminum has no effect upon arc-image furnace delays of PBAN propellants. Whether this holds for saturated binder systems was not determined.

Analysis of the problem of extinction permanence has received less attention than the initiation of extinction. Cohen[17] has attempted to use the ignition theory of Paul[27] for development of a reignition criteria. The Paul ignition model is based upon a thermal ignition delay plus a pressure-dependent

chemical delay. In utilizing this model, Cohen postulated that since the propellant has a thermal profile at the point of extinction, reignition will occur if the chamber pressure fails to fall below the minimum ignition pressure, P*, in a time period shorter than the chemical ignition delay. Vice versa, if the drop in pressure from the extinction pressure to below the P* occurs in an interval shorter than the time necessary to reinitiate combustion, extinction will be permanent.

The model obviously does not describe those situations where the P* is less than the ambient pressure. Since the pressure in the motor cannot fall below the P*, reignition would be predicted to always occur. The $\dot{P}$ results and the concurrent ignition studies[11] have shown this to be invalid. All the basic propellants with P* below the ambient pressure level were still extinguished. Furthermore, the light sensor data of table V indicate that at lower L* values, extinction of the UTREZ propellants was achieved at pressures considerably above the minimum ignition pressure. The film studies also demonstrated that propellant reignition was often caused by the retention of heat in the inhibitor used to control propellant burning area, a problem not considered in any analysis. These results demonstrate the need for development of an understanding of both termination and reignition phenomena which can provide a reliable basis for the development of engineering design methods.

THEORETICAL STUDIES

Theoretical studies were initiated late in the research program to provide a basis for the interpretation of combustion termination and reignition data. The basic approach will be to follow theoretically the response of the temperatures in the combustion zone to the pressure decay. By including the effects of chemical reactions on and within the solid phase and heat transfer from the gas phase, the thermal history following depressurization can be followed and the conditions producing reignition determined. The combustion model used in this investigation is currently under study at UTC in ignition and combustion instability research programs.

The transient behavior of the solid phase is modeled, at least to a first approximation, by the one-dimensional form of the transient heat conduction equation expanded to include the effects of exothermic reactions. This equation is

$$\frac{\partial T}{\partial t} = \alpha \frac{\partial^2 T}{\partial x^2} + \dot{r} \frac{\partial T}{\partial x} + Z_3 \exp(-E_3/RT) \tag{4}$$

where:

T = temperature

x = distance into the solid from the surface

t = time

α = propellant thermal diffusivity

$\dot{r}$ = linear burning rate of the propellant

Z_3 = Arrhenius preexponential factor for solid-phase combustion reactions.

At the surface of the propellant, a heat balance indicates that the total heat received by the surface is given by

$$-k\left(\frac{\partial T}{\partial x}\right)_{x=0} = \underset{(1)}{F} + \underset{(2)}{Z_1 P \exp(-E_1/RT)} - \underset{(3)}{\Delta H_v \rho \dot{r}} \qquad (5)$$

where:

k = thermal conductivity

ρ = propellant density

Z_1 = Arrhenius preexponential factor for exothermic surface reactions

E_1 = Activation energy factor for exothermic surface reactions

P = pressure

F = heat flux from gas-phase combustion zone to solid surface.

The terms on the right-hand side of equation 5 represent

(1) = heat supplied from the flame zone (gas-phase reaction zone a finite distance away from the surface)

(2) = heat generated at the surface by heterogeneous reactions between the solid oxidizer decomposition gases and the exposed fuel matrix

(3) = heat released because of gasification of propellant at the surface.

Deep within the propellant, the temperature remains constant at the initial temperature of the propellant. Mathematically, this can be expressed as

$$T = T_\infty \text{ at } x = \infty \qquad (6)$$

To complete the mathematical model, an expression also is needed for the regression rate in terms of the surface temperature. In this analysis, it has been assumed that the linear burning rate is determined by some overall pyrolysis rate of the solid phase. Mathematically, this can be expressed

$$\dot{r} = Z_2 \exp(-E/RT_s) \qquad (7)$$

Before the response of the preceding equations to pressure perturbations can be studied, the effect of pressure on the gas-phase heat transfer must be considered. This effect, which has received attention in several studies, is the result of a complex interaction between diffusional processes, which are independent of pressure, and chemical reaction processes, which are highly pressure dependent. The net pressure effect is thereby difficult to evaluate theoretically as shown by Penner.[28] For the purpose of these preliminary theoretical studies, the various complex theoretical relations for the effect of pressure on the gas-phase heat flux, F_o, can be approximated by the empirical expression

$$F = F_o \left(\frac{P}{P_o}\right)^{n'} \tag{8}$$

where the subscript o refers to steady-state conditions.

To study the reignition and termination problem, solutions to this set of equations will be sought assuming the pressure follows the relation

$$\left(P - P_f\right) = \left(P_o - P_f\right) \exp\left(-\lambda t\right) \tag{9}$$

where P_f is the steady-state pressure after chamber decompression. After the pressure has reached P_f, the temperature history of the combustion zone can be followed to determine if surface energy release or if auxiliary heating of the solid phase by gas-flow phenomena is sufficient to produce reignition or if extinguishment has indeed been achieved. In this way, both termination and reignition can be studied simultaneously.

To simplify the solution, the variables can be expressed in the following dimensionless forms

$$\theta = T/T_\infty \tag{10}$$

$$\theta_o = T_s^\circ/T_\infty = \frac{1}{\phi} \tag{11}$$

$$\tau = t\,(\dot{r}_o)^2/\alpha \tag{12}$$

$$\zeta = x\,\dot{r}_o/\alpha \tag{13}$$

Where $\dot{r}_o$ is the steady-state combustion velocity and $\alpha = k/C_p\rho$, the equations become

$$\frac{\partial\theta}{\partial\tau} = \frac{\partial^2\theta}{\partial\zeta^2} + \frac{\dot{r}}{r_o}\frac{\partial\theta}{\partial\zeta} + \bar{Z}_3 e^{-E_3/RT_\infty\theta} \tag{14}$$

at $\zeta = 0$

$$-\frac{\partial\theta}{\partial\zeta} = \frac{\eta}{\phi} + \bar{P}\exp\left[-E/RT_\infty\theta\right] - \frac{\beta}{\phi} \tag{15}$$

$$\zeta \to \infty \qquad\qquad \theta \to 1.0 \tag{15a}$$

where:

$$\bar{P} \equiv \frac{Z_1 P_o}{\dot{r}_o\rho T_\infty C_p}, \quad \bar{Z}_3 \equiv \frac{Z_3\alpha}{T_\infty r_o}, \quad \beta = \frac{\Delta H_v}{C_p T_s^\circ}, \text{ and } \eta = \frac{F_o}{\dot{r}_o\rho C_p T_s^\circ}$$

Exact solution of equations 14 and 15 is difficult because of the nonlinearity of these expressions. In order to circumvent this problem, a finite difference algorithm was developed for digital computer solution. Equation 14 in continuum form replaced the finite difference approximation as shown by equation 16 where the mesh points of the difference scheme are represented by i from i = 1 at the propellant surface to n at a point $n\Delta\zeta$ within the solid propellant.

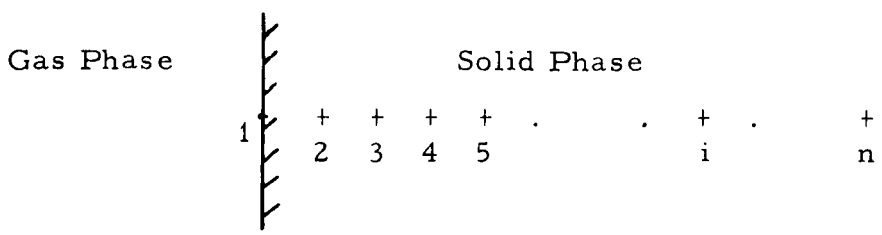

For i = 2, 3, 4, i, n

$$\left.\frac{\partial\theta_i}{\partial\tau}\right/ = \frac{\theta_{i+1} - 2\theta_i + \theta_{i-1}}{\Delta\zeta^2} + \frac{\dot{r}}{\dot{r}_o}\frac{\theta_{i+1} - \theta_{i-1}}{2\Delta\zeta} + B'e^{-E/RT_\infty\theta_i} \tag{16}$$

Writing the boundary condition equation at $\zeta = 0$ in finite difference form we obtain

$$-\frac{\partial \theta}{\partial \zeta} = \frac{\theta_3 - 4\theta_2 + 3\theta_1}{2\Delta\zeta} = \frac{\eta}{\phi} + \bar{P}\, e^{-E_2/RT_\infty \theta} - \frac{\beta}{\phi}\left(\frac{\dot{r}}{\dot{r}_o}\right) \tag{17}$$

This equation may be differentiated with respect to the time variable, τ, to give

$$\left(\frac{\partial\theta_3}{\partial\tau} - \frac{4\partial\theta_2}{\partial\tau} + 3\,\frac{\partial\theta_1}{\partial\tau}\right)\Big/ 2\Delta\zeta = \frac{\partial\eta/\phi}{\partial\tau} + \frac{\partial\bar{P}}{\partial\tau}\, e^{-E_2/RT_\infty\,\theta_1}$$

$$+ \bar{P}\,\frac{E_2}{\theta_1^2\, RT_\infty} \cdot e^{-E_2/RT_\infty\theta_1} \cdot \frac{\partial\theta_1}{\partial\tau} - \frac{\beta}{\phi}\left(\frac{E_3}{RT_\infty\theta_1^2}\right)\frac{\partial\theta_1}{\partial\tau}\left(\frac{\dot{r}}{\dot{r}_o}\right) \tag{18}$$

Rearranging gives

$$\frac{\partial\theta_1}{\partial\tau} = \frac{4\,\dfrac{\partial\theta_2}{\partial\tau} - \dfrac{\partial\theta_3}{\partial\tau} + 2\,\Delta\zeta\,\dfrac{\partial\bar{P}}{\partial\tau}\, e^{-E_2/RT_\infty\theta_1} + \dfrac{1}{\phi}\,\dfrac{\partial\eta}{\partial\tau}}{3 - 2\,\Delta\zeta\,\bar{P}\,\dfrac{E_2}{RT_\infty\theta_1^2}\, e^{-E_2/RT_\infty\theta_1} + 2\,\Delta\zeta\,\dfrac{\beta}{\phi}\,\dfrac{\dot{r}}{\dot{r}_o}\,\dfrac{E_3}{RT_\infty\,\theta_1^2}} \tag{19}$$

Thus, equation 16 plus the n-1 equations of the form of equation 14 provide a set of n simultaneous differential equations which can be solved with the aid of a digital computer. From equations 9 and 8, we obtained $\bar{P}$, $\partial\bar{P}/\partial\tau$, and $\partial\eta/\partial\tau$, and the time differential form of equation 7.

In these studies, a method of solution has been used which is quite unique in solving the transient diffusion and chemical reaction equations. First, a system of ordinary differential equations is generated from the relevant partial differential equation by discretization in terms of the space variable, and then the sequence of values of the dependent variable at the mesh points are regarded as new dependent variables. This leads to a system of ordinary differential equations (in derivatives with respect to time). This means of solution of boundary value problems was extensively exploited for some time in analogue computer work for solution of such problems as transient conduction of heat in solids.

In analogue computer work, the limitation is usually the capacity of the computer. The relatively recent development of digital computer subroutines ("package solvers") for solution of large order systems of differential equations has brought "analogue discretization" methods to a competitive means for solving certain types of partial differential equations.

The specific advantages of this approach to solution of boundary problems may be listed as follow:

A. The programming time is reduced to a minimum as most of the difficult programming has been done in the development of the ordinary differential equations subroutine. Also, the computer running time for the differential equations approach seems to offer an advantage compared to problems involving differencing in both the space and time steps.

B. Numerical convergence problems, i. e., convergence problems arising in numerical solution of the partial differential equations, are relegated to problems of convergence of solutions of systems of ordinary differential equations. Most subroutines for solution of ordinary differential equations have some means of assurance of numerical convergence of the solution.

C. Conversion of a boundary value problem into a system of ordinary differential equations provides a means of handling nonlinear difficulties. This point is particularly important because many of our equations involve an exponential Arrhenius term as well as reactant product terms.

D. The capacity of the differential equation "package solvers" is sufficiently large to allow use of a fairly large number of mesh points in the discretization.

Programming and computer checkout studies using the preceding equations has been completed.

CONCLUSIONS

Both the rapid-depressurization and critical chamber geometry combustion extinguishment characteristics of several series of composite propellants were examined in an effort to elucidate the mechanisms of combustion extinguishment. The effect of binder structure was examined with CTPB, PBAN, PEP, PU, and UTREZ nonaluminized propellants. The influence of catalysts, oxidizer loading level, AP particle size, AP coatings, and aluminum loading upon termination behavior were examined with a series of UTREZ propellants.

Significant differences in both $\dot{P}$ and L* termination characteristics were noted between propellants comprised of different binders, but the mechanism responsible for these changes have yet to be identified. While no exact measure of combustion properties of the binder systems was obtained, results suggest that the butadiene polymers are more easily degraded by oxidative mechanisms, while the UTREZ and polyurethane binders exhibit poorer resistance to degradation by thermal mechanisms. These differences resulted in high critical depressurization rates and low L* pressure levels for the polybutadiene propellants and lower $\dot{P}$ requirements but higher L* pressure for the UTREZ and PU propellants.

Concurrent arc-image furnace studies demonstrated the minimum ignition pressures of the PEP, CTPB, and PBAN propellants to be lower (0.1 to 0.03 atm) than the minimum ignition pressures of the PU and UTREZ propellants (0.2 and 0.4 atm, respectively). Also the L* pressure for large L* values (>400 in.) corresponded to the minimum ignition pressure levels.

Increasing the fuel content of a series of UTREZ propellants resulted in an increase of the L* pressure levels and a lowering of the critical depressurization rates. These findings suggest the endothermic thermal decomposition of the UTREZ binder has a significant influence on the termination process.

Substitution of large-particle, coarse AP (400μ) for the standard 190μ particles resulted in a slight increase of $\dot{P}$ termination requirements, while substitution of coarse AP coated with 1.5% Kel-F had no effect upon $\dot{P}$ or L* behavior.

The addition of different concentrations of iron-oxide and copper-chromite burning-rate catalysts had little or no effect upon $\dot{P}$ and L* behavior of the AP-UTREZ system, though these catalysts did modify the ballistic parameters. These and the results of the last paragraph above suggest subsurface decompositions have little effect upon the termination characteristics of UTREZ or other saturated polymer propellant systems.

Substitution of aluminum powder for AP resulted in but a slight increase of the $\dot{P}$ requirements of the UTREZ propellant system though the L* pressure

levels increased markedly with increasing aluminum concentration. Introduction of 4% aluminum needles into a propellant containing 16% total aluminum caused both the $\dot{P}$ termination requirements and the burning rate to be increased greatly.

Correlation of the experimental $\dot{P}$ termination requirements with Von Elbe-model-type predicted requirements showed qualitative agreement. However, a large number of exceptions to the general trend indicates this type of analysis had little potential for a priori predictions.

Photomicrograph examination of the L*-terminated UTREZ propellant surfaces showed tricalcium phosphate, other contaminants, and possibly AP to exist as a melt on the surface during combustion prior to extinction. Comparison with propellants formulated with other binders showed the extensive melting to be peculiar to the UTREZ and PEP binder systems.

Examination of the UTREZ propellants containing aluminum showed the surfaces to be covered with a sintered network of aluminum balls. Agglomeration of the original balls was evidenced by aluminum balls up to several hundred microns in diameter.

High-speed film studies showed reignition of $\dot{P}$-terminated grains to be caused in some instances by the propellant inhibitor. Thermal energy stored in the polymer inhibitor often caused reignition several seconds after complete combustion termination of the grain. Based on these observations, $\dot{P}$ data obtained in laboratory motors may not be directly applicable to working, well-inhibited motors unless the design is made sufficiently conservative.

The reignition criteria based on the critical depressurization time concept was shown to be invalid. Successful $\dot{P}$ and L* termination was achieved though the backpressure was greater than the minimum ignition pressure of the tested propellant.

A theoretical model of combustion termination behavior was developed and successfully programmed for future computer solution.

REFERENCES

1. Von Elbe, G.: Theory of Solid Propellant Ignition and Response to Pressure Transients. Bulletin of 19th ICRPG Conference, Silver Spring, Maryland, pp. 157-181, 1963.

2. Paul, B. E.; Lovine, R. L.; and Fong, L. Y.: A Ballistic Explanation of the Ignition Pressure Peak. AIAA Preprint 64-121, presented at the 5th AIAA Solid Propellant Rocket Conference, Palo Alto, California, January 1964.

3. Ciepluch, C. C.: Effect of Composition on Combustion of Solid Propellants During a Rapid Pressure Decrease. NASA TND-1559, December 1962.

4. Capener, E. L.; Dickinson, L. A.; and Marxman, G. A.: Propellant Combustion Phenomenon During Rapid Depressurization. Annual Report No. 1, Contract NAS 7-389, Stanford Research Institute, September 1966.

5. Levinsky, C. T.: Combustion Problems in Single Chamber Controllable Solid Rocket Development. ICRPG 3rd Combustion Conference, Cocoa Beach, Florida, 17-21 October 1966.

6. Horton, M. D.; Bruno, P. S.; and Graesser, E. C.: Depressurization Induced Extinction of Burning Solid Propellant. ICRPG/AIAA 2nd Solid Propulsion Conference, Anaheim, California, 6-8 June 1967.

7. Landers, L. C.; and Lou, R. L.: Development of an Extinguishable Solid Propellant. Final Report, Contract AF 04(611)-9889, Aerojet-General Corporation, July 1965 (CONFIDENTIAL).

8. Povinelli, L. A.; and Ciepluch, C. C.: Surface Phenomena in Solid Propellant Combustion. Presented at JANAF/ARPA/NASA Solid-Propellant Group Meeting, Pittsburgh, Pennsylvania, 5-7 June 1962.

9. Anderson, R.; Brown, R. S.; and Shannon, L. J.: Ignition Theories of Solid Propellants. AIAA Meeting, Palo Alto, California, January 1964.

10. Brown, R. S.: Research on Combustion of Solid Propellants. UTC 2136, Technical Summary Report, Contract No. DA-04-200-AMC-968(X), United Technology Center, July 1966.

11. Shannon, L. J.: Composite Solid Propellant Ignition Mechanisms. AFOSR Scientific Report, AFOSR 67-1765 (UTC 2138-ASR-2), Contract No. AF 49(638)-1557, United Technology Center, September 1967.

12. Horton, M. D.; Bruno, P. S.; and Graesser, E. C.: Depressurization Induced Extinction of Burning Solid Propellant. ICRPG/AIAA 2nd Solid Propulsion Conference, Anaheim, California, 6-8 June, 1967.

13. Nametz, R. C.: Self-Extinguishing Polyester Resins. Ind. Eng. Chem. 59, No. 5: pp. 99-116, May 1967.

14. Lou, R. L.; Landers, L. G.; and Lovine, R. L.: Theoretical and Experimental Study of Extinguishable Solid Propellants. Technical Report No. AFRPL-TR-66-128, Aerojet General Corp., July 1966 (CONFIDENTIAL).

15. Barrére, M.: Presentation Given at Stanford Research Institute, Menlo Park, California, 3 May 1967.

16. Coates, R. L.; and Cohen, N. S.: Correlation of Solid Propellant Extinguishment Data. Proceedings of ICRPG 3rd Combustion Conference, JFK Space Center, Florida, p. 213, 17-21 October 1966.

17. Cohen, N. S.: A Theory of Solid Propellant Extinguishment by Pressure Perturbation. Proceedings of ICRPG 2nd Combustion Conference, p. 677 (Aerospace Corporation, Los Angeles, California), 1-5 November 1965.

18. Parker, K. H.; and Summerfield, M.: Response of the Burning Rate of a Solid Propellant to a Pressure Transient. AIAA Preprint No. 66-683, presented at the AIAA Propulsion Joint Specialist Conference, Colorado Springs, Colorado, June 1966.

19. Donaldson, A. B.; et al: Extinguishment of Composite Propellants by Rapid Depressurization. Proceedings of ICRPG 2nd Combustion Conference, p. 697, (Aerospace Corporation, Los Angeles, California) 1-5 November 1965.

20. Madorsky, S. L.: Thermal Degradation of Organic Polymers. Interscience Publishers, New York, 1964.

21. Madorsky, S. L.: Modern Plastics, 38, No. 6: p. 134, 1961.

22. Jellinek, H. H. G.: Degradation of Vinyl Polymers. Academic Press Incorporated, New York, 1955.

23. Hansen, R. H.: Effects of Morphology, Antioxidants, and Copper on the Oxidation of Polypropylene. Bell Telephone Laboratories Report, Murray Hill, New Jersey.

24. Reed, Jr., R.; et al: Extinction Characteristics of Carboxyl Terminated Polybutadiene Propellant. ICRPG 3rd Combustion Conference, Cocoa Beach, Florida, 17-21 October 1966.

25. Waesche, R. H. W.; and Wenograd, J.: The Effect of Pressure and Additives on the Kinetics of Decomposition of Ammonium Perchlorate. Western States Section/Combustion Institute, Preprint No. 67-8, San Diego, California, April 1967.

26. Waesche, R. H. W.; Wenograd, J.; and Feinauer, L. R.: Investigation of Solid Propellant Decomposition Characteristics and their Relation to Observed Burning Rates. ICRPG/AIAA 2nd Solid Propulsion Conference, Anaheim, California, June 6-8, 1967.

27. Paul, B. E.; Lovine, R. L.; and Fong, L. Y.: Diffusional Analysis of Composite Propellant Ignition and its Application to Solid Rocket Ignition. AIAA Preprint 64-117, presented at the 5th AIAA Solid Propellant Rocket Conference, Palo Alto, California, January 1964.

28. Penner, S. S.: Chemical Rocket and Combustion Research. Gordon and Beech, New York, 1962.